The roles of clustered membrane proteins in T-cell signaling

by

Woo K. Chung

B.S., Northwestern University (2006)

Submitted to the Department of Chemical Engineering in Partial Fulfillment of the Requirements for the Degree of

Doctor of Philosophy
at the
Massachusetts Institute of Technology

May 2012

Signature of Author.....
Department of Chemical Engineering
May, 2012

Certified by.....
Arup K. Chakraborty
Robert T. Haslam Professor of Chemical Engineering
Professor of Chemistry and Biological Engineering
Thesis Supervisor

Accepted by.....
Patrick S. Doyle
Professor of Chemical Engineering
Graduate Officer of the Department

The roles of clustered membrane proteins in T-cell signaling

by

Woo K. Chung

Submitted to the Department of Chemical Engineering
on May 24, 2012 in Partial Fulfillment of the
Requirements for the Degree of Doctor of Philosophy in
Chemical Engineering

Abstract

Humans, like most other jawed vertebrates, are equipped with an adaptive immune system that can respond to diverse pathogens. Mature T cells, one of the most important immune cells generated from the thymus through a rigorous selection processes, are key orchestrators of the immune responses. Although many of the key signaling molecules in T cells have been discovered, the underlying mechanisms of how some of these signaling molecules interact with each other in space and time to trigger T cell activation have not yet been established. Furthermore, recent experimental results demonstrate that the membrane is a highly organized structure with some membrane proteins inhomogeneously distributed into clusters, which are often called protein islands or protein clusters. The roles of these clustered proteins remain to be established. For my thesis, to gain insights into the roles of protein islands in early T cell signaling, I have focused on important clustered proteins such as the T-cell receptor (TCR) and Linker of activated T cells (Lat). Active ZAP-70 molecules, which phosphorylate tyrosine residues of Lat molecules, are generated from the clustered TCR molecules. Using spatial Gillespie simulation and mathematical modeling, I found that clustered proteins may suppress the probability of spurious triggering of T cells. This finding may suggest an important role of clustered proteins, which may be relevant to other signaling networks and other cell types with spatially clustered proteins in the membrane. In addition, I have examined how the spatial organization of membrane proteins and the diffusivity of molecules affect the steady-state levels of key molecules required for T-cell activation: RasGTP and fully phosphorylated ITAM. I have also studied the correlation between the peptide repertoire presented by antigen-presenting cells in the thymus and the generation of autoreactive T cells as well as the TCR repertoire of peripheral T cells.

Thesis Supervisor: Arup K. Chakraborty
Title: Robert T. Haslam Professor of Chemical Engineering
Professor of Chemistry and Biological Engineering

To my parents and sister

Acknowledgement

My graduate years at MIT greatly have affected me in terms of maturity and intelligence. During my progress toward finishing my thesis, I have interacted with many people who positively influenced me. There are so many people that I should thank for my accomplishments as a researcher. Therefore, in this piece of paper, I would not be able to mention everyone who deserves to be acknowledged and I hope those of whom are not mentioned here understand my incapability.

Most of all, I regret I did not say enough to my father how he contributed to my life in positive ways, while he was in the world where I live. After my father passed away while I was a second year graduate student, I have had quite difficult times. My father's death made me realize that how life could be such fragile. My father's intelligence had inspired me since I was young. Although there is no my father, his spirit is still alive in my mind. I believe that I could overcome my difficult times in the United States because of cares of my parents. I should thank my mother and sister. I am very proud of their strengths and courage to overcome difficult years. I also thank my new country, the United States, which gave me opportunities to be educated in great schools as an American citizen. I should thank many professors and many friends whom I met while I was at Northwestern. They not only provided me great academic environment and opportunities, but also encouraged me to do well. They helped me prepare well to pursue further advanced education. I also thank many of my classmates and friends at MIT for sharing their time with me. As a graduate student, I spent most of my time in my lab, which means that my labmates greatly affected my life at MIT.

My lab consists of people with great mind from many fields. I appreciate all my fellow graduate students in my lab for their supports: Mikhail Wolfson, Chris Govern, Andrej Kosmrlj, Mieszko Lis, Arvind Prabhakar, Karthik Shekhar, Kevin Fowler, Maxim Artyomov, Jason Locasale, Ming Yang, Huan Zheng, and Allison Tovo-Dwyer. I especially thank Mikhail for his kind technical and emotional supports. I spent a brief period with Allison. Seeing her positive attitude and great spirit made my life in the lab much happier. Unfortunately, she got stomach cancer, and I hope she survive her cancer with her strong will. I also briefly spent a good time with new first-year graduate students in my lab. I also thank postdoctoral lab members: Steven Abel, Abhishek Jha, Vincent Dahriel, Jayajit Das, Ashok Prasad, Andrew Ferguson, Elizabeth Read, and Tom Butler. I especially want to acknowledge Steven. His love of science, sharp mind, humanism, and sincere care of his fellows inspired me greatly. I am so glad to meet him in my lab especially during a difficult time in my life, and I wish his great success as a scientist. I finally deeply appreciate my thesis advisor, Prof. Arup Chakraborty, and my thesis committee members: Prof. Narendra Maheshri and Prof. Darrell Irvine. My advisor and thesis committee members provided me great research advices and helped me progress in my work. As I was working in Prof. Chakraborty's lab, I had great opportunities to conduct research on important topics that could help improve understanding scientific phenomena related to health and medicine.

Table of contents

Chapter 1

Introduction

Chapter 2

The roles of protein clusters in the T-cell membrane in helping suppress spurious T cell triggering

Chapter 3

The effects of the configurations of membrane systems and the diffusivities of molecules on the amount of steady-state levels of downstream signals such as ITAM and RasGTP, in the presence of negative regulation of the downstream signals

Chapter 4

Stochastic error in thymic selection suggests the requirement of optimal peptide repertoire in the thymus

Chapter 5

Conclusion

Appendix

Chapter 1

Introduction

1.1 Background

Highly evolved jawed vertebrates have their own defense mechanisms against macro-scale organisms on the order of magnitude of their own sizes as well as micro-scale organisms or materials, such as fungi, bacteria, and viruses. Immunology focuses on the latter group. The field of this study has matured through enormous efforts by many experimental biologists, thus providing a large amount of information on the cellular and molecular levels about agents participating in immune responses. The expanding knowledge leaves many questions to be answered in order to more comprehensively understand the mechanisms of immune responses. Despite rapid discovery of new properties of cells and molecules that participate in the immune system, many unknown mechanisms and missing signaling pathways still have to be discovered to connect many spatiotemporal phenomena in immune responses, with advancing experimental technology and theories.

Theoretical and computational work can help us understand the mechanisms of biological systems by providing qualitative explanations based on well developed theory and software. This thesis presents my theoretical and computational work to suggest interesting mechanisms that account for experimental phenomena. The following sections in the introduction briefly describe the early-T cell signaling pathways and thymic selection that I have researched and which my future work will expand upon.

1.1.1 The early T-cell signaling event

T cells, the orchestrators of adaptive immune responses for almost all vertebrates, are equipped with intriguing features that enable them to detect the presence of pathogens and distinguish infected cells from normal cells. Once antigen-presenting cells (APCs), such as dendritic cells, detect and engulf pathogens, antigenic peptides, the peptide derivatives from the pathogens, are presented by a major-histocompatibility complex (MHC) on the surface membrane of an APC. A T-cell receptor (TCR), presented on the T-cell membrane, interacts with a complex of antigenic peptide and major histocompatibility complex (antigenic pMHC), and a few such interactions can stimulate the T cell. Many experimental results have indicated that the response of T cells to antigenic peptides is highly sensitive (they can recognize 1-10 antigenic pMHCs) and rapid (recognition takes about 30 seconds), thus making T cells highly effective detectors [1,2]. Such sensitive detection of many kinds of antigenic peptides, which is based on TCR's efficient translation of signals from the molecular level of interaction between TCR and antigenic pMHC, should be very specific as well as diverse [3]. In addition, the recognition of antigenic peptides by a T cell is rapid [4]. For example, the intracellular calcium fluxes occur within 10 seconds once a T cell interacts with a few antigenic pMHC [5].

While TCR interacts with pMHC, multiple immunoreceptor tyrosin-based activation motifs (ITAM), connected to a CD3 region of TCR [6,7], are efficiently phosphorylated by an Lck, which is brought by a molecule called a coreceptor [8]. The different types of coreceptors are expressed on the membrane of a T cell depending on the type of the cell. CD4 and CD8 proteins are coreceptors that are mainly expressed on

T helper cells and cytotoxic T lymphocytes (CTL), respectively [4,8,9,10,11]. The roles of these coreceptors in the early T cell signaling have been ambiguous. Recent experimental results suggest that TCR can interact with pMHC independently of CD4, and the interaction between TCR and pMHC is not significantly stabilized by CD4 [12]. In addition, cytotoxic T lymphocyte with no CD8 can still be triggered by antigenic pMHC with a high affinity interaction with TCR [11]. However, these coreceptors may help amplify the downstream signals induced by an antigenic pMHC interaction with TCR by means of several mechanisms, which will be described in detail later. After two tyrosine residues of each ITAM of the CD3 ζ chains become phosphorylated, the ZAP-70 protein can be bound to the phosphorylated ITAM and become activated by Lck [6,13,14,15]. The active ZAP-70 is an important kinase of a linker of activated T cells (Lat) [13,14,15,16,17,18]. The phosphorylation of multiple tyrosine sites of Lat is important for further generating downstream signals for T cell activation, the process which changes the morphology and function of T cells and initiates their differentiation and proliferation.

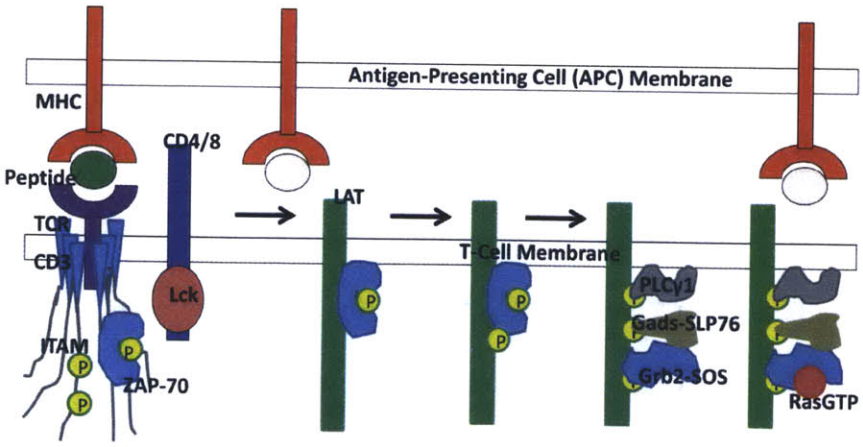

Figure 1-1. The early T cell signaling pathway. Key proteins participating in the early T cell signaling are shown.

T cells in peripheral tissues are able to distinguish between self cells and pathogen-infected cells. These normally functional T cells are produced through the selection process in the thymus, which will be described in more detail in the next section. Through thymic selection, only T cells that interact moderately with self (endogenous) pMHC should survive to interact with antigenic pMHC but avoid too strong an interaction with endogenous pMHC, which could lead to autoimmune responses. No clearly defined mechanism explains how this moderately interacting T cells minimize the accidental activation from their numerous interactions with many types of endogenous pMHC, but maximize the probability of activation by the T cells' few interactions with antigenic pMHCs.

Several models have suggested possible mechanisms for these phenomena. One of the plausible models, which is called the pseudodimer model [19,20] provides the following mechanism. Once the TCR binds to a strongly interacting antigenic pMHC complex, CD4 is recruited to the pMHC, and consequently CD4's Lck is activated. Then the activated Lck can phosphorylate many of the short-life complexes of TCR bound to endogenous pMHC, which frequently interact with the coreceptor bound to the antigenic pMHC. This model suggests that the highly sensitive detection of a small amount of antigenic pMHC comes from the "ready and waiting" mechanism that requires the CD4 dimer where two TCR-pMHC complexes bind to the common CD4 [19,20]. CD4 is highly specific because it is initially activated only by the antigenic pMHC complex. However, the CD8 that helps the activation of CTL is not so specific, but rather promiscuous. The CD8 can bind to a complex of TCR with a strong agonist (antigenic peptide), a weak agonist, and an antagonist (the peptide that nullifies signals induced by

an agonist) [21]. The strength of signaling of TCR is usually related to the strength of binding of CD8 to complexes of TCR-pMHC [21]. In contrast to CD4, CD8 may enhance the stability of a complex of TCR and pMHC [22,23]. Therefore, CD8 can improve the sensitive detection of antigenic pMHC by enhancing the stability of a complex of TCR and antigenic pMHC [24,25].

One of the mechanisms that explains the specific recognition of antigenic peptides is called kinetic proofreading [26]. The kinetic proofreading basically relies on the relative time scales of phosphorylation of ITAM and the association between TCR and pMHC. The model suggests that ITAM has multiple sites to be phosphorylated in order to generate further downstream signals, and the mean time scale for the full phosphorylation of ITAM of a TCR might be much longer than most of the time scales for the dissociation between TCR and endogenous pMHC [26,27]. Assuming that dephosphorylation of ITAM only occurs immediately upon dissociation between TCR and pMHC, most of the phosphorylated ITAM produced by the interaction between TCR and endogenous pMHC will be dephosphorylated. Otherwise, because the time scale for the dissociation of TCR from antigenic pMHC is longer than that of TCR from endogenous pMHC, the probability that the ITAM will be fully phosphorylated by the antigenic pMHC interaction is higher. The conventional kinetic proofreading is based mainly on the reaction rate constant for the dissociation between TCR and pMHC (k_{off}), but recent papers indicate that kinetic proofreading also depends on the reaction rate constant for the association between TCR and pMHC (k_{on}) because both k_{on} and k_{off} affect the effective lifetime of a complex of pMHC-TCR [1,2,27].

Another important theory that characterizes behaviors derived from the kinetic binding between TCR and pMHC is called the serial engagement hypothesis [1,18,28]. The total amount of early downstream signals in a T cell depends on the probability of full phosphorylation per interaction between pMHC and TCR as described by the kinetic proofreading model, but it also depends on how many distinct TCR molecules that a pMHC molecule can interact with per unit time. Therefore, the total downstream signal can be greatest for any pMHC that can both bind stably to each TCR for sufficient time for the complete phosphorylation of ITAM and can bind to many TCRs in a given time interval. This phenomenon, indicating that the rate of interaction between pMHC and TCR might be an import factor for determining the level of downstream signals, is called the serial triggering hypothesis. The pMHC that too strongly interact with TCR would not be able to debind as quickly and to interact with other TCRs as frequently as those pMHCs that weakly interact with TCR. However, based on the kinetic proofreading model, if the pMHC has too high a value of k_{off}, it would have fewer chances to fully phosphorylate ITAMs of any TCR that it interacts with. Consequently, it is natural for us to hypothesize that there should be an optimal value of k_{off} that maximizes the amount of downstream signal by improving both the probability for inducing effective signals such as fully phosphorylated ITAM per interaction between reactants and the rate of interaction between reactants. This hypothesis can be easily verified by solving the ordinary differential equations for the following reaction scheme that considers the generation of only singly phosphorylated ITAM:

$$\text{TCR+pMHC} \underset{k_{off}}{\overset{k_{on}}{\rightleftarrows}} \text{TCR-pMHC} \xrightarrow{k_p} \text{pTCR-pMHC} \xrightarrow{k_{off}} \text{pTCR+pMHC}$$

At fixed values of the association and phosphorylation rate constants, we examined how the downstream signals such as singly phosphorylated TCR depend on the lifetime of dissociation. As can be seen in Fig. 1-2, at a value of k_{off} of 1 sec^{-1}, the strength of the downstream signals such as phosphorylated ITAM (pTCR) at early times of reaction is greater than those at lower or greater k_{off}.

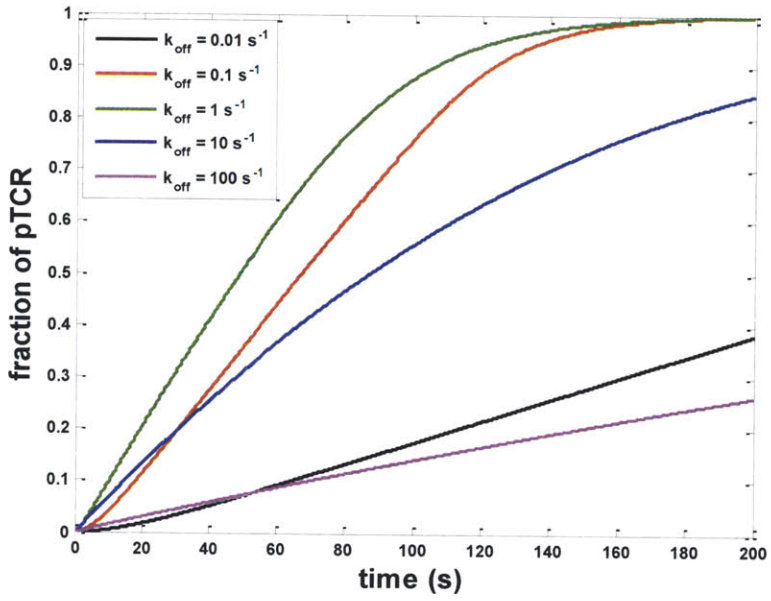

Figure 1-2. The fraction of singly phosphorylated TCR over time at various affinity interaction with pMHC. The simulation results are obtained by solving ordinary differential equations based on the above reaction scheme (kon=0.07 $\mu m^2/s$, kp=0.05 s^{-1}, $[TCR]_{t=0}$=200 μm^{-2}, $[pMHC]_{t=0}$=50 μm^{-2}).

After multiple sites of Lat are phosphorylated by an active ZAP-70, Lat becomes a docking site for many other proteins, such as PLC-γ, Gads-SLP76, and GRb2-SOS

[17,29,30,31,32]. These proteins cooperatively interact with each other, while binding to the phosphorylated Lat, and form a stable signalsome when they are bound to Lat in a certain order [17,32]. SLP-76 is associated with Itk, the kinase of PLC-γ [17]. The phosphorylated PLC-γ then cleaves PIP2 and produces a DAG molecule [17]. DAG can bring RasGRP molecules to the membrane and activate them [17]. The activated RasGRP can then convert RasGDP to RasGTP [17]. RasGTP is an important second messenger that can activate further downstream signals and eventually trigger T cell activation.

SOS is an interesting enzyme, which consists of two active sites: a catalytic site and an Ras exchanger motif (REM) domain (allosteric pocket) [16,17,33,34,35]. Catalytic sites can convert RasGDP to RasGTP molecules, and an allosteric pocket can interact with either RasGDP or RasGTP molecules [33]. Although SOS can convert RasGDP to RasGTP with basal activity when its allosteric pocket is empty, when the pocket is occupied by either RasGDP or RasGTP, SOS's catalytic site becomes more active [16]. Especially when SOS interacts with RasGTP at its allosteric site, the catalytic activity can be raised to 75 times the basal activity [36]. Therefore, this is one example of positive feedback because the activity of SOS is positively regulated when SOS interacts with its own product, RasGTP. Such a positive feedback reaction, coupled with the negative regulation of RasGTP by RasGAP, can induce the bimodality of the steady-state levels of RasGTP [16,36,37], which might be important for the effective decision of T cells upon receiving signals from the environment. For example, Fig. 1-3 shows bimodality in the level of RasGTP at a steady state based on our simulation results for the homogenous system which initially contains 350 RasGDP, 150 RasGTP, and 25 RasGAP

molecules per π μm^2. Because Lat is an important mediator for producing second messengers such as RasGTP through SOS, its deletion hinders T cell activation [38].

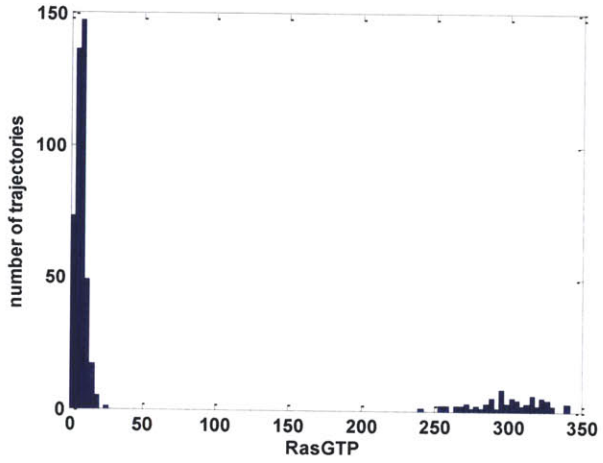

Figure 1-3. The steady-state levels of RasGTP and the number of cells containing a given steady-state level of RasGTP in the homogenous system. The diffusivity of molecules is 0.0167 $\mu m^2/s$. Each system initially consists of 350 RasGDP, 150 RasGTP, and 25 RasGAP molecules per π μm^2. The total number of cells or trajectories is 500. The reaction scheme, reaction kinetic parameters, and concentration of other reactants are the same as those listed in Reaction network S3-2, Table S3-3, and Rate constants for reaction network S3-2, respectively in Supporting Information for Chapter 3.

1.1.2 Spatially organized proteins in the T-cell membrane

Traditionally, the membrane of many types of cells was regarded as the homogeneous system by many experimental and theoretical scientists in order to characterize the mechanism of signaling events, following the principle of the "fluid mosaic" model suggested by Singer and Nicolson [39]. However, it turned out that the mobility of proteins in the membrane and their topology are non-uniform and strongly correlate with the changes of spatiotemporal modifications of cytosolic proteins such as cytoskeletons [7,40,41,42,43]. Lillemeier et al. suggest that almost all plasma membrane-

associated proteins are clustered into regions called "protein islands" [39]. Like all other membrane-associated proteins, Lat and TCR molecules can also form protein islands. Although the causes of the formation of protein islands have not yet been established, studies suggest that modifications of cytoskeletons as well as spontaneous phase separations (into raft and non-raft phases) induce the stable formation of protein islands [7,39,41,42,44,45]. The movement of most transmembrane proteins is restricted to a confinement zone of size ranging from 30 nm to 700 nm, which constitutes the picket-fence model [39].

Upon T cell activation, the contact interface between a T cell and an APC develops a complicated dynamic spatial rearrangement to form a highly patterned region called an immunogical synapse (IS) [38,46]. The IS develops mainly three concentric regions: the central supramolecular activation cluster (cSMAC), the peripheral supramolecular activation cluster (pSMAC), and the distal supramolecular activation cluster (dSMAC), induced by cytoskeletal rearrangement [38]. cSMAC mainly consists of TCR and CD28, while pSMAC contains many cytoskeletal proteins [38,46,47]. Otherwise, CD43, CD44, and CD45 are highly localized in dSMAC [46]. Although an active ZAP-70 is a well known primary kinase of Lat molecules, it is suggested that CD28 can also phosphorylate Lat molecules without active ZAP-70 [48]. Interestingly, the largest amounts of active Lck and active ZAP-70 are located in pSMAC, which suggests that cSMAC is not the region that produces the greatest amount of downstream signals [38]. The dynamic change of the cytoskeleton and the elevation of intracellular calcium level occur within seconds, and the calcium level reaches a peak within 2 to 3 minutes after the detection of antigenic peptides [38]. Yokosuka et al. have shown that

clustered active or inactive ZAP-70 islands are colocalized with CD3ζ chain clusters at initial times of T cell activation throughout the entire contact area between a T cell and an APC, but after 3 minutes since the initial T cell activation, inactive or active ZAP-70 clusters move toward the periphery of the contact region between the T cell and APC [14]. However, CD3ζ chain clusters move toward the center of the contact region. These experimental results suggest that the initial signal for T cell activation is generated even before the formation of cSMAC. However, they indicate that TCRs are internalized into the cytosol at cSMAC, while active signals persist at pSMAC [1,14].

Recently, Ras nanocluster formation was also observed by many experimentalists [36,49,50,51]. Three types of Ras exist: H-ras, N-ras, and K-ras [49,50,52]. It was shown that membrane bound K-ras recruits Raf, which has a Ras binding domain (RBD) [51,53]. The recruited Raf can then bind to MEK, which can also interact with Erk [51]. Therefore, a Ras nanocluster becomes a highly concentrated site for Erk, which is a mitogen activated protein kinase (MAPK) pathway second messenger, as well as become a protector of MEK and ERK from phosphatases [50,51]. Although the exact mechanism of a Ras nanocluster formation is not clear, there are several suggested mechanisms. Das et al. have shown that RasGTP clusters could form in the initially homogeneously mixed reactants such as RasGDP and SOS when the diffusion of molecules is slow (diffusivity of molecules on the plasma membrane is about 100-fold slower than in the cytoplasm) compared to the positive feedback reaction rate [36,49]. In addition, Tian et al. suggest that oligomerization of Gal3 that can interact with K-Ras contributes to the formation of Ras nanoclusters [54], while Gurry et al. hypothesize that the cluster formation might be due to the short-range attraction and long-term repulsion between Ras molecules, based

on the observation of lipid microphase separation [55]. The size of the nanocluster is very small, as 6-12 nm in radii. In addition, the cluster can live as long as 0.4 to 1 seconds and contains around 7 Ras molecules [49,51]. Such internalization and disintegration of islands could lead to digital signaling from each island, which would lead to analog downstream signaling in the whole cell [49]. RasGTP cluster formation can be terminated by the detachment of SOS from the membrane, which can be initiated by the activation of Erk, one of the downstream products of positive feedback [36].

1.1.3 Thymic selection

Thymic selection is a process during which the thymus, an organ located in the chest, detects and removes any harmful or useless T cells. The selection process is thought to help prevent autoimmune diseases that could be caused by harmful T cells and to delete T cells that would be unable to detect molecular signatures of pathogens. Such an important selection involves two major processes: positive selection and negative selection [10,56,57,58,59,60].

Understanding the selection process requires understanding the molecular level interaction between TCR and pMHC. TCR recognition of an antigenic peptide is quite sensitive, but still cross-reactive. For example, T cells cannot recognize point mutation of antigenic peptides, but they can recognize many peptides. This fact is called the specificity/degeneracy conundrum. TCR consists of a hypervariable region and a conserved region that directly bind to a peptide sequence and a part of the MHC sequence, respectively. As discussed before, the stability of interaction, or the duration of

binding, between a TCR and a pMHC determines the magnitude of downstream signaling from the TCR, and eventually the fate of the T cell during the selection process.

One of the selection processes, called positive selection, filters all useless naive T cells [3,60]. The main functions of T cells are to detect any pathogens and kill any infected cells. To perform these roles, T cells should be able to detect an antigen, a molecular mark on the surface of a pathogen, by interacting with it. Positive selection ensures removal of weakly interacting T cells with pMHCs in the thymus because these T cells will be unable to effectively interact with pMHC in the peripheral tissue and cannot recognize antigenic peptides. To summarize, to be positively selected, a T cell should interact with at least one pMHC with an interaction free energy that exceeds a certain threshold for its survival, called the positive selection threshold.

The other important selection process is negative selection [3,61]. This selection removes T cells that bind too strongly to any endogenous pMHC presented in the thymus. For example, a T cell should be eliminated once it binds to an endogenous pMHC with an interaction free energy greater than the negative selection threshold. If the T cell strongly interacts with endogenous pMHC, it can promiscuously react with infected cells as well as non-infected cells. This adverse effect is called an autoimmune response. Therefore, negative selection should delete any autoreactive T cells.

Positive selection is known to be important for ensuring MHC restriction, but not for antigen specificity [3]. Košmrlj et al. and Huseby et al. suggest that negative selection plays a role in mediating specificity [3,62]. The experimental results from Huseby indicate that antigen-specific T cells produced through normal thymic selection sensitively recognize the mutations of certain amino acid sites, which are called hot spots

[62]. However, if the thymus expresses only one type (sequence) of peptides, T cells cannot recognize most mutations of antigenic peptides. Considering that the free energy of the interaction between a TCR and a pMHC in the thymus is important in determining whether a T cell will be negatively or positively selected, Košmrlj et al. developed simple models to examine the development of TCR sequences through the thymic selection based on the interaction free energy [3].

The string model developed by Košmrlj et al. assumes one-to-one interaction only between the two closest neighboring amino acids. According to the model, the total interaction free energy between a TCR and a pMHC can be found as the sum of F_C and the free energy of the interaction between the hypervariable region of TCR (CDR3) and an endogenous peptide presented by the MHC, where F_C is the free energy of interaction between the conserved region of TCR (CDR1 and CDR2) and the region of MHC that directly binds to TCR. The qualitative results are independent of the choice of potential [3]. For example, when the interaction between juxtaposed residues is influenced by neighboring residues, the qualitative result does not change [3]. Košmrlj et al. employed a sharp threshold model for the probability of T cells' survival based on the interaction free energy between a TCR and a pMHC to find how the number of types of peptides affects the mature T cell repertoire. According to the sharp threshold model, the boundaries determining the positive and negative selection thresholds are very sharp. Therefore, if a T cell interacts with any pMHC stronger than the negative selection threshold, it is certainly killed by negative selection. Otherwise, to be positively selected, a T cell should interact sufficiently strongly with at least one of the pMHCs larger than the positive selection threshold.

Košmrlj's results show that the negative selection process plays an important role in shaping antigen-specific TCRs by enriching weakly interacting amino acids in TCRs. These TCRs enriched by weakly interacting amino acids would not recognize antigens if one of the amino acids of antigens is mutated because all interactions between two neighboring amino acids significantly contribute to the overall interaction between TCRs and endogenous peptides.

1.2 Thesis outline

As described in previous sections, immunology provides many interesting phenomena to scientists. The mechanisms behind any of these phenomena are still open questions to us. For my research, I focus on some of these phenomena. The discovery of protein islands in T-cell activation has excited many scientists, but their roles have not yet been well defined. Consequently, I have been interested in finding what kinds of roles that clustered proteins might have in the early and later T-cell signaling pathway with computer simulation and mathematical modeling. The second chapter of my thesis describes my research findings that suggest possible roles of clustered proteins in helping suppress spurious T-cell triggering that might be caused by numerous interactions between TCR and endogenous pMHC molecules.

The third chapter suggests possible mechanisms of how the cluster system induces the greater amount of steady-state downstream signals such as fully phosphorylated ITAM and RasGTP as well as the enhanced bimodality of the amount of RasGTP. I have investigated the role of negative regulator of phosphorylated ITAM in a T cell's fine discrimination of antigenic pMHC from endogenous pMHC molecules based

on the strengths of their affinity interaction with TCR molecules. In addition, the effects of diffusivity of molecules on the steady-state level of doubly phosphorylated ITAM and RasGTP are discussed.

The fourth chapter addresses how stochastic errors in thymic selection controlled by repertoires of peptides presented in the thymus influence the generation of autoreactive T cells and the repertoire of TCR sequences of peripheral T cells. This work implements the experimental data obtained by Huseby et al. and Daniels et al. that indicate that the thymic selection process might not be perfect in selecting functional normal T cells [63,64].

Finally, I suggest the possible future works that can be further pursued from my current work. As described in the previous sections, many interesting questions should be addressed and answered in order to comprehend the mechanisms of immune responses. Big tasks remain ahead for both experimental and theoretical scientists who explore immunological phenomena.

Chapter 2

The roles of protein clusters in the T-cell membrane in helping suppress spurious T cell triggering

T cells play an important role in the adaptive immune system, quickly activating effector functions in response to small numbers of antigenic peptides but rarely activating in response to constant interaction with most endogenous peptides. Emerging experimental evidence suggests that key membrane-bound signaling proteins such as the T cell receptor and the adaptor protein Lat are spatially organized into small clusters on the T cell membrane. We use spatially resolved, stochastic computer simulations to study how the inhomogeneous distribution of molecules affects the portion of the T cell signaling network in which the kinase ZAP-70, originating in T cell receptor clusters, phosphorylates Lat. To gain insight into the effects of protein clustering, we compare the signaling response from membranes with clustered proteins to the signaling response from membranes with homogeneously distributed proteins. Given a fixed amount of ZAP-70 (a proxy for degree of TCR stimulation) that must diffuse into contact with Lat molecules, the spatially homogeneous system responds faster and results in higher levels of phosphorylated Lat. Analysis of the spatial distribution of proteins demonstrates that, in the homogeneous system, nearest ZAP-70 and Lat proteins are closer on average and fewer Lat molecules share the same closest ZAP-70 molecule, leading to the faster response time. The results presented here suggest that spatial clustering of proteins on the T cell membrane may suppress the propagation of signal from ZAP-70 to Lat, thus providing a regulatory mechanism by which T cells suppress transient, spurious signals

induced by stimulation of T cell receptors by endogenous peptides. Because this suppression of spurious signals may occur at a cost to sensitivity, we discuss recent experimental results suggesting other potential mechanisms by which ZAP-70 and Lat may interact to initiate T cell activation.

2.1 Introduction

Nearly all vertebrates, including humans, are equipped with an adaptive immune system that can respond to diverse and previously unencountered pathogens. T lymphocytes (T cells), the primary orchestrators of adaptive immunity, are equipped with molecular features that enable them to distinguish molecular markers of pathogens from "self." The identification of foreign pathogens is accomplished largely through the T cell receptor (TCR), which is a transmembrane protein that interacts with short peptide fragments complexed with host proteins known as major-histocompatibility complexes (MHCs) displayed on other cells. If the TCR and peptide-MHC (pMHC) complex bind sufficiently strongly, then the T cell can become activated through a network of biochemical reactions that originate with the TCR and ultimately change the gene transcription program of the cell [10]. T cell activation can be elicited by a small number of antigenic peptides.

While a T cell can be activated upon encountering a few antigenic pMHC, it is important to note that T cells nearly constantly encounter endogenous peptide fragments bound to MHC, yet rarely activate upon numerous such interactions. This feature of cell signaling is essential for the integrity of the immune system, as frequent activation of T cells against self peptides could lead to uncontrolled proliferation of T cells, a hallmark

of autoimmunity. Although the key biochemical components of the early T cell signaling network are known, in spite of advances [16,65,66], how the network of biochemical reactions yields a fast and specific response against small numbers of antigenic pMHC remains an open question.

The earliest step in T cell signaling through the TCR involves the cytoplasmic portion of the TCR complex, which contains several immunoreceptor tyrosine-based activation motifs (ITAMs). These motifs can be phosphorylated by the tyrosine kinase Lck when the TCR is bound to a peptide-MHC complex. Once phosphorylated, the ITAMs act as binding domains for the kinase ZAP-70 [14,15,46,66,67]. When recruited, ZAP-70 can be phosphorylated by Lck [15], turning it into an active tyrosine kinase. Active ZAP-70 can phosphorylate several tyrosine residues on Lat (linker of activated T cells), an essential adaptor protein that serves as a docking site for many other proteins involved in downstream signaling. The activation of a T cell is controlled largely by early signaling events that occur quickly, with markers of productive signaling downstream of the TCR detectable on order of 10 seconds after TCR engagement with agonist pMHC ligands [5]. Productive signaling, starting from these earliest events, eventually transforms a T cell into an active state [16].

Both TCRs and Lat molecules are transmembrane proteins, suggesting that it may be important to consider features of the membrane environment when analyzing the spatiotemporal control of T cell signaling. The cell membrane has traditionally been difficult to study experimentally, although emerging experimental evidence suggests that the molecules on resting T cell membrane are not homogeneously distributed, but are spatially organized into clusters of proteins [14,39,44,68,69,70,71,72,73]. Recent results

by Lillemeier et al. indicate that TCRs and Lat are each clustered into distinct regions on the surface of resting T cells, with the cluster sizes ranging between 30nm and 700nm [39,69]. Additionally, the average distance between neighboring TCR and Lat clusters apparently decreases upon T cell activation [69]. These results differ from the traditional fluid mosaic model which regards the membrane as a lipid bilayer containing a homogeneous distribution of membrane proteins. How the spatial organization of proteins affects signaling is a topic of current interest, as spatiotemporal dynamics of proteins may play key roles in regulating cell signaling. In this paper, we use computational methods to examine effects of TCR and Lat clustering on early T cell signaling events using the experimental results of Lillemeier et al. as motivation. We start with a fixed amount of active ZAP-70 as a proxy for TCR stimulation and study a model in which ZAP-70 must diffuse into spatial proximity of Lat to phosphorylate it. We find that the clustering of proteins leads to a slower signaling response (as measured by the amount of phosphorylated Lat) compared with the case in which all proteins are homogeneously distributed. Analysis of the spatial distribution of proteins demonstrates that, in the homogeneous system, neighboring ZAP-70 and Lat proteins are closer on average and fewer Lat molecules share the same neighboring ZAP-70 molecule, leading to faster response times. In the Discussion section, we discuss alternative mechanisms suggested by recent experiments in which protein clusters may enhance TCR signal transduction.

2.2 Methods

2.2.1 Signaling network

The methods we use explicitly consider both spatial aspects of the membrane surface and the stochastic nature of diffusion and chemical reactions. We compare systems in which proteins are inhomogeneously distributed in clusters with systems in which key proteins are distributed homogenously. We focus on a small portion of the T cell signaling network in which a kinase (ZAP-70) searches for and modifies a target molecule (Lat) [15], while other proteins (phosphatases such as SHP-1) in the system can inactivate the kinase protein [74]:

$$\text{Lat} + \text{pZAP-70} \rightleftarrows \text{Lat} \cdot \text{pZAP-70} \rightarrow \text{pLat} \cdot \text{pZAP-70} \rightarrow \text{pLat} + \text{pZAP-70}$$
$$\text{P} + \text{pZAP-70} \rightleftarrows \text{P} \cdot \text{pZAP-70} \rightarrow \text{P} \cdot \text{ZAP-70} \rightarrow \text{P} + \text{ZAP-70}$$

Here, pZAP-70 denotes phosphorylated, active ZAP-70, which acts as a kinase of Lat, and P denotes a phosphatase that binds and dephosphorylates pZAP-70, thus abrogating its catalytic function. This generic scheme is common in cellular signaling networks, so insights gained here are likely to be relevant to other signaling networks with similar motifs. Note that in reality Lat has multiple phosphorylation sites, but we consider only a single modification in order to gain qualitative insight into the effects of clustering.

2.2.2 Computational framework

We consider discrete-space, continuous-time dynamics in which two-dimensional space is divided into a square lattice with lattice spacing 0.01 μm. The dynamics are governed

by a chemical master equation in which molecules diffuse by hopping to nearest neighbor lattice sites and proteins can react when they co-occupy the same lattice site. Typical reported diffusivities of proteins on the membrane range from 0.01 to 0.5 μm^2/sec [1,8,69]. We use our previously developed Stochastic Simulation Compiler to simulate trajectories consistent with the dynamics [75].

Recent experimental studies suggest that the radius of typical TCR and Lat clusters varies from 35 to 70 nm, and can be up to 300 nm [2,69,76]. Additionally, TCR and Lat clusters apparently do not intermix their own components (Lat and TCR molecules) and their domains do not overlap [69]. To model the clustered distribution of proteins, we consider three types of domains: TCR clusters, Lat clusters, and the remaining membrane space not occupied by the clusters (see Fig. 2-1). Since ZAP-70 is recruited to phosphorylated ITAM regions on the cytoplasmic domain of the TCR complex during early T cell signaling [13,14,15,38], we begin by assuming a fixed amount of active ZAP-70 exists in each TCR cluster and focus on the dynamics of Lat phosphorylation. The fixed amount of ZAP-70 corresponds to ZAP-70 recruited upon TCR stimulation. Thus we do not explicitly consider the dynamics of TCRs and instead focus on slightly downstream signaling reactions. Each simulation is initiated by placing clusters of fixed radius at random positions subject to the constraint that they do not overlap. The entire patch of simulated membrane is circular with a diameter of 2 μm, and reflecting boundary conditions are used. Each cluster is 0.2 μm in diameter. The system size is appropriate for a cell-cell contact region, and we have tested that increasing the system size does not change the results presented below.

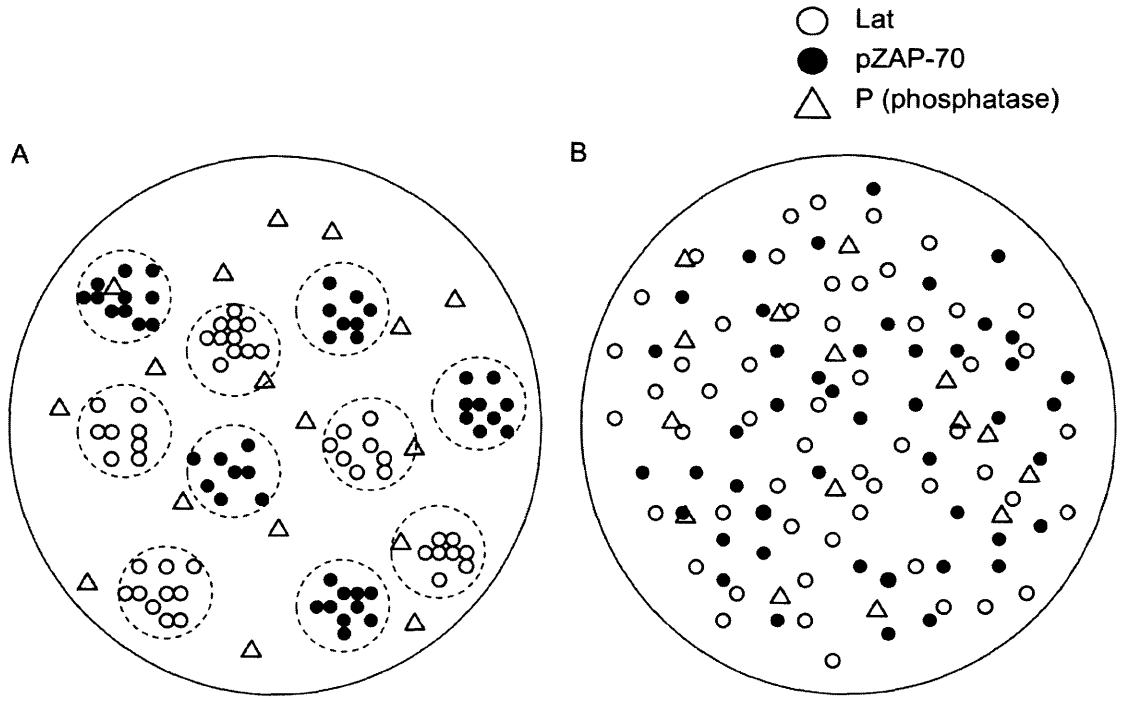

Figure 2-1. Schematic depiction of the initial distribution of proteins. (A) depicts the membrane with clustered proteins, with Lat and pZAP-70 molecules initially located in non-overlapping clusters. Lat molecules are confined to diffuse only within their initial cluster domain, while ZAP-70 molecules can diffuse anywhere on the membrane. **(B)** depicts the homogeneously distributed system, with Lat and pZAP-70 molecules homogeneously distributed initially. In both cases, phosphatase molecules that can deactivate pZAP-70 can diffuse through all domains and are homogeneously distributed initially.

For each trajectory, we place a fixed number of ZAP-70 uniformly at random in each TCR cluster and a fixed number of Lat at random in each Lat cluster. Phosphatases are placed uniformly at random over the entire membrane, irrespective of the domain, and are meant to be representative of membrane-proximal cytosolic phosphatases such as SHP-1. Each protein diffuses with a fixed diffusion coefficient, with Lat molecules restricted to diffuse within their initial cluster domain. ZAP-70 and phosphatases can diffuse throughout any domain. In the homogeneous system, there are no cluster domains and all proteins are placed uniformly at random over the entire membrane. For

comparison, for each set of conditions with clustered proteins, we consider the homogeneous case with the same number of molecules. The only difference is the initial configuration and the fact that Lat can diffuse anywhere in the homogeneous system. Unless noted otherwise, all simulations are performed using a diffusion coefficient of D = 0.0033 $\mu m^2/s$.

In the system with clustered proteins, we place twenty Lat molecules per cluster and vary the concentration of ZAP-70 molecules per TCR cluster. It is not clear whether stronger antigenic peptides induce higher concentrations ZAP-70 per cluster. The typical number used was 20 ZAP-70 per cluster. In addition, since the membrane is two-dimensional, kinetic rate constants are converted to appropriate two-dimensional units (see SI). For every set of conditions and parameters, we generate 500 independent trajectories, which we use to determine the mean and standard deviation of the number of pLat molecules as a function of time. For cases in which proteins are homogeneously distributed, each trajectory is initiated from a random configuration of proteins. For cases in which proteins are clustered, we first generate 20 different random configurations of clusters. For each configuration, we then run 25 independent trajectories in which proteins are initially placed at random positions within their clusters.

2.3 Results

2.3.1 Pre-existing clusters suppress the phosphorylation of Lat.

Intuiting the influence of clusters on the speed and magnitude of downstream signaling is difficult. For example, it is possible that the system with clustered proteins might enhance

downstream signals due to the high local concentration of Lat molecules in clusters. Once a few active ZAP-70 molecules enter Lat clusters, they might be able to quickly phosphorylate many Lat molecules through the serial engagement of Lat within the cluster.

We begin by investigating the time required for ZAP-70 molecules to phosphorylate the Lat molecules in the absence of phosphatase. Figure 2-2 shows that in the homogeneous system, it takes less time to reach a given amount of phosphorylated Lat than in the case with clustered proteins. Hence, in the absence of phosphatase, the system with homogeneously distributed proteins has a faster response than the system with clustered proteins. We explore the physical reasons for this difference in the next section.

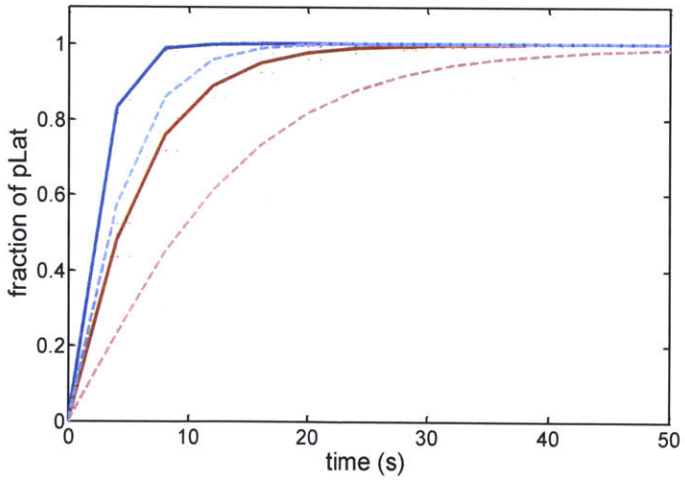

Figure 2-2. Fraction of phosphorylated Lat as a function of time without phosphatase. The fraction of phosphorylated Lat (pLat) measures the ratio of the number of phosphorylated Lat molecules to the total number of Lat molecules. Solid lines (dark) correspond to the homogeneous system and dashed lines (lighter) correspond to the system with clustered proteins. Dashed red curves have 5 ZAP-70 and 5 Lat clusters, and dashed blue curves have 20 ZAP-70 and 20 Lat clusters. Each cluster initially contains 20 proteins. The homogeneous systems have the same number of molecules but in a homogeneous initial configuration.

When we include phosphatase proteins in the system, pZAP-70 molecules can be deactivated by the phosphatase. Since we start with a fixed number of pZAP-70 molecules, it is possible for all of the pZAP-70 to be deactivated before they phosphorylate all of the Lat proteins. Figure 2-3 compares signaling responses of systems with homogeneous and clustered proteins in the presence of phosphatase, for various numbers of clusters and various amounts of ZAP-70 per cluster. Figure 2-4 compares the number of pLat at steady state in the homogeneous system and the system with clustered proteins for a variety of conditions, including varied cluster size and varied number of pZAP-70 per cluster. For all conditions, the homogeneous system produces larger amounts of phosphorylated Lat on average than system with the same number of clustered proteins. Hence, in our simulation model, pre-existing clusters on the membrane suppress the signaling output (as measured by pLat), given a fixed amount of pZAP-70 as input. It is known that Lat dephosphorylation can occur on similar timescales to those appearing in Figs. 2-2 and 2-3 [77]. Figure S2-5 presents simulation results showing that explicitly considering phosphatases of Lat does not change the qualitative results: Protein clustering suppresses the magnitude of transient peaks in the number of pLat compared with homogeneously distributed proteins.

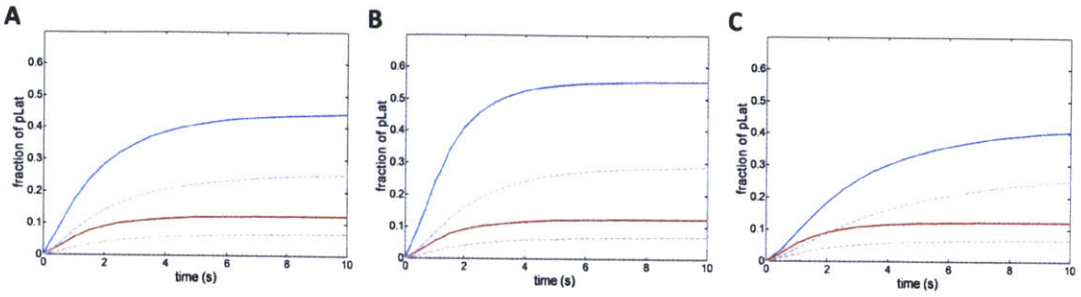

Figure 2-3. Fraction of phosphorylated Lat as a function of time with phosphatase. Solid lines correspond to the homogeneous system and dashed lines correspond to the system with clustered proteins. **(A)** The effect of increasing the number of clusters at fixed phosphatase concentration (800 phosphatase molecules per π μm^2). Dashed red curves have 5 ZAP-70 and 5 Lat clusters, and dashed blue curves have 20 ZAP-70 and 20 Lat clusters. Each cluster contains 20 molecules, with solid lines (dark) corresponding to the equivalent homogeneously distributed initial conditions. **(B)** The effect of increasing the initial concentration of active ZAP-70. The results are shown for 5 ZAP-70 and 5 Lat clusters. Blue curves have 100 pZAP-70 per cluster, red curves have 20 pZAP-70 per cluster, and the concentration of phosphatase is 800 per π μm^2. **(C)** The effect of decreasing the concentration of phosphatase. Results are shown for 5 ZAP-70 and 5 Lat clusters, each of which contains 20 molecules. Red curves have 800 phosphatase per π μm^2 and blue curves have 200 phosphatase per π μm^2.

In the simulations, we have not accounted for the dynamics of pZAP-70 production, which could be influenced by the presence of TCR clusters. As discussed in the Introduction, the production of pZAP-70 begins with the ligation of TCRs by pMHC and involves multiple signaling molecules, including the kinase Lck. It is possible that clustering enhances the production of pZAP-70 by locally increasing the concentration of relevant signaling molecules. If this is the case and TCR clustering leads to larger numbers of pZAP-70 compared with an equivalent homogeneously distributed system, then the system with clustered proteins could lead to higher levels of downstream signaling. For example, in Fig. 2-3C, if each cluster starts with 100 pZAP-70, the system with clustered proteins results in higher amounts of pLat than the homogeneous case with 5 times fewer pZAP-70 molecules. Note that starting with 100 pZAP-70 per cluster is a

physiologically unlikely number, given that TCR clusters on resting cells contain on order of 10 to 20 TCR molecules. As we discuss in the Discussion section, clustering of TCR and Lat on the cell surface may be a means for the T cell to suppress spurious triggering caused by small amounts of transiently produced ZAP-70 in the absence of antigenic peptides.

2.3.2 Analysis of the effects of the initial molecule distribution.

Our simulation results indicate that given a fixed amount of active ZAP-70, a system with homogeneously distributed proteins responds faster on average than a system with clustered proteins. Additionally, in the presence of phosphatases, the homogenous system produces a larger amount of phosphorylated Lat at long times, implying that the magnitude of the response is larger in the homogeneous case. By independently varying the initial concentration of active ZAP-70 and phosphatases, we consistently find that the homogenous system produces a faster response and a greater fraction of phosphorylated Lat at long times (see SI for additional results). In this section, we first explore features of the short-time dynamics by using scaling analysis to determine the characteristic time associated with the nearest ZAP-70 molecule diffusing into contact with a generic Lat molecule. We then compute numerically the average distance from a Lat molecule to the k^{th} nearest pZAP-70 molecule and investigate how many Lat share the same nearest neighbor. We are interested in how differences in the initial distribution of proteins lead to differences in signaling output.

We begin by considering a specific Lat molecule and estimate the characteristic distance to the nearest ZAP-70 molecule. From this we can obtain a characteristic time

for the two molecules to diffuse into contact and compare the effects of the distribution of molecules on the time for the two to first meet. In the system with homogeneously distributed molecules, the ZAP-70 molecules are distributed uniformly at random, and the average distance from a Lat molecule to the nearest ZAP-70 molecule is well-approximated by

$$d_h = \frac{1}{2\sqrt{\rho_z}}$$

where ρ_z is the concentration of ZAP-70 molecules and d_h is given by the first moment of the spatial Poisson process of density ρ_z in continuous space. The expected time for the two molecules to diffuse this distance, with D_{tot} the sum of the individual diffusion coefficients, is

$$\tau_h \sim d_h^2 / D_{tot}$$

In the system with clustered proteins, the concentration of ZAP-70 clusters is $\rho_c = \rho_z/n_z$, where n_z denotes the number of ZAP-70 molecules per cluster. Hence, the expected distance from the edge of a Lat cluster to the edge of a ZAP-70 cluster is

$$d_c = \frac{1}{2\sqrt{\rho_c}} - 2r_c$$

where r_c denotes the radius of a cluster. Thus, the expected time for a ZAP-70 molecule to diffuse into contact with a Lat molecule scales as $\rho_c \sim d_c^2/D$, plus corrections due to the molecules not being at the edge of the cluster on average (these corrections are typically small compared with ρ_c). Note that the diffusion coefficient used here is solely that of the ZAP-70 molecule, since Lat remains confined in its cluster. By comparing ρ_c and ρ_h, we find that the homogeneous system is characterized by a shorter expected time for the first encounter when the number of clusters is sufficiently small. For example, with 5 TCR

and 5 Lat clusters, each containing 20 molecules, the expected first encounter time is an order of magnitude faster in the homogeneously distributed system. As the number of clusters increases, the difference between ρ_c with ρ_h becomes smaller, suggesting the need for more detailed analysis and leading us to address the distribution of distances from a Lat molecule to ZAP-70 molecules numerically.

We begin by computing the average distance from a Lat molecule to the k^{th} nearest ZAP-70 molecule for various initial conditions. Figure 2-5 demonstrates that reactants are farther apart on average when all molecules are confined to clusters compared with cases in which at least one of the species is homogeneously distributed. As suggested above, it follows that the average time for reactants to first diffuse into contact is larger in the system in which proteins are clustered. In Fig. S2-8, we present simulation results for a typical system and plot the cumulative probability, as a function of time, that a single pZAP-70 molecule has bound a Lat molecule.

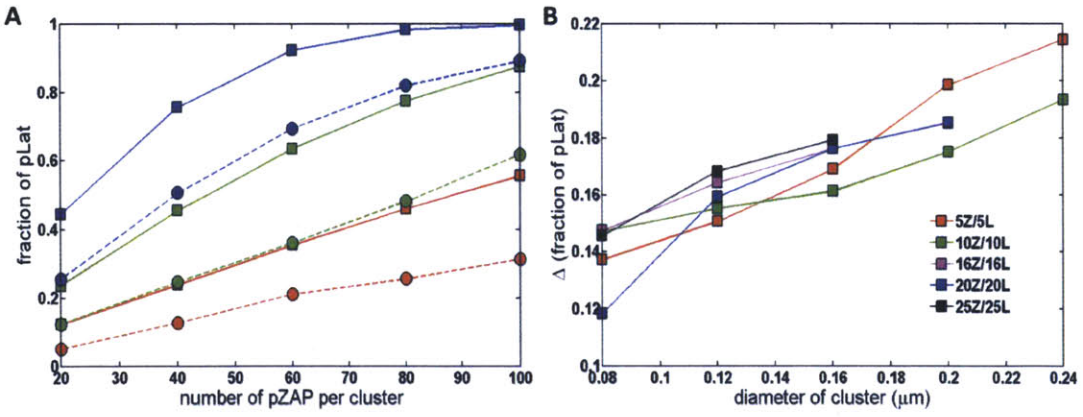

Figure 2-4. Steady state fraction of pLat for various conditions. Each system contains 800 phosphatases of pZAP-70. We obtain the fraction of pLat over 60 different configurations of clusters with 25 trajectories for each configuration. The homogenous system produces larger quantities of pLat at all conditions. **(A)** compares the steady state fraction of pLat for various numbers of pZAP-70 per cluster. In the system with clustered proteins, 20 Lat molecules and a variable number of pZAP-70 molecules are initially located inside each cluster. Solid curves with

squares and dashed curves with circles represent the homogenous systems and the cluster systems, respectively. Colors correspond to the following conditions: 20 ZAP-70 and 20 Lat clusters (blue), 10 ZAP-70 and 10 Lat clusters (green), 5 ZAP-70 and 5 Lat clusters (red). **(B)** shows the difference between the fraction of pLat in the homogenous system and the fraction of pLat in the cluster system for various diameters of clusters. Each system contains 400 Lat, and 400 pZAP-70 molecules. "5Z/5L" stands for the cluster system that contains 5 pZAP-70 and 5 Lat clusters, each of which initially contains 80 molecules.

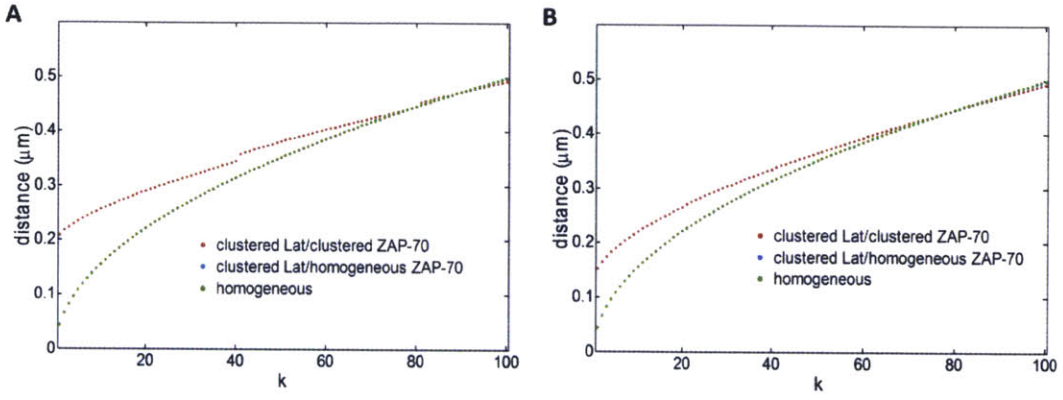

Figure 2-5. The mean distance from a Lat molecule to the k^{th} nearest pZAP-70. Results are averaged over 1000 initial configurations. Note that in both figures, blue and green data points are nearly indistinguishable. **(A)** Results for 10 Lat clusters, each of which contains 40 molecules (400 Lat molecules are distributed homogeneously in the green results). There are 400 pZAP-70 molecules, either homogeneously distributed or distributed into 10 clusters. **(B)** Results for 20 Lat clusters, each of which contains 20 molecules. There are 400 pZAP-70 molecules, either homogeneously distributed or distributed into 20 clusters. To avoid edge effects, numerical results were obtained by considering only Lat molecules near the center of the system.

As can be seen from results in Figs. 2-3 and 2-4, for a fixed number of phosphatases, the magnitude of the signaling response is smaller in the system with clustered proteins than in the homogeneous system. In order to phosphorylate a Lat molecule, an active ZAP-70 must not be dephosphorylated by a phosphatase before it encounters the Lat molecule. Since the phosphatases are uniformly distributed, the longer a ZAP-70 molecule takes to diffuse into contact with a Lat molecule, the more likely it is to be inactivated. To first approximation, the probability that a ZAP-70 molecule is active

when encountering a Lat molecule is $(1-p_{deact})^{\lambda}$, where p_{deact} is the probability that a phosphatase deactivates a ZAP-70 molecule when they occupy the same lattice site and λ denotes the expected number of encounters between the ZAP-70 and a phosphatase before the ZAP-70 encounters a Lat molecule. Assuming the phosphatases are well mixed, λ is expected to increase linearly with time. Hence, there is a smaller probability for a ZAP-70 molecule to be active when it first encounters a Lat molecule in the case with clustered proteins since the expected time for such an encounter is longer than in the homogeneous case.

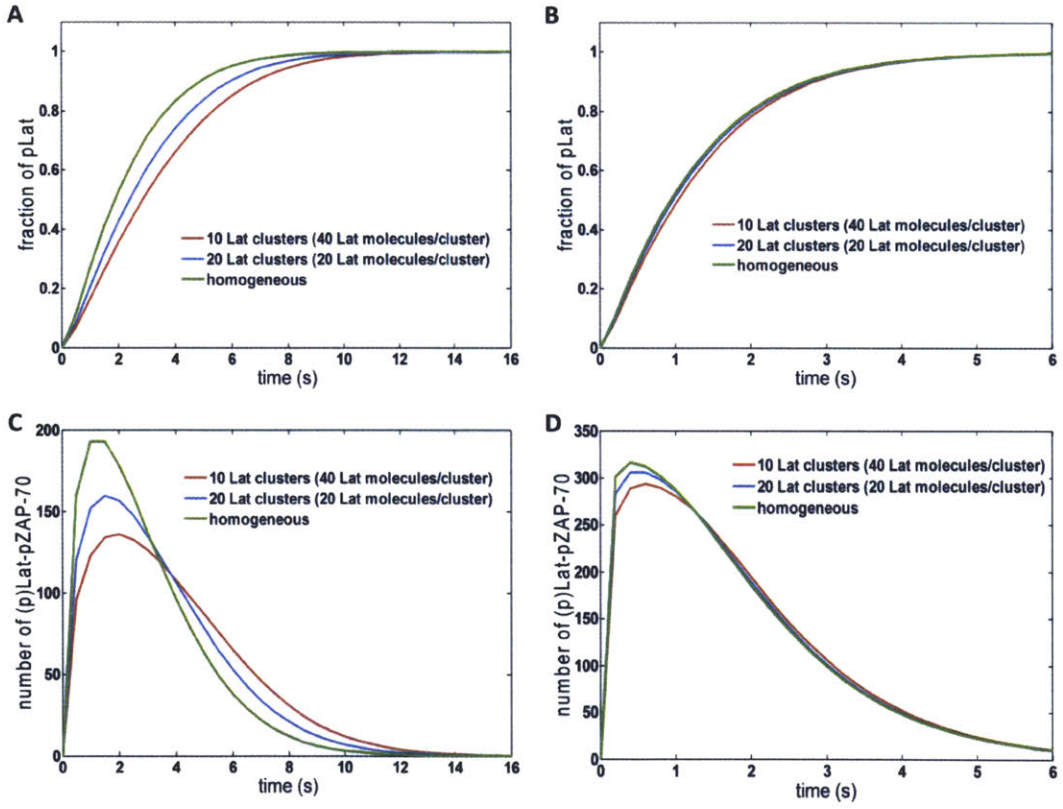

Figure 2-6. The effect of distributing a fixed number of LAT molecules in different numbers of clusters. Simulation results for 400 Lat molecules placed in 10 clusters (red), 20 clusters (blue), or homogeneously (geen). In all cases, 400 pZAP-70 molecules are homogeneously distributed initially and can diffuse through all domains. No phosphatase is present. **(A)** and **(B)** display the

fraction of pLat as a function of time for D = 0.0033 $\mu m^2/s$ and D = 0.33 $\mu m^2/s$, respectively. **(C)** and **(D)** measure the number of ZAP-70 bound to Lat as a function of time and correspond to the diffusivities of (A) and (B), respectively. The differences between the different initial configurations are more pronounced at slower diffusion rates.

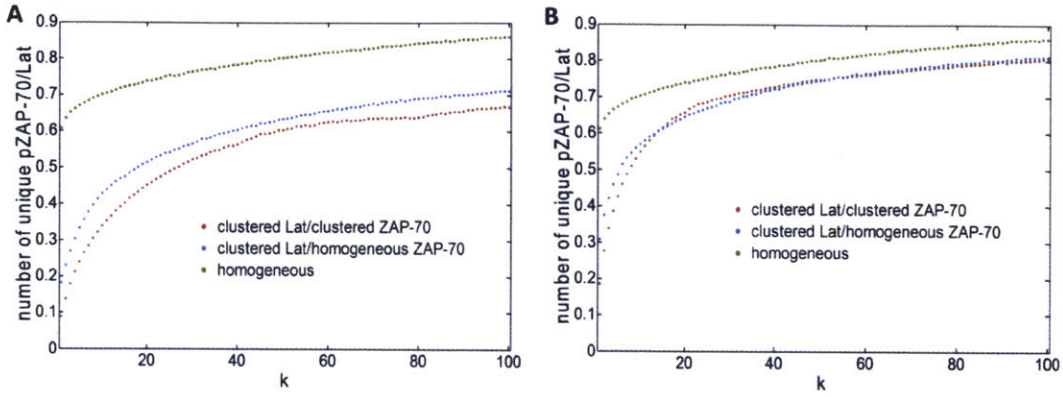

Figure 2-7. The number of unique neighboring pZAP-70 per Lat molecule. Results are averaged over 1000 initial configurations. **(A)** Results for 10 Lat clusters, each of which contains 40 molecules (400 Lat molecules are homogeneously distributed in the green results). There are 400 pZAP-70 molecules, either homogeneously distributed or distributed into 10 clusters. **(B)** Results for 20 Lat clusters, each of which contains 20 molecules. There are 400 pZAP-70 molecules, either homogeneously distributed or distributed into 20 clusters.

We further investigated how the initial distribution of proteins affects the overall signaling response when ZAP-70 molecules are homogenously distributed but Lat is clustered. In this case, the distance from a Lat molecule to the k^{th} nearest ZAP-70 is the same as in the homogenous system (see Fig. 2-5). However, at low concentrations of pZAP-70 or in systems with small clusters, few pZAP-70 are initially found within the clusters, and the time to diffuse into a cluster increases the first encounter time relative to the homogeneous case since the time for ZAP-70 to diffuse into a cluster depends only on the ZAP-70 diffusion coefficient. At sufficiently high pZAP-70 concentrations, such as those used to obtain the results in Fig. 2-6, the characteristic time to a first encounter is expected to occur on a comparable time scale to the homogenous system. Even with a

comparable time scale, we find that the overall response of this system is slower than the homogeneous system. To illustrate another physical feature that accounts for differences in the signaling response, we find the average number of unique neighboring ZAP-70 per Lat molecule. For a given initial configuration, we find the nearest ZAP-70 molecule to every Lat molecule and determine the total number of unique ZAP-70 molecules represented. This gives the number of unique neighboring ZAP-70 per Lat molecule, which provides a measure of how many Lat share the same ZAP-70 as a nearest neighbor. If the number is small, many Lat share the same nearest neighbor ZAP-70. Hence, the expected first encounter time is not representative of the characteristic time for most Lat to first encounter a ZAP-70, since the first Lat to bind the neighboring ZAP-70 will effectively sequester it and ZAP-70 from greater distances must diffuse into contact with the other Lat. In Fig. 2-7, we present the average number of unique neighboring ZAP-70 per Lat molecule, showing that it is highest in the homogeneous case. Additionally, in Fig. 2-6, it is seen that increasing the number of Lat clusters while keeping the total number of Lat and ZAP-70 fixed leads to a faster response time. Increasing the number of clusters does not change the average closest distance from a Lat molecule to a ZAP-70 molecule, but it increases the average number of distinct nearest ZAP-70 molecules per Lat molecule, as can be seen by comparing Figs. 2-7A and 2-7B. This implies that, at early times, increasing the number of clusters increases the number of encounters per unit time by increasing the number of distinct nearest ZAP-70 molecules per Lat. As is seen in Fig. 2-6, increasing the number of Lat clusters with fixed number of molecules increases the number of pZAP-70 bound to Lat and increases phosphorylated Lat production at early times. We also considered how the changes of

other parameters affect the production of pLat (see SI for further details). For example, reducing the size of clusters decreases the number of unique neighboring ZAP-70 per Lat and increases the diffusion time for pZAP-70 to enter Lat clusters, thus reducing the speed of the signaling response (see Figures S2-4, S2-7, and S2-11).

2.3.3 Analysis of hitting rate between two reactants in the membrane

Several important features can affect the generation of the downstream signal at much later times since the first encounter between active ZAP-70 and Lat molecules. For example, the number of rebinding and the duration of interaction between an active ZAP-70 molecule and a Lat molecule can influence the probability for the Lat to be phosphorylated by an active ZAP-70 per interaction. The effect of rebinding between reactants on the T-cell signaling was carefully examined by Govern et al. and Dushek et al. [2,78]. Both the amount of rebinding between two reactants and the duration of binding between molecules strongly depend on the association reaction rate constant between reactants and the diffusivities of molecules, while the duration of binding depends on the dissociation rate constant as well. If the concentration of reactants is not too high to cause a reactant of one species that is already bound to a reactant of another species to interact immediately with one of nearby reactants rather than the same reactant that it has previously interacted with, once it dissociates with the reactant, the total number of rebinding and the duration of interaction between reactants are the same in between the homogenous system and the cluster system. However, when the size of cluster or the diffusivity of molecules becomes smaller, or the association reaction rate constant between reactants becomes larger, the rebinding between reactants can be

enhanced. If the number of one species of reactants that modifies the state of another species of reactants is much less than that of species that is modified, the rebinding could make the cluster system induce greater downstream signals, but we need further investigation to confirm our hypothesis. However, at various sizes of clusters and concentrations of active ZAP-70 in the regime of kinetic parameters and diffusivities of molecules in our systems, the homogenous system consistently induces the greater reaction rate.

The total number of distinct Lat molecules interacted with an active ZAP-70 molecule per unit time is also important in determining the overall amount of phosphorylated Lat molecules. Wofsy et al. analyzed the effect of serial engagement of TCR by a pMHC molecule on the amount of downstream signals based on the hitting rate between them [79]. Wofsy et al. defined the hitting rate as the number of reactants of one species interacted by a reactant molecule of another species per unit time in the system, when there are only the association and dissociation reactions between reactants. Assuming that there are two species of reacting molecules such as A and B, and the concentration of B molecules is much greater than that of A, thus minimizing the competition among A molecules for binding to a B molecule, Wofsy et al. approximated the hitting rate as the inverse of the sum of time scales of the association and dissociation between reactants, which will be described in detail in this section.

As we have already discussed, the cluster system with initially homogenously distributed active ZAP-70 does not induce a greater reaction rate with Lat molecules than the homogenous system. We found that the greater number of unique ZAP-70 per Lat at any k^{th} nearest distances in the homogenous system can result in the greater reaction rate

in the homogenous system at early time of reactions. In the steady-state system with the simple reaction that only considers the association and dissociation between reactants and with no competition among reactants of one species for binding to a reactant of another species, we explored the hitting rate between reactants in the cluster system to find whether the cluster system can induces the greater hitting rate than the homogenous system. We note that the concentration of one species of reactants such as unphosphorylated Lat in our system changes over time. Therefore, the hitting rate comparison might be useful for the cases when the rate of phosphorylation of Lat is much smaller than the dissociation rate constant in the presence of small concentration of active ZAP-70 molecules compared to that of Lat, which could be seen at the early time of reaction. In addition, the hitting rate analysis can be useful for exploring the effect of configuration on the generation of fully phosphorylated ITAM led by the interactions between pMHC and TCR molecules because pMHC molecules can continually interact with TCR independently of whether ITAM of TCR is modified or not.

When A is bound to B, there can be multiple rebindings between them before an A molecule completely dissociates and diffuses away from a reaction volume. The following simple reaction describes the event of binding and unbinding of A to B molecules.

$$A + B \underset{k_{off,eff}}{\overset{k_{on,eff}}{\rightleftarrows}} A - B$$

The rate constants for the association and dissociation between A and B molecules denoted by $k_{on,eff}$ and $k_{off,eff}$ may depend on both diffusivities of molecules and intrinsic k_{on} and k_{off} values, such as the following.

$$A + B \underset{k_-}{\overset{k_+}{\rightleftarrows}} A \cdots B \underset{k_{off}}{\overset{k_{on}}{\rightleftarrows}} A - B$$

In the above reactions, there are intermediate steps before an A molecule is completely bound to a B molecule. The first event of the association between A and B molecules is diffusion of A molecule into the reaction volume of B molecule. The rate of diffusion of A into the reaction radius from B, or simply the diffusion rate constant, is denoted by k_+. When A and B molecules are in a reaction radius, as described in the intermediate state in the above reaction scheme, A and B molecules can either diffuse away with a diffusion rate constant, k_-, or react with an intrinsic association rate constant, k_{on}. Once A and B are bound, they will dissociate with an intrinsic dissociation rate constant, k_{off}. The above reaction scheme was examined by many scientists to find the analytical description of effective rate constants for the association ($k_{on,eff}$) and dissociation ($k_{off,eff}$) between reactants in terms of diffusivity and intrinsic reaction rate constants, hoping to reduce the partial differential equations to the rather simple ordinary differential equations. The earliest works on the effective rate constant at steady state were done by George Bell; Goldstein et al.; Berg and Purcell; Shoup and Szabo; and Lauffenburger and Linderman, while work on the effective rate constant at non-steady state was done by Torney and McConnell [80,81,82,83,84,85]. Bell suggested that each

effective reaction rate constant can be related to each elementary rate constant as followings [80].

$$k_{on.eff} = \frac{k_+ k_{on}}{k_- + k_{on}}$$
$$k_{off.eff} = \frac{k_- k_{off}}{k_- + k_{on}} \qquad 2.4$$

For three dimensional interaction between reactants,

$$k_+ = 4\pi (D_A + D_B) s$$
$$k_- = 3(D_A + D_B) s^{-2} \qquad 2.5$$

where D_A and D_B are diffusivities of A and B molecules, respectively, and s is a reaction radius between two reactants. For two-dimensional interaction on the membrane,

$$k_+ = 2\pi (D_A + D_B)$$
$$k_- = 2(D_A + D_B) s^{-2} \qquad 2.6$$

Shoup and Szabo have derived the analytical form of effective rate constants for interaction between ligands in a solution and receptors on the membrane. Lauffenburger and Linderman derived their own form based on a similar method that Shoup and Szabo developed. Lauffenburger and Linderman found each effective rate constant for the interaction between reactants in two-dimensional membranes as the following.

$$
\begin{aligned}
k_{on,eff} &= \gamma k_{on} \\
k_{off,eff} &= (1-\gamma) k_{off} \\
\gamma &= \frac{k_{on}}{k_{on} + k_{+}} \\
k_{+} &= \frac{2\pi (D_A + D_B)}{\ln(b/s)}
\end{aligned}
\qquad 2.7
$$

The above solution basically has the same form of the capture probability, γ, that Shoup and Szabo suggested for their solution. The diffusion rate constant k_+ depends on not only diffusivity, but also reaction radius s and one-half mean distance between B molecules, which is denoted by b $\left(\approx (\pi[B])^{-1/2}\right)$, which depends on the concentration of B molecules, [B].

$$
A + B \underset{k_{off,eff}}{\overset{k_{on,eff}}{\rightleftarrows}} A - B
$$

The hitting rate in the homogeneous system for the above simple reaction scheme for the two-dimensional interactions can be obtained by calculating one period time for complete association ($\tau_{association}$) and dissociation ($\tau_{dissociation}$) between two reactants, A and B:

$$
H \approx \frac{1}{\tau_{association} + \tau_{dissociation}} \qquad 2.8
$$

The above hitting rate is valid for the case in which $[B]_h \gg [A]_h$, so that there exists minimal competition among A molecules to interact with the same B molecule. Then, the hitting rate between A and B molecules in the membrane after implementing the analytical forms of two dimensional diffusion rate constants suggested by Bell can be found as

$$H_h \approx \frac{1}{\frac{1}{k_{on,eff}[B]_h} + \frac{1}{k_{off,eff}}} = \frac{2\pi(D_A + D_B)k_{on}k_{off}[B]_h}{(2\pi(D_A + D_B) + k_{on})(k_{off} + k_{on}[B]_h)}$$
$$= \frac{k_{on}[B]_h}{\left(1 + \frac{k_{on}}{2\pi(D_A + D_B)}\right)(1 + K[B]_h)} \qquad 2.9$$

From the above form, we notice that the hitting rate H_h inversely correlates with the number of rebinding, $\frac{k_{on}}{2\pi(D_A + D_B)}$, which implies that as the number of rebindings of A to a given B molecule increases, the number of interactions between A and unique B molecules per unit time decreases. The probability for rebinding can be significantly reduced as the relative magnitude of the sum of diffusivities of A and B molecules becomes much greater than the association rate constant between reactants. For the asymptotic limit to a well-mixed system, H_h approaches that of Wofsy et al.:

$$H_h(D \to \infty) \approx \frac{k_{on}[B]_h}{(1 + K[B]_h)} = k_{on}[B]_h\left(\frac{\tau_{on}}{\tau_{on} + \tau_{off}}\right) \qquad 2.10$$

If the value of dissociation rate constant increases infinitely, the hitting rate is limited by the time required for the association and the number of rebinding between two reactants. However, when the concentration of B molecules becomes very large, the hitting rate only depends on the effective duration of binding.

$$H_h\left(k_{off} \to \infty\right) = \frac{k_{on}\left[B\right]_h}{\left(1 + \frac{k_{on}}{2\pi\left(D_A + D_B\right)}\right)} \tag{2.11}$$

$$H_h\left(\left[B\right]_h \to \infty\right) = \frac{k_{off}}{\left(1 + \frac{k_{on}}{2\pi\left(D_A + D_B\right)}\right)} = \frac{\ln(2)}{\left(t_{1/2} + \frac{\ln(2)K}{2\pi\left(D_A + D_B\right)}\right)} \tag{2.12}$$

$$H_h\left(k_{on} \to \infty\right) = 0 \tag{2.13}$$

To calculate the hitting rate in our cluster system, we discretized the system into subdomains, each of which consists of one A molecule and one B cluster that confines B molecules (see Fig. 2-8). Therefore, we are examining the specific case where there exists no competition among A molecules for binding to the same B molecule. We then compared the hitting rate between reactants in this cluster system with the homogenous system that contains the same amount of A and B molecules.

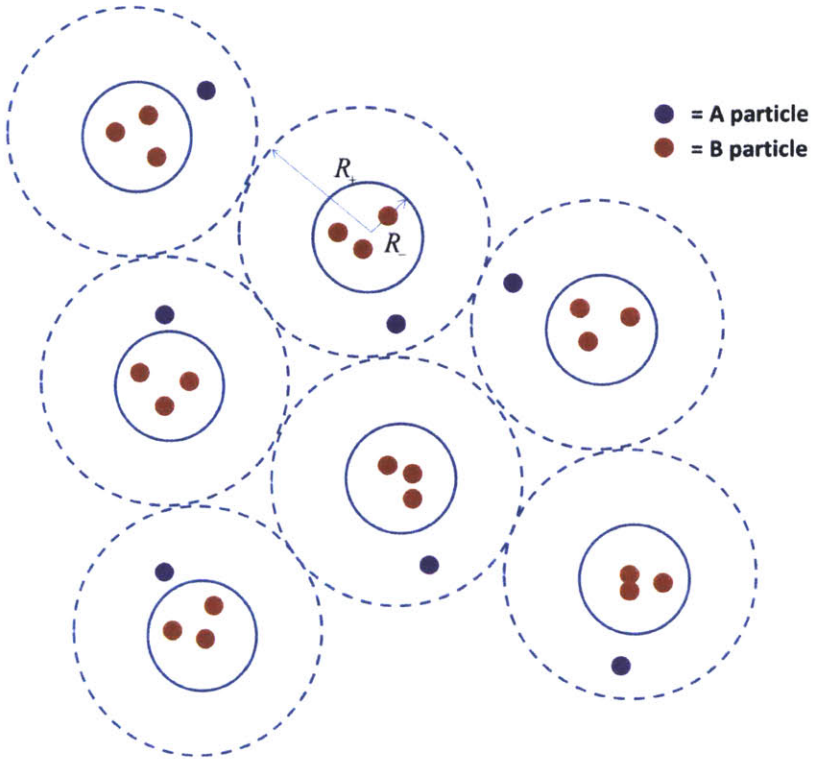

Figure 2-8. The system with clustered proteins. The membrane system is discretized into subdomains, each of which consists of one A molecule and one cluster that confines B molecules.

The one subdomain that contains one cluster is our elementary system is our focus in order to calculate the hitting rate in the cluster system. As can be seen in Fig. 2-9, we denote the radius of the subdomain by R_+ and the radius of the cluster by R_-.

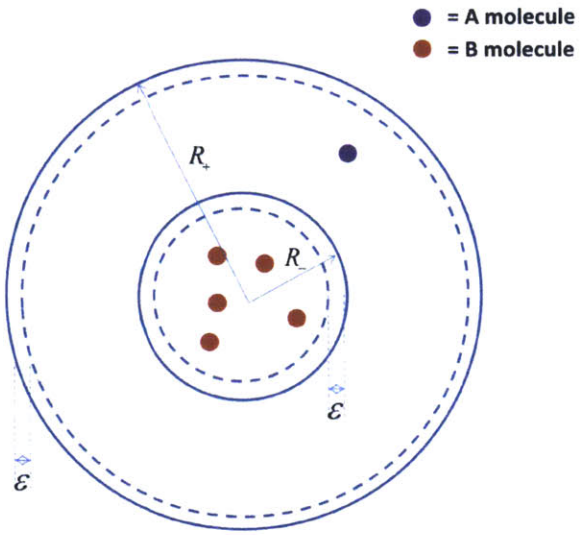

Figure 2-9. The diagram of one subdomain. This elementary system contains one A molecule and one cluster that confines B molecules.

The mean hitting rate in our cluster system is derived based on the periodic event considering that A molecule, which is initially located at the edge of the reflective boundary R_+, comes back to R_+. We can decompose the time period into two time scales: the time required for an A molecule to reach the boundary of a cluster, R_-, for the first time ($\tau_{R_+ \to R_-}$) since its diffusion from the edge of the subdomain, and the time duration for an A molecule starting diffusing from R_- until it comes back to R_+ ($\tau_{R_- \to R_+}$). During the latter fraction of the period time ($\frac{\tau_{R_- \to R_+}}{\tau_{R_+ \to R_-} + \tau_{R_- \to R_+}}$), there can be multiple crossings of A molecule over the boundary R_-. While A molecules is inside the cluster, there exists an expected number of interactions between A and B molecule, which can be approximately estimated by the product of the hitting rate and the duration of stay of A molecule in a cluster. Then the total number of interactions between A and B molecules can be

approximated by the expected number of hitting between A and B molecules per crossing of an A molecule over the boundary of a cluster multiplied by the expected number of crossing until an A molecule comes back to the boundary of the subdomain. For both the case in which the diffusivities of A, B and a complex of A and B (AB) are the same and the case in which only the diffusivity of a AB complex is zero, we obtain the following total time duration of an A molecule that spends in a cluster per period (τ_{cl}).

$$\tau_{R_+ \to R_-} = -\frac{\left(R_+^2 - R_-^2\right)}{4D} + \frac{R_+^2}{2D}\ln\left(\frac{R_+}{R_-}\right) \qquad 2.14$$

$$\tau_{R_- \to R_+} = \frac{\left(R_+^2 - R_-^2\right)}{4D} \qquad 2.15$$

$$\tau_{cl} = \frac{R_-^2}{2D}\ln\left(\frac{R_+}{R_-}\right) \qquad 2.16$$

$$D = D_A$$

With the diffusion rate constant, k_+, suggested by George Bell, we can find the expected hitting rate in the cluster system is comparable to that in the homogenous system after normalizing the concentration of B in the cluster ($[B]_c$) to the concentration of B in the homogenous system ($[B]_h$).

$$[B]_h = [B]_c \frac{R_-^2}{R_+^2} \qquad 2.17$$

$$H_c \approx H_h$$

However, implementing the analytical form of the diffusion rate constant suggested by Lauffenburger and Linderman, we obtain different results (see supporting information for Chapter 2 in appendix). We note that each analytical form of two dimensional diffusion rate constant suggested by scientists has its own assumptions and is valid for certain situations. For example, Lauffenburger and Linderman assumed that the concentration of one species of reactants at one-half the mean distance between different species of reactants is the bulk concentration of the species, and the flux of one species of reactants to the reaction radius of another species of reactants is the same as the reaction rate between reactants at the reaction radius. However, the bulk concentration of one species of reactants might be the mean concentration over the membrane rather than the concentration at the one-half the mean distance between different reactants. Nevertheless, Lauffenburger and Linderman's results capture the possible important relationship between the concentration of one species of reactants and the diffusion rate constant. For the comprehensive comparison of hitting rates between two different systems, we have to further investigate to develop analytical forms of diffusion influenced kinetic parameter. When there is no competition among A molecules for binding to the same B molecule in the cluster system as shown in Fig. 2-9, the number of unique A molecules per B molecule in the cluster system is the same as that in the homogenous system. Therefore, the hitting rate might be a dominant factor to be considered to analyze the rate of production of downstream signals in different configurations of systems at a steady state. However, when A molecules compete each other for binding to B molecules, the homogenous system induces the greater number of unique A molecules per B molecule at any k^{th} nearest distances between reactants. This implies that, at the concentration of A

molecules that causes competitions among A molecules, the greater number of unique A molecules per B molecule in the homogenous system may induce a greater reaction rate at early reaction events.

2.4 Discussion

In this paper, we investigated effects of protein clustering at the cell membrane on early signaling events in T cell activation against antigen. This was accomplished by comparing the output of a model system in which the initial distribution of proteins was either homogeneous or clustered. We focused on the phosphorylation of Lat by active ZAP-70 molecules that originate from TCR clusters, using stochastic computer simulations to study the dynamics of Lat phosphorylation. Our main finding is that the clustering of Lat and TCR suppresses signaling when active ZAP-70 must diffuse into contact with Lat.

We examined two different systems with clustered proteins, comparing their signaling response to the homogeneously distributed system. In the first, active pZAP-70 molecules originate from TCR clusters and diffuse on the membrane in search of clustered Lat molecules. We found that the characteristic time for the initial encounters between pZAP-70 and Lat is greater than in the homogenous system. Since the pZAP-70 takes longer to find Lat, in the presence of a phosphatase of ZAP-70, the chance for a pZAP-70 to phosphorylate Lat molecules is smaller in the system with clustered proteins than in the homogeneous system. This is because it is more likely that active ZAP-70 will be dephosphorylated before encountering Lat when proteins are clustered. In the second inhomogeneous system, Lat is confined to clusters, but pZAP-70 is initially distributed

homogeneously. From analysis of this system, it was found that reducing the number of Lat clusters with a fixed total number of Lat molecules resulted in slower production of phosphorylated Lat, even though the nearest neighbor distribution is identical. This highlights that the number of Lat molecules sharing the same nearest ZAP-70 molecule also plays a role in the signaling response. Overall, the fact that the homogeneous system reaches steady state faster and yields a larger signaling output (as measured by phosphorylated Lat) suggests that the clustering of proteins inhibits the phosphorylation of Lat molecules on the membrane.

Recent experimental results suggest novel signaling mechanisms that may give insight into how T cells produce large amounts of downstream signal even though protein clustering on the membrane seems to suppress such production [69,73,76]. The results of Lillemeier et al. reveal that clusters of TCR and Lat molecules appear to come closer together upon stimulation by antigen [69], while the recent findings of Williamson et al. suggest that most surface-bound Lat do not participate in T cell activation and that most Lat phosphorylated during T cell activation reside on intracellular, membrane-recruited vesicles [76,86]. Additionally, recent work by Sherman et al. suggests that TCR and Lat clusters partially overlap, leading the authors to propose that Lat is phosphorylated by ZAP-70 in or near the overlapping regions [73]. Each of these mechanisms relies on ZAP-70 and Lat being in close proximity to facilitate phosphorylation. In the first mechanism, clusters brought into close proximity would result in ZAP-70 having to diffuse shorter distances to phosphorylate Lat. Additionally, the proximity could facilitate direct interaction in which ZAP-70 bound to TCR complexes near the edge of T cell clusters could directly phosphorylate Lat molecules. In the second mechanism, the

recruitment of vesicles containing Lat molecules to the membrane could result in direct contact between TCR clusters and Lat-containing vesicles, yielding a highly concentrated local environment in which interactions between ZAP-70 and Lat are very likely. Since membrane-bound Lat are apparently not used to initiate downstream signaling in this model, it is likely beneficial for the resting T cell to keep them organized into clusters, since this decreases the chance of spurious activation by transiently-bound endogenous peptides. In each of the proposed mechanisms, it is possible that ZAP-70 can be transiently activated and unbind from the cytoplasmic region of the TCR complex. Having molecules clustered may help to suppress spurious downstream signaling events, while the mechanisms above may provide a means for cells to amplify signals when antigenic peptides are encountered by TCR.

It remains to explore other features of clusters that may influence T cell activation. As discussed previously, clustering of TCR on the cell membrane may enhance the production of pZAP-70 in response to antigenic peptides as a result of the enhancement of Lck activity within the cluster. The clustering of Lat may also enhance downstream signaling events by increasing the local concentration of various signaling proteins. One example is the production of active Ras, an important downstream signaling protein, by the protein SOS, which binds to phosphorylated Lat and activates Ras using a positive feedback loop. But, the early signaling event of Lat phosphorylation seems to be suppressed by the clustering of proteins on the T cell surface.

Chapter 3

The effects of the configurations of membrane systems and the diffusivities of molecules on the amount of steady-state levels of downstream signals such as ITAM and RasGTP, in the presence of negative regulation of the downstream signals

T-cell signaling involves modifications of the distribution and mobility of proteins. It seems that such complexity of signaling events correlates with T cells' effective detection of and response to the presence of antigenic pMHC molecules. We implemented a spatial Gillespie method [75,87,88] to examine the roles of clustered proteins in the membrane, the change of mobility of proteins, and the negative regulation of downstream signals in inducing the generation of effective signals originated from clustered TCR and Lat molecules. In this chapter, we especially focus on the negative regulation of ITAM and RasGTP. Our model suggests that, in the early stage of T cell interaction with pMHC molecules, the negative regulation of ITAM may help a T cell discriminate antigenic pMHC from endogenous pMHC molecules. Our work also suggests that the slow diffusion of proteins such as pMHC and TCR may help boost T cell activation. In addition, we show that the inhomogenous membrane system with clustered proteins may help amplify certain types of downstream signals such as phosphorylated ITAM and RasGTP and induce stable bimodality in the amount of RasGTP at equilibrium, compared to the hypothetical membrane system with homogenously distributed molecules.

3.1 Introduction

Many species of animals owe their integrity to their efficient immune systems, which recognize the invasion of pathogens and eliminates those harmful foreign bodies. One of most important cells that mediate such important immune responses is a T cell. To detect the presence of foreign bodies, the T-cell receptor (TCR) presented on the surface membrane of a T cell scans the surface of antigen-presenting cells (APC) by interacting with complexes of peptide and major histocompatibility complex (MHC) molecules (pMHC). Most MHC molecules present peptides that are derived from the organism's body, which are called endogenous peptides. The interaction with complexes of endogenous pMHC usually does not induce T cell activation, the process which modifies the functions and morphology of T cells. If a T cell falsely reacts against an APC presenting only endogenous pMHC, a harmful autoimmune response will result. However, when APC expresses a minute amount of peptides derived from a foreign body mainly as a result of endocytosis of a foreign body by APC, a T cells becomes activated by effectively reacting with these antigenic pMHC molecules. These interesting phenomena have been topics for many scientists for many years and they have suggested possible mechanisms for the way T cells could only respond to a small amount of antigenic pMHC molecules presented by APC. However, it is still hard to define the mechanism of how T cells discriminate antigenic pMHC from endogenous pMHC molecules based on the potency of the interaction between TCR and pMHC. TCR consists of 10 ITAM regions and each ITAM has two tyrosine regions, which can be phosphorylated by an Lck molecule [6]. When ITAM of CD3 ζ chain of TCR becomes phosphorylated, ZAP-70 can interact with the ITAM and become activated by Lck

[6,13,14,15]. The active ZAP-70 can initiate further downstream signals. There is an important molecule such as a coreceptor that might enhance the phosphorylation of ITAM [8]. Although CD4 may not enhance the stability of a complex of TCR and pMHC, the coreceptor might bring Lck molecules in proximity to ITAM, thus increasing chances for Lck near TCR to phosphorylated ITAM [8,12]. Otherwise, CD8 in cytotoxic T lymphocyte (CTL) can enhance the stability between TCR and pMHC and improve sensitivity [22,23,24,25]. In our paper, we propose a model that could explain how these coreceptors could play roles in helping T cells to detect a minute amount of antigenic pMHC molecules among the sea of endogenous pMHC molecules in the presence of negative regulators of ITAM.

Recent experimental results indicate that the membrane of T cells is highly organized. For example, contrary to the traditional view that the membrane has homogenously mixed proteins, as supported by the fluid mosaic model, most proteins on the membrane are clustered [39]. The discovery of these protein clusters has drawn great interest from many experimental biologists. Many of them have suggested that cytoskeletal modifications and spontaneous phase separation of membrane components into raft and non-raft phases induce the formation of protein islands [39,44,45]. Recent results by Lillemeier et al. indicate that TCRs and Lat proteins are pre-clustered as well even before T cell activation [69]. The results suggest that the average distance between neighboring TCR and Lat clusters apparently decreases upon T cell activation [69]. The roles of the spatial organization of proteins such as TCR and Lat in T-cell signaling are still open to question, but the organization may play key roles in regulating cell signaling.

We therefore use computational methods to examine effects of clustered TCR and Lat in T-cell signaling.

Lat is an important mediator for producing second messengers such as RasGTP, and deletion of it may hinder T cell activation [68]. Lat consists of multiple tyrosine sites that can be phosphorylated by active ZAP-70 molecules, which are generated from TCR. It is still not clear how ZAP-70 molecules activate Lat molecules. When Lat molecule's tyrosine becomes phosphorylated, it becomes a docking site for a specific protein. For example, PLCγ1 can interact with the tyrosine 132 of Lat, while Grb2-SOS and Gads can either interact with the tyrosine 191 or 226. Once all these three molecules interact with a Lat molecule in a certain order, they form a stable signalsome, and the dissociation rate between any of these molecules and Lat molecule significantly becomes reduced. While bound to Lat, PLCγ1 can interact with IP3 and produces DAG molecule, which can interact with RasGRP. Then, RasGRP converts RasGDP to RasGTP [17].

SOS is an especially important catalyst in producing a large amount of second messengers such as RasGTP [17]. SOS consists of an allosteric pocket and a catalytic site. The catalytic site can interact with RasGDP and converts it to RasGTP. When an allosteric site is empty, SOS is basally active in producing RasGTP. The allosteric pocket can interact with either RasGDP or RasGTP molecules, and such interaction makes SOS catalytic in converting RasGDP to RasGTP at its catalytic site. However, when the allosteric pocket is occupied by RasGTP, SOS becomes most catalytic, and this is one example of positive feedback.

RasGTP is an important signal that triggers further downstream molecules and eventually activates a T cell. Therefore, the amount of RasGTP is an important factor in

triggering T cell activation. However, at the same amount of reactants, the amount of RasGTP can be either in the lower state or higher state, mainly because of the stochastic nature of T-cell signaling [16,17]. In our paper, we discuss interesting features of the diffusivity of molecules that can influence such bimodality of T cell activation.

3.2 Results

3.2.1 Strong negative regulation of ITAM before stimulation may help a T cell discriminate antigenic pMHC from endogenous pMHC

The kinetic proofreading model suggested by McKeithan captures the important mechanism of how stronger antigenic pMHC with lower k_{off} can induce greater chances for a TCR to be fully phosphorylated [26]. However, the serial triggering hypothesis suggests that an antigenic pMHC with a stronger affinity interaction with a TCR interacts with fewer distinct TCR molecules per unit time [1,28]. The strong antigenic pMHC with very low k_{off} might cause pMHC to interact with TCR for a longer time, thus decreasing the total number of TCR molecules that can be fully phosphorylated in a given time. However, too high k_{off} would not be able to fully phosphorylate any TCR. Therefore, there could be an optimal k_{off} value that might maximize the amount of fully phosphrylated TCR. However, it is known that very strong antigenic pMHC such as a super antigen still causes T cell activation, thus casting doubt on the validity of the serial engagement hypothesis. For example, Holler et al. have shown that antigenic pMHC with a very strong affinity interaction (low k_{off}) with TCR can still trigger T cell activation [11,24].

The kinetic proofreading model does not consider the role of coreceptors and assumes the immediate dephosphorylation of ITAM upon the disassociation between TCR and pMHC. Therefore, the model may also not capture the roles of coreceptors and the strength of negative regulation, which can be controlled by the concentration of phosphatases, in the real system. There are two major types of coreceptors such as CD4 and CD8 that can interact with pMHC and TCR. As suggested by Artyomov et al., the main role of coreceptors might be enhancing the Lck recruitment, rather than stabilizing the interaction between TCR and pMHC. We implemented the same model that Artyomov et al. used, but we considered the explicit phosphatases that can randomly diffuse through all domains in the membrane.

There are several known phosphatases for phosphorylated ITAM of TCR such as PTPN4 and PTPH1 (PTPN3) [89,90]. Although PTPH1 is membrane-bound, further experiments are required to determine the topology of it. In addition, several papers suggest that CD45, SHP-1 and SHP-2 may dephosphorylate ITAM, but whether or not SHP-1 and SHP-2 are true phosphatases of ITAM is still in debate, although SHP-1 is a well known phosphatase of active ZAP-70 and is highly localized near the membrane upon the generation of active ZAP-70 [89,90,91,92]. In our model, we explicitly implemented phosphatases of ITAM that diffuse in a Brownian motion. Many models assume that spontaneous dephosphorylation happens upon the dissociation between TCR and pMHC, and dephosphorylation does not occur while TCR interacts with pMHC [2,8,26]. This is a reasonable assumption in that the interaction between pMHC and TCR might enhance the phosphorylation of TCR, which implies that a pMHC molecule bound to TCR might protect phosphorylated TCR with unknown mechanisms. Furthermore, the

phosphorylation rate of ITAM should be at least greater than the rate of dephosphoryaltion if the dephosphrylation could happen while TCR interacts with pMHC in order to generate effective downstream signals. We have loosened the assumption for the inhibition of dephosphorylation of phosphorylated TCR implement by McKeithan. For example, we assume that while a coreceptor interacts with a complex of TCR-pMHC, a phosphatase cannot interact with the ITAM. In our model, the coreceptor somewhat protects the phosphorylated ITAM from the phosphatase while it interacts with a complex of TCR-pMHC molecules mainly due to the steric hindrance. Davis et al. hypothesize that the phosphorylated TCR is likely to be protected from bulky phosphatases [66]. We did not consider the effect of cooperative enhancement of T-cell signaling by endogenous pMHC, suggested by the pseudodimer model [19,20], and autophosphorylation of Lck regulated by CD4 and CD28 [93]. The possible future work related to the pseudodimer model in the cluster system is discussed in Chapter 5. This chapter focuses on how the potency of pMHC and configuration of the system affect the downstream signals in the presence of phosphatases of ITAM.

Our reference cluster and homogenous systems consist of 30 pMHC that can have a different k_{off} from or the same one as that of the rest of the 300 endogenous pMHC molecules. If these 30 pMHC have the same k_{off} as the endogenous pMHC (20 sec^{-1}), they are endogenous pMHC, but if k_{off} of 30 pMHC molecules is lower than that of the endogenous pMHC, we denote them as the weak or strong antigenic pMHC depending on the value of k_{off}. The lifetime of a complex of TCR-pMHC, which depends on both association and dissociation rate constants, might be important in determining the overall amount of downstream signals. Because Holler et al. carefully examined the level of T

cell activation at various dissociation rate constants in order to find the correlation between the activity of CTL and the affinity between pMHC and TCR, we mainly varied k_{off} to differentiate affinity potencies. Each TCR in our model consists of one ITAM, which consists of two tyrosine residues, and assumes that only doubly phosphorylated ITAM can initiate the further downstream signals. We examined how the configuration of the system and the concentration of antigenic pMHC molecules affect the doubly phosphorylated TCR at a steady state in the presence or absence of phosphatases of ITAM.

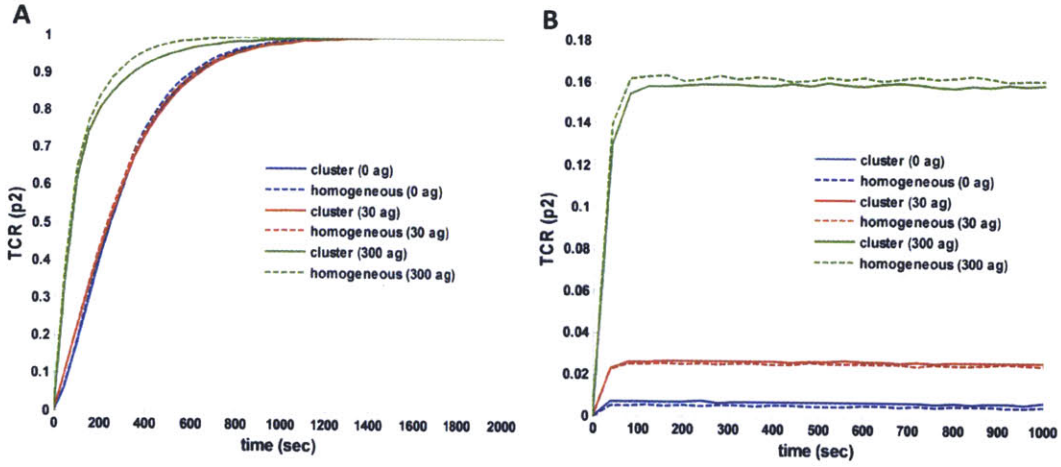

Figure 3-1. The levels of singly phosphorylated ITAM at various concentrations of antigenic pMHC. Simulation results for the cluster system in which 20 TCR molecules are placed in each of 20 TCR clusters and the homogeneous system which contains randomly distributed 400 TCR molecules. The fraction of doubly phosphorylated TCR is obtained by the number of doubly phosphorylated TCR divided by 400. Each system contains a fixed amount of pMHC molecules (330 pMHC molecules); only the number of antigenic pMHC is varied to examine the effect of the concentration of antigenic pMHC on the downstream signals. The "cluster (30 ag)" denotes the cluster system that contains 30 antigenic pMHC (k_{off}=0.02 s^{-1}) and 300 endogenous pMHC molecules (k_{off}=20 s^{-1}). The "homogeneous (30 ag)" denotes the homogenous system that is compared to the system "cluster (30 ag)." The diffusivity of molecules is 0.0033 $\mu m^2/s$. **(A)** The system with no phosphatase of ITAM. **(B)** The system with 600 phosphatases of ITAM per π μm^2.

We located different concentrations of antigenic pMHC with k_{off} of 0.02 s^{-1} by changing the ratio of antigenic pMCH to endogenous pMHC at a fixed amount of pMHC molecules, assuming that APC presents a fixed amount of pMHC molecules to a T cell. When there is no phosphatase in the systems, we observe no significant differences in the rate of production of doubly phosphorylated ITAM between the homogenous and cluster systems as shown in Fig. 3-1. We notice that the high concentration of pMHC molecules makes a short diffusion time scale for interaction between pMHC and TCR for both cluster and homogenous systems, thus making little discrepancy between the rates of production of doubly phosphorylated ITAM of the two different systems. In addition, there is no significant discrepancy between the reaction rates in the system that consists of 30 antigenic pMHC molecules and the system that consists of only endogenous pMHC molecules. Because of the small concentration of antigenic pMHC molecules, most of the phosphorylated ITAM are generated by the interaction between the endogenous pMHC and TCR molecules for the system with 30 antigenic pMHC molecules.

In the presence of a high concentration of phosphatases of ITAM (600 phosphatases of ITAM per π μm^2), we observe that a short time (around 1 minute) is required to reach the steady state. In addition, there are clear differences in the steady-state level of doubly phosphorylated ITAM between the systems with 30 antigenic pMHC molecules and those with no antigenic pMHC molecules. These interesting results suggest the importance of negative regulation in discriminating the APC presenting antigenic pMHC from APC presenting no antigenic pMHC molecules in a short time. The high concentration of phosphatases quickly remove phosphoryalted ITAM of free

TCR, thus making the system with a larger amount of antigenic pMHC molecules induce the greater amount of TCR to be protected from being dephosphorylated.

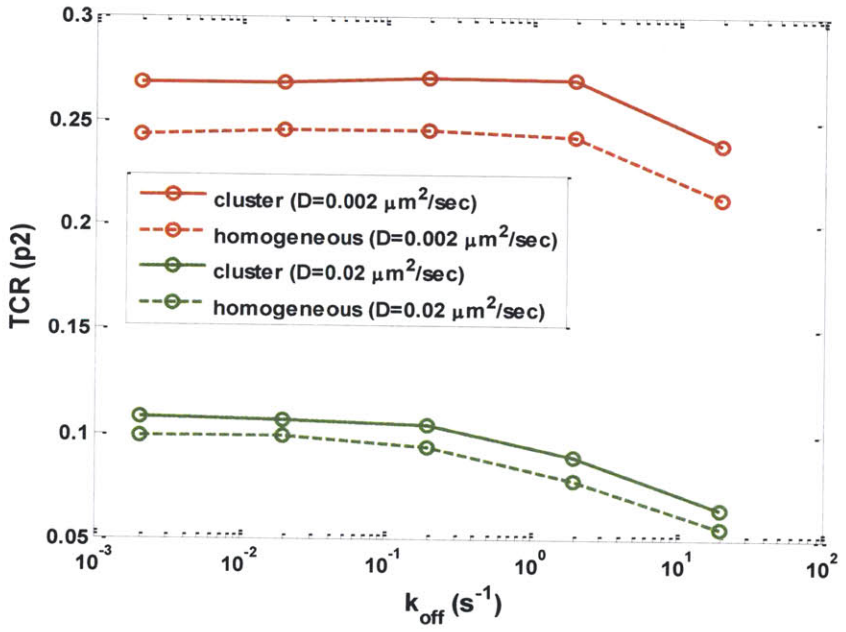

Figure 3-2. The effect of clustering of proteins, diffusivity of molecules, and potency of antigenic pMHC on the level of doubly phosphorylated ITAM at equilibrium. Simulation results for the cluster system in which 20 TCR molecules are placed in each of 20 TCR clusters and the homogenous system which contains randomly distributed 400 TCR molecules. Each system consists of 300 endogenous pMHC, 30 antigenic pMHC molecules, and 60 phosphatases of ITAM per π μm^2.

We then focused on the effect of diffusivity of molecules and the configuration of systems on the steady-state levels of doubly phosphoryalted ITAM in the presence of 60 phosphates in systems. In our system, there are 330 pMHC molecules, and we change the potencies of 30 pMHC molecules among them by varying the value of a dissociation rate constant between these 30 pMHC and TCR. As Fig. 3-2 shows, when the k_{off} value of antigenic pMHC is smaller, the amount of doubly phosphorylated ITAM increases, and

then no more significant change occurs in the amount of TCR with doubly phosphorylated ITAM although the value of k_{off} is significantly further reduced.

We could expect that there should be an optimal k_{off} that maximizes the amount of fully phosphorylated TCR as suggested by the serial engagement hypothesis. We hypothesized that because the amount of antigenic pMHC is much smaller than that of endogenous pMHC, antigenic pMHC molecules compete with large numbers of endogenous pMHC molecules for binding to TCR molecules, thus reducing the chances for antigenic pMHC molecules to serially engage with distinct TCR molecules. However, we find the most significant factor for observing no serial engagement effect is the rapid dephosphorylation of ITAM by the phosphatases at a given concentration of phosphatase (60 phosphatases per π μm^2). For example, when the concentration of phosphatase is reduced by a factor of 10, we observe the serial engagement effect (see Figures S3-12 and S3-13). Because of rapid dephosphorylation, the moderately interacting antigenic pMHC cannot trigger a larger amount of doubly phosphorylated ITAM compared to very strong antigenic pMHC as most of the phosphorylated TCR that is not bound to pMHC will be quickly dephosphorylated.

Consequently, at a given number of pMHC molecules, a greater fraction of endogenous pMHC molecules induces a lesser amount of doubly phosphorylated ITAM at equilibrium (see Figures S3-9 and S3-10). These results indicate that the downstream signal is strongly positively correlated with the amount of the antigenic pMHC because the stronger pMHC with lower k_{off} will increase the chances for full phosphorylation of ITAM and the duration of the protection of phosphorylated ITAM from phosphatases.

We also examined the effect of diffusivity of molecules on the level of fully phosphorylated TCR. We can expect if the diffusivity is lowered too much, there will be a longer diffusion time scale for any reaction between molecules, thus reducing the reaction rate between molecules. However, as we can see from Fig. 3-2, the moderate reduction of diffusivity of molecules increases the level of fully phosphorylated TCR. The reduced diffusivity of molecules lowers the hitting rate among the pMHC, TCR, and coreceptors as well as the hitting rate between phosphorylated ITAM and phosphatases. However, reduced diffusivity may enhance rebinding between molecules. Such enhanced rebinding will increase the probability of full phosphorylation of ITAM as well as dephosphorylation of any phosphorylated ITAM. As mentioned before, because of the high concentration of endogenous pMHC molecules, the serial engagement effect among antigenic pMHC molecules might not be significant. In addition, for those strong antigenic pMHCs with low k_{off}, the hitting rate with TCR will be much lower than that for those endogenous pMHC molecules, because of the longer time scale of dissociation. The low hitting rate for strong pMHC implies that the reduced diffusivity will not significantly affect the overall distinct numbers of TCR interacting with antigenic pMHC per unit time.

On the other hand, the probability of the full phosphorylation of those ITAM of TCR molecules that interact with pMHC molecules with moderate or weak k_{off} is increased significantly by the reduced diffusivity of molecules. Because of the high concentration of endogenous pMHC molecules, such increased probability of the full phosphorylation of ITAM by slower diffusion can significantly affect the total amount of downstream signals. In addition, the long diffusion time scale for the interaction between

a phosphatase and a phosphorylated ITAM due to the small concentration of phosphatases significantly further lowers the interaction rate between phosphatases and phosphorylated TCR when the diffusivity of molecules is reduced. Therefore, moderately reduced diffusivity might enhance the overall level of fully phosphorylated TCR.

To gain insight into the roles of protein islands, we compared the level of doubly phosphorylated ITAM in both the system with homogeneously distributed proteins and the system with clustered proteins. The previous chapter shows that the cluster system can induce a lower early reaction rate between two reactants when one species is confined in clusters, while another species is homogeneously distributed initially, compared to the homogenous system. Then, we notice that the reaction rates among TCR, pMHC, and coreceptors as well as reaction rate between phosphorylated ITAM and phosphatases in the cluster system are lower than those in the homogenous system. Figure 3-2 shows that the downstream signal in the cluster system is greater than that in the homogenous system. The reduction of the number of unique reactants, such as pMHC or coreceptors, per another species of reactants, such as TCR, less severely affects the overall reaction rate for the reaction among pMHC, coreceptors, and TCR, mainly due to the high concentrations of pMHC and coreceptor molecules (see Figure S3-11). However, the long diffusion time scale for the interaction between a phophatase and a phosphorylated ITAM in the cluster system results in the lower reaction rate between phosphatases and TCR molecules compared to the reaction rate in the homogenous system.

3.2.2 The diffusivity of molecules and configuration of systems affect bimodality in the amount of RasGTP at equilibrium

Experimental results indicate that clusters of phosphorylated Lat molecules are expressed on the membrane after a T cell is initially triggered by antigenic pMHC molecules [76]. As previously discussed, the phosphorylated Lat molecules can associate with SOS molecules and initiate the positive feedback loop for the rapid production of RasGTP molecules. There are also RasGAP molecules that can convert RasGTP back to RasGDP molecules. In the presence of such a positive feedback loop and negative regulation, the T cell can exhibit bimodality in the steady-state levels of RasGTP [16,17,37].

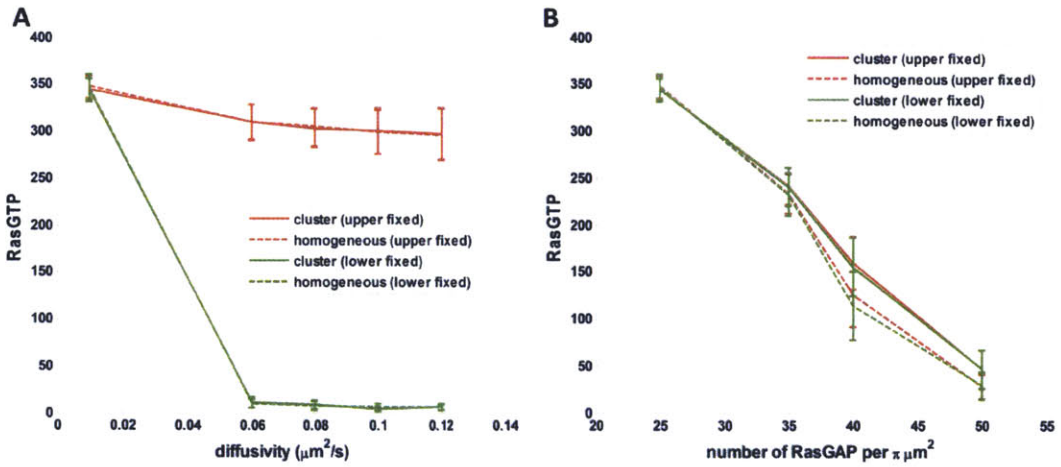

Figure 3-3. The effect of diffusivity of molecules, the concentration of RasGAP, and the configuration of systems on the level of RasGTP at equilibrium. The upper or lower fixed points are obtained by simulating the system initially containing Ras as a form of RasGTP or RasGDP, respectively. **(A)** The effect of diffusivity and configuration of the system. Each system contains 25 RasGAP molecules. **(B)** The effect of the concentration of RasGAP and configuration of the system. The diffusivity of molecules is 0.00167 $\mu m^2/s$

To examine the effect of the configurations of systems and the diffusivity of molecules on bimodality, we first examined the simple reaction network, which mainly

consists of the positive feedback reaction and the negative regulation by RasGAP (see reaction network S3-2 in appendix). Figure 3-3 (A) shows the bimodality of the system from moderate diffusivity to fast diffusivity in both cluster and homogenous systems. To obtain the upper or lower fixed points as shown in the figure, we simulated the system in which all Ras molecules are initially RasGTP or RasGDT, respectively. Therefore, based on our notations, if the upper and the lower steady states are the same, the system exhibits unimodality. We note that the bimodality in the steady-state levels of RasGTP disappears at low diffusivities of molecules. The time scale for converting RasGDP to RasGTP when the allosteric pocket of SOS is occupied by RasGTP (~25 sec) or RasGDP (~300 sec) and the time scale for the hydrolysis of RasGTP (~10 sec) are greater than the time scale for RasGTP to diffuse over the half of the mean distance between clusters (~1.3 sec). Therefore, the distribution of RasGTP in the cluster system might be similar to the distribution in the homogeneous system. However, as the diffusivity of molecules is reduced, we observe the disappearance of bimodality. The hitting rate between reactants for either producing RasGTP or destroying RasGTP will decrease when the diffusivity is reduced. However, we notice that the reduction of diffusivity may boost the positive feedback reaction and suppress the negative regulation reaction because the rebinding of RasGTP to the allosteric pocket of SOS is enhanced [37], as suggested by Abel et al., and the diffusion time scale for the interaction between RasGAP and RasGTP is increased upon the reduction of diffusivities of molecules.

We then examined whether the unimodality of the system exhibited at a low diffusivity of molecules can revive bimodality at a higher concentrations of RasGAP. However, we observe no bimodality, but a difference in the amounts of RasGTP between

the homogenous and cluster systems. The greater concentration of RasGAP will result in the more dramatic increase in the number of unique RasGAP per RasGTP for the homogeneous system at any given k^{th} nearest distances between reactants. In addition, mean distances between any k^{th} nearest reactants are reduced for both the homogenous and cluster systems. Therefore, most RasGTPs will more rapidly interact with RasGAP molecules once they are produced as the concentration of RasGAP increases. Therefore, most RasGTP in the cluster system will be located in or near Lat clusters at high concentrations of RasGAP and low diffusivity of Ras molecules, while the distribution of RasGTP is rather uniform in the homogenous system. Consequently, locally generated RasGTP molecules in the cluster system induce the lower reaction rate between RasGTP and RasGAP molecules.

We further developed our system to implement cooperative binding between reactants to form a signalsome on a Lat molecule. We simplified the whole reaction network for the cooperative binding between proteins as in the following paragraph (see reaction network S3-3 in Appendix).

Our model has two phosphorylated tyrosine residues on a Lat molecule. PLC-γ and GRb2-SOS molecules can independently interact with an upper and a lower tyrosine residue, respectively. When both of them are bound to tyrosine residues, they form a stable signalsome, and the dissociation rate constant for each molecule with its tyrosine residue is lower than the case when only one of them is bound to Lat. As described before, PLC-γ can cleave IP3 and produce DAG molecules, which activate RasGRP. RasGRP then converts RasGDP to RasGTP.

Depending on the concentration of RasGAP molecules, our system coupled with a cooperative binding model exhibits either bimodality or unimodality in the steady-state level of RasGTP molecules. For example, as can be seen in Fig. 3-4, when the system consists of 20 RasGAP molecules, we observe an imperfect bimodality, while the system shows only unimodality when it contains 15 RasGAP molecules (see Fig. S3-14). Simulation results shown in Fig. 3-4 indicate that the lower fixed point is stable for both the cluster and homogenous systems. However, we notice that the upper fixed point is unstable for both systems, but the homogenous system exhibits more unstable bimodality.

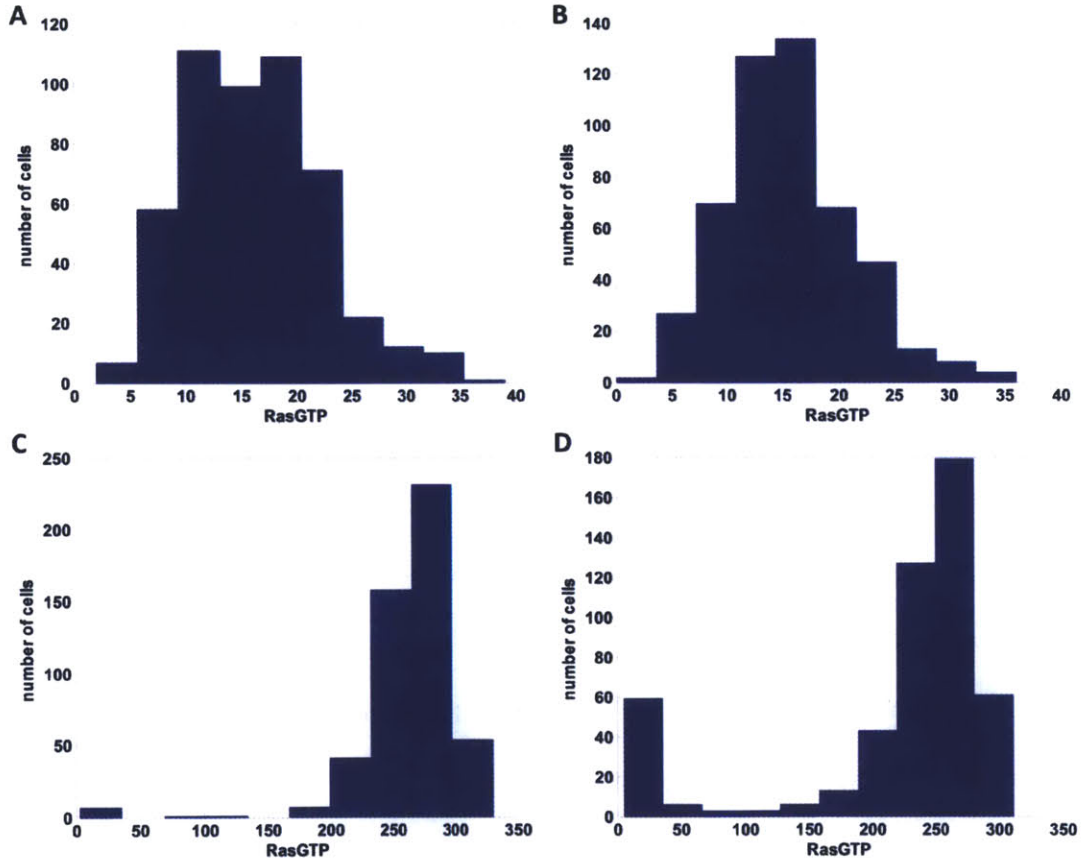

Figure 3-4. The steady-state levels of RasGTP and the number of cells containing a given steady-state level of RasGTP. The diffusivity of molecules is 0.0167 $\mu m^2/s$. Each system consists of 500 Ras and 20 RasGAP molecules per π μm^2. The total number of

cells or trajectories is 500. **(A)** The cluster system that initially consists of Ras as a form of RasGDP. **(B)** The homogenous system that initially consists of Ras as a form of RasGDP. **(C)** The cluster system that initially consists of Ras as a form of RasGTP. **(D)** The homogenous system that initially consists of Ras as a form of RasGTP.

When the membrane of a T cell initially contains Ras as a form of RasGTP, the homogenous membrane system has a higher tendency to contain a greater number of RasGDP at a steady state, compared to the cluster system, which implies that the homogenous system induces a higher transition rate from the upper fixed point to the lower fixed point. As discussed before, the cluster system may result in a lower reaction rate between reactants when there is the same amount of reactants in both the cluster and homogenous systems. Likewise, the cluster system may induce a lower reaction rate between RasGTP and RasGAP molecules, thus stabilizing the upper steady-state level of RasGTP. We also hypothesize that the cluster system may enhance rebinding of RasGTP to the allosteric pocket of the nearby SOS molecule, once it dissociates from a SOS molecule, mainly due to the close proximity between SOS molecules in a cluster.

3.3 Discussion

In this chapter, we extensively discussed how the configuration of membrane systems, diffusivity of molecules, and the negative regulation of downstream signals such as phosphorylated ITAM and RasGTP can affect the behavior of T cells. Our simulation results suggest that the cluster system may enhance the production of downstream signals at equilibrium. For example, in the presence of phosphatases of ITAM, we observed that the cluster system induces the greater amount of doubly phosphorylated ITAM. In addition, in a certain range of concentrations of RasGAP and diffusivities of molecules,

the cluster system generates greater numbers of steady-state RasGTP molecules when both systems exhibit unimodality in the level of RasGTP and results in the more stable upper fixed level of RasGTP when the systems show the bimodality in the amount of RasGTP at equilibrium.

As discussed above, the cluster system may reduce the reaction rate between downstream signals and their negative regulators. We have already shown that the cluster system can induce the slower reaction rate at early times of reaction in the second chapter. When the downstream signals are generated from the cluster system, they face a smaller number of unique negative regulators at any k^{th} nearest distances, and the diffusion time scale for the reaction between them and their negative regulators is longer than in the homogenous system. The stability of the upper steady-state level of RasGTP is greater in the cluster system mainly for two reasons: the lower reaction rate between RasGTP and RasGAP in the cluster system and the enhanced positive feedback reaction caused by rapid rebinding of RasGTP to the allosteric pocket of neighboring SOS molecule in the same cluster. The recently published paper by Mugler et al. suggests the enhanced rebinding of one species of reactants to another species of reactants which are confined in the cluster [94]. It suggests that if enzymes that can doubly phosphorylate cytosolic substrates are confined in a cluster in the membrane, then a greater fraction of doubly phosphorylated substrate is observed than in the membrane system where enzymes are randomly distributed, in the presence of cytosolic phosphatases of the substrates. Mugler et al. claim that singly phosphorylated substrate can rebind to one of the nearby enzymes in a cluster once it debinds to an enzyme and is less susceptible to phosphatases before the enzyme diffuses far from the cluster of enzymes.

We have shown that the slower diffusion of molecules surprisingly induces the greater downstream signals. The steady-state numbers of doubly phosphorylated ITAM can be increased upon reducing the diffusivity of molecules because of the increased chances of rebinding of pMHC with moderate affinity or endogenous pMHC to a TCR molecule. In addition, the increased rebinding between RasGTP and the allosteric pocket of SOS molecules can enhance the positive feedback reaction. Furthermore, the diffusion time scale for the interaction between ITAM and its phosphatase or between RasGTP and RasGAP can be significantly increased upon the decrease in the diffusivities of molecules.

Chapter 4

Stochastic error in thymic selection suggests the requirement of optimal peptide repertoire in the thymus

The thymus is an important organ that produces highly antigen specific as well as cross-reactive T cells, the orchestrators of the adaptive immune response. It achieves this by means of two major processes called negative and positive selection. These occur when naive T-cell receptors (TCR) interact with complexes comprising of endogenous peptides bound to protein products of the major histocompatibility complex (MHC) gene. Recognizing that the thymus is susceptible to stochastic errors during the selection processes, we have explored scenarios which result in the escape of autoreactive T cells, particularly those resulting from varying the types and copy numbers of endogenous peptides presented in the thymus. The results from our computational models suggest significant roles of intra-thymic diversity and concentrations of endogenous peptides as variables that mediate central tolerance in the presence of unavoidable stochastic errors from thymic selection.

4.1 Introduction

MHC proteins bind to short peptides cleaved from both antigenic and endogenous proteins, and the resulting peptide-MHC complex (pMHC) is presented on the plasma membrane of antigen-presenting cells (APCs). T cells are responsible for discriminating between self and non-self markers on APCs and mounting an immune response in case of

a genuine infection. A T cell interacts with an APC by means of the T-cell receptor molecule on its surface engaging with the pMHC complex.

TCRs are generated through stochastic rearrangement and the naive T cells bearing them migrate to the thymus to undergo selection through interaction with endogenous (or self) pMHC molecules [3,10,63,95,96]. The role of thymic selection is to detect and remove two kinds of T cells- ones that bind with high affinity to any self pMHC molecule (negative selection) and those that are unable to bind with reasonable affinity to even a single self-pMHC molecule (positive selection or death by neglect) [3,56,57,59,60]. The selection process is thought to ensure prevention of autoimmune diseases that could be caused by autoreactive T cells, and deletion of T cells that would be unable to competently detect molecular signatures of pathogens.

During positive selection, T cells that have weak interactions with all pMHCs in the thymus are removed. Therefore, positive selection results in MHC restriction, ensuring that only those T cells that can stably interact with the MHCs survive and migrate out of the thymus. On the other hand if any T cell strongly interacts with an endogenous pMHC, it can potentially react against a specific normal tissue resulting in an autoimmune response [96,97,98,99]. Negative selection eliminates such autoreactive T cells.

TCR recognition of an antigenic peptide is highly specific, but it is also degenerate [3,63]. A T cell that can recognize a particular pMHC complex usually fails to do so if point mutations are introduced in the peptide, hence specificity. Degeneracy or cross-reactivity arises from the ability of a given T cell to recognize several antigenic pMHC. This counter-intuitive dichotomy has been referred to as the specificity-

degeneracy conundrum. It was originally believed that the specificity of TCR to single point mutations in a peptide was a consequence of positive selection.

However, recent experimental work by Huseby et al. and synergistic computational investigations by Košmrlj et al. suggest that negative selection plays the dominant role in mediating specificity of TCRs [3,62,63]. The experimental results from Huseby et al. showed that a normal repertoire of peptides in the thymus produces antigen-specific T cells which are sensitive to mutations of certain amino acid sites (hot spots). However, if there are only peptides of one type (amino acid sequence) in the thymus, T cells become more tolerant to most mutations of antigenic peptides [63].

Because the free energy of interaction between a TCR and endogenous-pMHCs in the thymus is important in mediating selection, a simple model was developed by Košmrlj et al. to calculate this quantity [3]. In their model, the TCR and peptide backbones sat parallel to each other and only opposite residues on either backbone interacted with each other in a purely energetic manner.

Košmrlj et al. employed sharp thresholds for negative and positive selection to compute the survival statistics of naive T cells and to understand the characteristics of amino acid residues that populate them [3]. Implicating negative selection as the dominant mediator in shaping antigen-specific TCRs, computational results showed that these TCRs were enriched with weakly interacting amino acids. These kinds of TCRs would usually fail to recognize point mutations in antigens because each contact makes a significant contribution to the overall interaction energy and disrupting any of these leads to the abrogation of recognition. On the contrary, having only one type of peptide in the thymus produces TCRs that possess few strongly interacting amino acids in their

sequences. These T cells retain the ability to recognize point-mutated antigenic peptides with high probability because the interaction between the few strongly interacting residues on the TCR with their apposing counterparts on the pMHC dominate the overall interaction energy and point mutations on the rest do not affect recognition.

Despite the undoubted importance of the thymus in adaptive immunity, it can turn against the body by producing autoreactive T cells. Even healthy individuals can potentially have low-levels of autoreactive T cells [96,100,101]. Fortunately, these autoreactive T cells can be checked and suppressed by other immune cells, such as regulatory T cells (T_{reg}) [10,96,97,100,101]. However, if there are high concentrations of autoreactive T cells in the body, the system of checks and balances can be subverted to produce an autoimmune response. The production of autoreactive T cells in a normal individual is inevitable because of stochastic errors in thymic selection as indicated by experimental data [102]. Events such as escape of autoreactive T cells from negative selection and survival of incompetent T cells could result from molecular fluctuations during binding [61,102,103,104].

It is experimentally challenging to analyze the influence of the endogenous peptide repertoire on the generation of autoreactive T cells in vivo. Consequently, there has been no clear understanding on the effect of the numbers of types of endogenous peptides and copies of each type of endogenous peptide on autoimmunity. Therefore, we have focused on these two aspects of endogenous peptide profile in our computations.

Daniels et al. suggest that a ligand whose stimulatory potency lies between the weakest negative selector and strongest-biding positive selector peptide can itself be a negative selector or a positive selector depending on its concentration at the physiological

condition [64]. Furthermore, even weak agonists that binds stably to the respective MHC, but usually do not activate T cells in the physiological concentration in the thymus, can activate T cells at high concentrations [102,103,104]. These results indicate imperfections in the selection processes and suggest soft thresholds for negative and positive selections.

In addition, Autoimmune regulator (Aire) is known to be an important gene in enabling epithelial cells in the thymus to express antigens for certain types of peripheral tissues such as insulin and salivary protein-1 [98,101]. Mutation or deletion of Aire results in serious autoimmune diseases such as type 1 diabetes [98]. This suggests that the thymus should present a diverse set of endogenous peptides representative of most peripheral tissues in the body to avoid autoimmune reactions. In addition, each type of peptide can have several copies in the thymus enabling multiple interactions of a TCR with a given pMHC type. An investigation into the significance of these effects through a computational model could facilitate a deeper understanding of the causal relationships between the endogenous peptides repertoire and autoimmunity.

4.2 Models and methods

The work by Košmrlj et al. describe thymic selection of TCRs by a simple 'string model' that considers the free energy of interaction between the hypervariable regions of the TCR and the peptide bound to the MHC [3]. The TCR and the pMHC complexes are represented as strings of residues. The total free energy of interaction between a TCR and a pMHC takes a contribution from the interaction energy between the conserved parts of the TCR and pMHC and that between the hypervariable CD3 loop of TCR and the peptide. Although Miyazawa and Jernigan's empirical interaction potential energy

between two amino acids (MJ matrix) was used in the numerical computations, it was also shown that the qualitative results are independent of the choice of potential [3,105].

For a given number of endogenous-peptides in the thymus, we generate a panel of one million TCRs by picking amino acid residues for the hypervariable CDR3 loop of the TCR. The amino acid residues in the endogenous-peptides and the TCRs are picked according to their frequency of appearance in the human proteome. The interaction energy between the conserved CDR1 and CDR2 regions of the TCR and MHC is assigned a constant value, F_C. On the other hand, the interaction energy for a given TCR CDR3 residue t_i and its corresponding pMHC residue s_i, $F(t_i, s_i)$, is calculated based on the parameterized potential from the MJ matrix [105]. Though this is not quantitatively precise, we emphasize that our objective is to obtain qualitative mechanistic insights and not exact numerical answers.

Our interest in this study is to illustrate what kind of residues populate the selected TCRs as a consequence the thymic environment and energetic criteria through the simple TCR-pMHC interaction model we have proposed. The thymic environment is characterized by the number of endogenous peptides that the thymus presents in order to design its repertoire of self-tolerant TCR sequences that recognize antigenic peptides. Our simulations results illustrate the consequences of selecting TCRs against varying number of self-peptides in the thymus.

Following the principle of positive selection and negative selection, a given TCR is selected if its free energy of interaction is stronger than F_P with at least one endogenous peptide and is never stronger than F_N for any peptide (note that F_N and F_P are negative

values). This is a 'sharp threshold model' since the boundaries for positive and negative selections are sharply defined.

To understand the effects of the thymic environment characterized by the endogenous peptide profile on the generation of autoreactive T cells, the probability density for the survival of T cells with respect to the interaction energy has been modified in the light experimental results from Daniels et al. [64]. The results suggest using a soft threshold that resembles a half Gaussian distribution. As mentioned before, these thresholds can represent stochastic effects during association of TCR from endogenous pMHC. Therefore, in our model for the generation of autoreactive T cells, half Gaussian distributions for negative and positive selections were added to represent the stochastic error in the thymic selection processes as indicated in Fig. 4-1.

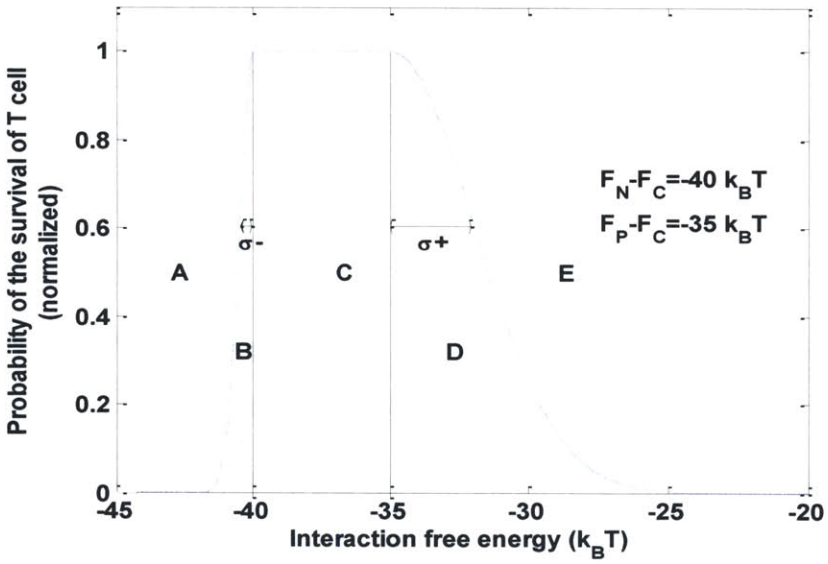

Figure 4-1 Probability of survival of T cells based on the interaction free energy. σ_- and σ_+ denote the standard deviations for the left and the right half Gaussian distributions, respectively. The negative threshold (F_N-F_C) is set to be -40 k_BT and the positive selection threshold (F_P-F_C) is set at -35 k_BT. The probability of the survival of T cells that

interact with endogenous pMHC stronger than the positive selection threshold and weaker than the negative selection threshold is normalized to unity. A, B, C, D, and E represent regions of qualitatively different reaction events. If the interaction free energy falls in region A, the T cell is negatively selected out, while in region B the T cell can still escape negative selection with a finite probability. If the T cell interacts with all of the endogenous pMHCs weaker than the positive selection threshold and all events fall into the region E, the T cell dies by neglect, but it can be positively selected if at least one interaction event falls into the region D.

Because T cell activation threshold in peripheral tissues is similar to the negative selection threshold, we assumed those T cells that have escaped the negative selection threshold can be autoreactive [102]. In our model, each interaction event involves generating a random number between zero and one and comparing it with the value of probability density at a given interaction free energy. For example, when a TCR reacts with an endogenous pMHC with an interaction free energy of -42 k_BT, a T cell has two fates; either it escapes the negative selection (event falling into the region B of Fig. 4-1) or it is simply killed (event falling into the region A of Fig. 4-1). Likewise, T cells that interact with all peptides with a free energy weaker than the positive selection threshold (F_P) can potentially still be positively selected. The σ value for the left half Gaussian (σ_-) is set to be k_BT while the σ value for the right half Gaussian (σ_+) is assigned to be 5 k_BT. The values for σ of two half Gaussians may not be quantitatively correct, but their relative magnitudes are assigned to explain the qualitative phenomena of the generation of autoreactive T cells inspired by experimental data that indicate the relatively steep threshold of negative selection and analog character of positive selection [17,64]. Daniels et al. show that upon binding to a ligand, depending on the strength of the binding, different compartmentalization of intermediates for downstream signaling pathways such as MAPK can occur in T cells, explaining the different responses of T cells to positive

and negative selectors [64]. In addition, relatively broad soft threshold for positive selection is set to explain its relatively low fidelity that can convert even weak agonist peptides to strong agonists at high concentrations.

Košmrlj et al. generated endogenous peptides and TCRs of length ten by picking out residues according to their frequency of appearance in the human or mouse proteome and investigated the statistics of interaction between the two sets [3]. Since the set of possible sequences is very large ($\sim 10^{20}$) compared to the number of randomly generated endogenous peptides in simulation, nearly all of them end up having single copies. However, each type of peptide can have several copies and the level of expression of each type is highly correlated with its binding affinity to the corresponding MHC protein. In our computations, we allow each type of endogenous peptide to have several copies to examine the effect on the number of autoreactive T cells as well as surviving T cells. However, we have neglected the correlation between endogenous peptide concentration and MHC type, which saves us from great computational cost as well as complexity derived from MHC structure. Because there is no significant correlation between the binding affinity of TCRs to endogenous peptides and the binding affinity of endogenous peptides to MHCs, it is hard to predict peptide concentration based on these parameters [103]. For simplicity, we have assumed equal numbers of copies for each type of peptide in our calculations. Although this model cannot extract the effects of MHC haplotype on the endogenous peptide repertoire, it can yield insights into how the number of copies affect the generation of autoreactive T cells based on the interaction level between a TCR and pMHC.

4.3 Results

4.3.1 The effect of number of types

We have calculated the overall free energy to explore the relation between the endogenous peptide profile and the generation of autoreactive T cells. To find the effects of the number of types of peptides on the survival of T cells as well as on the generation of autoreactive T cells, the number of types was varied at a fixed number of copies.

A few definitions are in order. The 'fraction of surviving T cells' is defined as the ratio of the number of surviving T cells to the original number of T cells made in the thymus. The 'fraction of autoreactive cells' is defined as the ratio of the number of autoreactive T cells to the number of original T cells. We performed numerical simulations to characterize the effects of positive and negative selection on the generation of autoreactive T cells. Here, a moderate value interaction free energy between the conserved regions of a TCR (CDR1 and CDR2) and a MHC (F_C) was used, as explained in Košmrlj et al. [3].

For the sharp threshold model, the survival fraction of T cells increases as the number of types of peptides increases up to a certain point and then it begins to decrease (see Fig. S4-1). This pattern can be explained as follows. As the number of types of peptides increases, so does the chance of having peptides that interact with a given T cell with energy stronger than the positive selection threshold. But there is a critical value of peptide types, beyond which the higher propensity of a given T cell to interact with some peptide with strength exceeding the negative selection threshold starts to dominate the selection statistics. The effects of negative selection overshadow positive selection

beyond this point. In conclusion, for a large number of types of peptides, the survival fraction of T cells continuously decreases as the number of types of peptides increases.

Imposing soft thresholds for negative and positive selection changes the qualitative behavior for the number of surviving T cells and autoreactive T cells as compared to the sharp threshold model. Fig. 4-2 illustrates the effect of the number of peptide types at a fixed number of copies for each type. For most our simulations, we make 1000 T cells interact with a given amount of peptides and repeat this process for several hundreds and obtain the mean values and standard deviations of fractions of surviving T cells and autoreactive T cells. We have also examined the quality of T cells in peripheral tissues by observing the percentage of autoreactive T cells that escape.

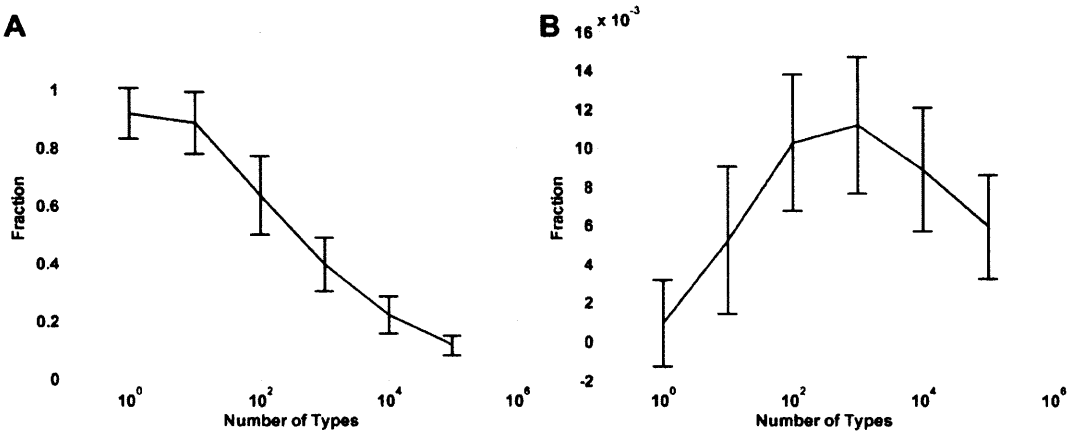

Figure 4-2 The effect of the number of types of peptides. The number of copies for each type of peptide is fixed at 100. **(A)** Fraction of surviving T cells (the number of surviving T cells/the original number of T cells made in the thymus) **(B)** Fraction of autoreactive T cells (the number of autoreative T cells/the original number of T cells made in the thymus)

We see that as the number of types of peptides increases, the number of surviving T cells decreases monotonically; the number of autoreactive T cells increases up to about

1000 types of peptides and then begins to decrease. High copy numbers and the soft threshold attenuate the effect of positive selection at low values of peptide types in contrast to the sharp threshold case ensuring that most weakly interacting T cells with interaction inside region D end up being positively selected. However, as can be expected, the effects of positive selection start to resurface at low copy numbers; the number of surviving T cells initially increases and then decreases as the number of types of peptides increases (see Fig. S4-2 A).

Negative selection continues to play a significant role in determining the fate of T cells. For a given number of original T cells, as the number of types of peptides increases, the numbers of T cells that interact with any pMHC stronger than the negative selection threshold increase, while weakly interacting T cells decrease in number. Up to a critical number of peptide types (1000 in our simulations), this causes an increase not only in the number of T cells that are negatively selected out, but also the escaping autoreactive ones owing to the soft threshold. However, as the number of peptide types increases further, the chance for strongly interacting T cells to be negatively selected out becomes much higher than the chance of escape causing the number of autoreactive T cells to decrease. On the other hand, as the larger numbers of types are generated, the number of the peptides enriched by strongly interacting amino acids increases, making both the non-autoreactive and autoreactive TCR to be enriched in weakly interacting amino acids (see Figs. S4-5, A and B) because T cells of which TCR mainly composed of strongly interacting amino acids have higher chances to be negatively selected out. As a result, increasing the number of types of peptides makes autoreactive T cells to less strongly react with endogenous as well as antigenic peptides.

The quality of T cells (1-number of autoreactive T cells/number of surviving T cells) is also important aspect to be examined. Although the number of autoreactive T cells decreases as the number of types of peptides exceeds the certain value, the number of surviving T cells decreases more sensitively. As a result, as can be seen from Fig. S4-2, the quality of peripheral T cells becomes worse as the number of types of peptides increases.

4.3.2 The effect of number of copies

Although many experiments suggest the presence of multiple copies of peptides expressed by MHCs of antigen-presenting cells (APCs) [10,106], the significance of having such properties on autoimmunity remains to be understood. As we can see from Fig. 4-3, both the number of surviving T cells as well as the number of autoreactive T cells decrease as the number of copies of each type of peptide increases. With increasing copy numbers, more reaction events can be made to occur at a particular value of the interaction free energy between a T cell and an endogenous pMHC resulting in increased sampling.

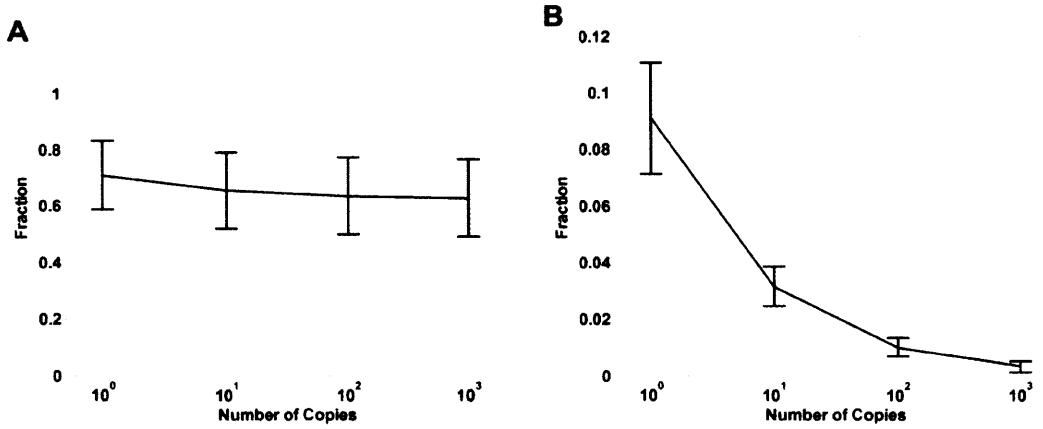

Figure 4-3 The effect of the number of copies (repeats) of each type of peptide. The number of types of peptides is fixed at 100. **(A)** Fraction of surviving T cells (the number of surviving T cells/the original number of T cells made in the thymus) **(B)** Fraction of autoreactive T cells (the number of autoreative T cells/the original number of T cells made in the thymus)

For a fixed number of types of peptides (e.g. 100), naive T cells can be classified as strongly interacting (interacting with any pMHC stronger than the negative selection threshold), moderately interacting (interacting with at least one pMHC stronger than the positive selection threshold, but interacting with all pMHCs weaker than the negative selection threshold), and weakly interacting (interacting with all pMHCs weaker than the positive selection threshold) with endogenous peptides. As the number of copies of peptides or concentration of peptides increases, the chances of weakly interacting T cells to be positively selected and strongly interacting T cells to be negatively selected out increase respectively, a phenomenon which follows from known experimental results [64,102,103].

While increasing number of weakly interacting T cells end up positively selected as peptide copy numbers increase, the magnitude of the increase is small because the total number of weakly interacting T cells is quite small at a large number of types of peptides for moderate values of F_C. Our simulations showed that amino acid frequencies of non-autoreactive TCRs do not change with varying copy numbers (see Fig. 4-3 B). Although the change of amino acid frequencies is not visible as seen from the case where only the number of types of peptides is varied at a fixed number of copies, the subtle change is observed. This happens because TCR with higher frequencies of strongly interacting amino acids have higher chances to be eliminated at a higher copy numbers in accordance with the soft threshold (see Fig. S4-6, A and C). Negative selection continues to

predominantly determine the overall number of surviving T cells. More T cells are negatively selected out and consequently fewer numbers of autoreactive T cells escape.

As the number of copies increase infinitely, any T cell interacting with an endogenous pMHC type with a free energy larger than the negative selection threshold will be negatively selected out, and the number of autoreactive T cells will be zero. As expected, the soft threshold for negative selection becomes sharp in the limit of infinite copy numbers. At an infinite number of copies the only surviving T cells are those having interaction energies less than the negative selection threshold with all peptides. This observation suggests advantages that multiple copy numbers can confer in terms of reducing the number of autoreactive T cells.

4.3.3 The effect of constraining the total number of peptides

The other possible scenario of interest is when the total number of peptides is fixed while number of types and copies are varied inversely with each other. Our simulations show that as the number of types of peptides increases for fixed total number, the number of surviving T cells and the number of autoreactive T cells continuously decreases and increase respectively (Fig. 4-4).

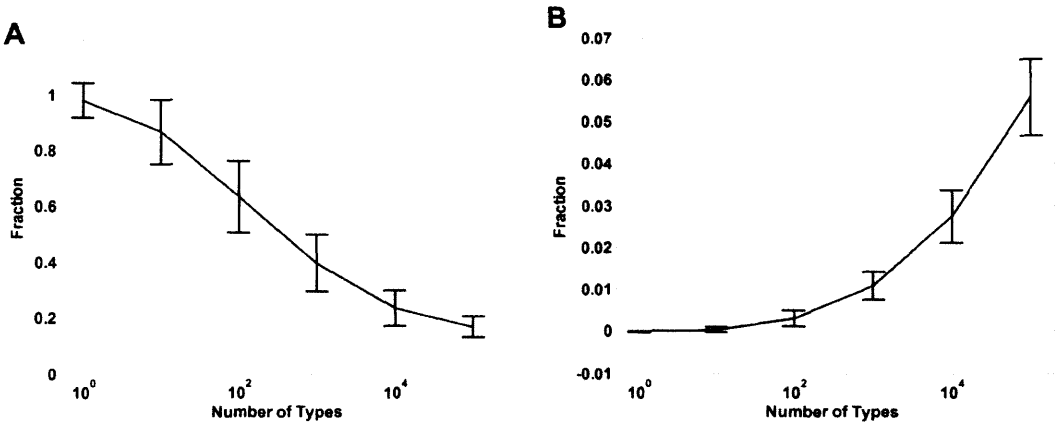

Figure 4-4 The effect of the number of types of peptide for a fixed total number of peptides. The total number of peptides is fixed at 10^4 **(A)** Fraction of surviving T cells (the number of surviving T cells/the original number of T cells made in the thymus) **(B)** Fraction of autoreactive T cells (the number of autoreative T cells/the original number of T cells made in the thymus)

As the number of types of peptides increases, the number of TCRs that interact with some peptide stronger than the negative selection threshold increases. Despite this, decreasing number of copies lowers the probability of negative selection for strongly interacting T cells since the number of reaction events decreases. This leads to the escape of a larger fraction of autoreactive T cells. Further, we observed that the frequency profiles for amino acid sequences for autoreactive and non-autoreactive TCRs are qualitatively similar to those observed in the case where the number of types of peptides is varied at a fixed number of copies (see Fig. S4-7, A and B).

The role of positive selection in determining the overall number of surviving T cells becomes less important as the number of types of peptides increases. Consider the case for total number of peptides fixed at 10^5 (see Fig. 4-4). When only one type of peptide is generated with 10^5 copies, most T cells are positively selected owing to the soft threshold for positive selection. However, when there are 10^5 peptide types with single

copies, most weakly interacting T cells fail to get positively selected. Increasing the number of peptide types also increases the fraction of T cells that get negatively selected. Interestingly though, we observe that the fraction of autoreactive T cells also increases. This is because strongly interacting T cells that would have ordinarily been negatively selected in the presence of higher copy numbers escape in this situation.

4.4 Discussion

Although thymic stromal cells present many types of endogenous peptides and many copies for each type, the significance of having such properties in the thymus, especially its implications on autoimmunity have not been investigated from a theoretical standpoint. Here we have attempted to shed light on these issues through computational analysis.

Our calculations show that as the number of types of peptides increases, the fraction of autoreactive T cells among surviving T cells increases although the absolute number of autoreactive T cells initially increases and then decreases for moderate values of F_N-F_C. The extent of autoimmunity is determined by both the quantity of autoreactive T cells produced and the quality of peripheral T cells. Minimizing the number of autoreactive T cells would require the thymus to increase or decrease the number of types of peptides from the critical value where the number of autoreactive T cells reaches a maximum (Fig. 4-2). Considering the quality of the peripheral T cells, the number of types of peptides should be small. However, as indicated by Košmrlj et al., large number of types of peptides are essential in making antigen-specific T cells which ought not to be compromised for the quality of peripheral T cells. Although the level of production of

autoreactive T cells varies over different values of F_N-F_C, the quality of peripheral T cells declines regardless of the value of F_N-F_C (see Fig. S4-8 C). My work suggests that there might be optimal number of peptides with distinct amino acid sequences presented in the thymus that maximized the number of normal T cells, while minimizing the number of autoreactive T cells.

Where large number of types of peptides increases the fraction of autoreactive T cells, increasing the copy numbers does the opposite regardless of value of F_N-F_C (see Fig. S4-9). This clearly suggests an important evolutionary role that multiple copies of endogenous peptides in the thymus play. The thymus has to thus tune the number of peptide types and copy numbers in order to design an antigen-specific robust T cell repertoire that has a low fraction of autoreactive T cells.

Constraining the total number of peptides, we observe that as the number of types of peptides increases, the number of autoreactive T cells as well as the fraction of autoreactive T cells increases. Once again, diverse peptides types are essential to make the T cells antigen specific. Our simulations reveal that larger the total number of endogenous peptides, smaller is the number of autoreactive T cells and also their fraction over the surviving T cells (see Figs. S4-4, B and C). Therefore, from an evolutionary standpoint, one would not expect the thymus to constrain the total number of peptides presented but only increase the diversity at reasonable copy numbers.

In physiological conditions, only a small fraction of naive T cells (less than one percent) end up surviving. This may be a consequence of the cumulative effect of many types of peptides as well as multiple copies of each of them presented by numerous MHCs of many alleles in the thymus. At first glance, there are huge disadvantages to

having both many types of peptides and many copies of each type in the thymus since these conditions result in the elimination of many T cells by negative selection. Nevertheless, as we have argued, such a sacrifice seems inevitable for the thymus in its ultimate goal of designing a self-tolerant but highly competent T cell repertoire.

Chapter 5

Conclusion

5.1 Summary

The recent discovery of clustered proteins provides us challenging and exciting problems in immunology. Although many scientists have struggled to find the roles and properties of these clustered proteins, they are still ambiguous. As a researcher in a computational immunology lab, I formulated the following research topic, hoping to provide insight into the roles of clustered proteins. Lillemeier at al. suggested that TCR and Lat molecules are preclustered on the membrane of T cells [69]. I hypothesized that these clustered proteins should have roles in early T-cell signaling because the formation of these clustered proteins causes entropic costs for T cells. Therefore, I focused on finding the possible benefits of having this highly organized structure for a T cell by comparing the behavior of T cells between the membrane system containing protein clusters (cluster system) and the membrane with randomly mixed proteins (homogenous system) at a given amount of signaling proteins.

I have examined whether spatial segregation between TCR and Lat molecules due to the cluster formation might affect the downstream signals differently from the homogenous membrane system. The mechanism of the correlation between the amount of active ZAP-70 generated from TCR and the potency of antigenic pMHC molecule that the TCR interacts with remain unclear. In addition, how active ZAP-70 phosphorylates Lat molecules is still unknown. However, we know that inactive ZAP-70 is recruited to TCR after ITAM becomes phosphorylated, which implies that active ZAP-70 probably

can also diffuse away from TCR. Yokosuka et al. have shown that active ZAP-70 can be located out of TCR clusters [14]. Assuming that active ZAP-70 diffuse and react with Lat molecules, my simulation results indicate that the cluster system can reduce the amount of downstream signals.

We investigated the reaction that considers the binding and unbinding between two reactants, which leads to the modification of the state of one of the reactants by another reactant. For example, in our cluster and homogenous systems, the Lat molecules interact with and become phosphorylated by active ZAP-70. In our system, we examined how the amount of downstream signals, which are singly phosphorylated Lat molecules, changes over time. In the absence of phosphatases that can dephosphorylate Lat molecules, we found that the homogenous system induces a greater reaction rate compared to the cluster system at early reaction times. In the presence of phosphatases, the steady-state level of phosphorylated Lat molecules was greater in the homogenous system.

To analyze the effect of configuration of systems on the generation of downstream signals, we first compared downstream signals generated by the homogenous system and the cluster system that confines only Lat molecules inside clusters and initially homogenously distributes active ZAP-70, which can diffuse through all domains. In this comparison, we also found that the homogenous system still induces a greater initial reaction rate between Lat and active ZAP-70. Interestingly, when we increase the number of Lat clusters at a fixed total amount of Lat molecules in the cluster systems, we observe a greater reaction rate that approaches that of the homogenous system. We notice that increasing either the number of Lat clusters or the size of clusters

makes the topology of reactants in the cluster system become more similar to that in the homogenous system. We find that increasing the number of Lat clusters does not change the distance profile between reactants, but increases the number of unique ZAP-70 per Lat molecule. Increasing the number of unique ZAP-70 per Lat can increase the initial reaction rate because of the increased number of Lat molecules interacting with the ZAP-70 molecules in a given time interval.

When the cluster system initially confines ZAP-70 molecules inside TCR clusters, the system induces a larger diffusion time scale for active ZAP-70 to encounter Lat molecules at early reaction, compared to the cluster system that initially distributes ZAP-70 molecules homogenously. As expected, our simulation results indicate that the further discrepancy between the reaction rates in the homogenous system and the cluster system that confines the ZAP-70 molecules initially inside clusters. In the presence of phosphatases, we observe the greater fraction of phosphorylated Lat at a steady state in the homogenous system compared to the cluster system. The probability of an active ZAP-70 encountering a Lat molecule for the first time exponentially reduces by the number of encounters between the active ZAP-70 and phosphatases. This number is greater in the cluster system, thus inducing the more rapid decrease in the amount of active ZAP-70 molecules in the cluster system.

We then focused on the effect of the configurations of the T-cell membranes on the detection of antigenic pMHC molecules and the bimodality of the production of RasGTP. The mechanism of how a T cell recognizes the presence of antigenic pMHC molecules has been ambiguous. McKeithan proposed the kinetic proofreading model to describe how antigenic pMHC molecule can induce a higher probability of full

phosphorylation of the TCR that the pMHC interacts with [26]. However, his model has shortcomings in explaining why stronger antigenic pMHC molecules induce the greater amount of downstream signals, because this phenomenon contradicts serial engagement hypothesis, proposed by scientists such as Valitutti et al. and Dushek et al. The serial engagement hypothesis suggests that very strong antigenic pMHC with a low dissociation rate constant with TCR, k_{off}, does not necessarily induce the stronger downstream signals in terms of the amount of fully phosphorylated TCR, compared to the moderately interacting pMHC [1,28]. Because a strong antigenic pMHC has a lower k_{off}, the total amount of unique TCR proteins that the antigenic pMHC can interact with per unit time might be lower than the amount that the weaker antigenic pMHC can interact with. Therefore, pMHC with moderate k_{off} can induce the maximal amount of fully phosphorylated TCR according to the serial engagement hypothesis. Nevertheless, Holler et al. have shown that antigenic pMHC with very strong affinity interaction with TCR can still trigger T-cell activation [11,24]. Holler et al. examined the strong affinity interaction that is out of the range of k_{off} observed in vivo and found that the strong affinity with low k_{off} actually still induces the strong response of cytotoxic T lymphocytes (CTL). Both the kinetic proofreading model and serial engagement hypothesis have their own merit in explaining the mechanism of a T cell's response to antigenic pMHC. However, each model alone insufficiently describes the experimental observation, which indicates that the stronger antigenic pMHC, with a longer lifetime of interaction with TCR, triggers the T cell more strongly [11,24].

We examined our membrane system that consists of both endogenous and antigenic pMHC molecules. The concentration of antigenic pMHC may vary among

antigen-presenting cells, but it is typically much lower than that of endogenous pMHC molecules. Our system also consists of coreceptors and phosphatases of ITAM. Our simulation results indicate that, in a certain range of kinetic parameters and concentrations of reactants, as we increase the potency of antigenic pMHC molecules by lowering k_{off}, a T cell tends to generate stronger downstream signals, the amount of which is measured by doubly phosphorylated ITAM. In other words, we did not observe the prominent peak of downstream signals at a moderate value of k_{off}. Therefore, our results qualitatively correspond to the experimental results suggested by Holler et al. We hypothesized that this phenomenon might be explained by the reduced serial engagement effect of antigenic pMHC molecules, mainly because highly concentrated endogenous pMHC molecules compete with antigenic pMHC molecules for binding to TCR. However, we have found that rapid dephosphorylation by phosphatases were the main cause of observing no optimal k_{off}. For example, when we reduced the concentration of phosphatases significantly, our system begins to show the serial engagement effect. Therefore, our system captures the significances of concentration of phosphatases in fine detection of antigen pMHC. McKeithan's simple model that assumes spontaneous rapid dephosphorylation of ITAM upon the dissociation between TCR and pMHC does not capture the effect of the concentration of phosphatases on the qualitative response of a T cell to pMHC at various affinities. Based on our results, we can hypothesize that a sufficiently strong negative regulation on the phosphorylated ITAM might be necessary for the fine detection of antigenic pMHC. However, it would be necessary to reduce the strength of negative regulation for maximizing the production of effective downstream

signals upon the stimulation of T cell. This hypothesis will be discussed in more detail with experimental data in the next section.

The effect of diffusivity of proteins as well as the configuration of systems on the steady-state level of fully phosphorylated ITAM was discussed. The reduced diffusivity of proteins interestingly increased the level of downstream signals. The decrease in the diffusivity of molecules can increase the probability of rebinding between molecules. This suggests that chances for the weakly or moderately interacting pMHC molecules with TCR to fully phosphorylate ITAM increases significantly by the reduction of diffusivity of molecules. It is obvious that too slow diffusion or no diffusion of molecules might cause a very long or infinitely long diffusion time scale for interaction between reactants, so there will be a very slow reaction rate or almost no reaction between reactants. Nevertheless, in a range of kinetic and diffusion parameters of our system, we observe the increase in the downstream signals mainly due to enhanced rebinding between molecules. In addition, our cluster system also results in a greater amount of downstream signals. As discussed before, the cluster system can cause the slower response of dephosphorylation of phosphorylated ITAM by phosphatases.

The positive feedback mediated by SOS molecules can cause the bimodality in the level of RasGTP in a T cell at a steady state in the presence of RasGAP molecules. Such bimodality might be important for T cells in optimal decision based on the incoming signals from the environment. For example, a resting T cell has a low number of RasGTP molecules at the steady state. However, when TCR interacts with antigenic pMHC molecules, the initial abrupt increase in concentrations of certain molecules such as phosphorylated Lat molecules will enable a T cell to produce a large amount of

RasGTP molecules, maintain such a level for a long time, and remain in an active state to change its morphology and function. Therefore, the bimodal decision with a given number of key proteins for T cell activation, such as Ras molecules, is crucial for proper immune responses. We extended bimodality of RasGTP to our cluster system to see how the configurations of the membrane system as well as the diffusivity of molecules affect the bimodality. We observe bimodality in the amount of steady-state level of RasGTP at moderate or fast diffusion of molecules. However, the bimodality disappears when the diffusion becomes very slow because of enhanced rebinding of RasGTP to the allosteric pocket of a SOS molecule and the very long diffusion time scale for the interaction between RasGTP and RasGAP. In addition, the cluster system enhances the bimodality more than the homogenous system. The cluster system can cause the less reaction rate between RasGTP and RasGAP and enhance the rebinding of RasGTP to an allosteric pocket of the neighboring SOS molecule in a cluster. In other words, the cluster system improves chances for RasGTP to rebind to an allosteric pocket before being hydrolyzed by RasGAP molecules.

The macroscale immune response such as thymic selection is susceptible to stochastic error. Naive T cells undergo the selection process by interacting with numerous endogenous peptides present on the epithelial and bone-marrow-derived antigen-presenting cell in the thymus [59,107]. The repertoire of the endogenous peptides present in the thymus is diverse in terms of a sequence of amino acids [3]. In addition, APC can present multiple copies of the same peptide sequence [10,106]. Through the selection process, T cells' recognition of antigenic peptides becomes diverse and specific [3]. Among two main selection processes, negative selection removes strongly interacting

T cells, thus reducing the chances of escape of autoimmune T cells. Another process called positive selection eliminates those weakly interacting T cells, which would not be able to recognize antigenic peptides. However, thymic selection might not be perfect, because even healthy people have a small number of autoreactive T cells in their peripheral tissues [96,100,101]. We implemented soft thresholds for the probability of survival of a T cell that depends on the affinity interaction between pMHC and TCR following the experimental observation of an imperfect selection process.

We examined the effect of numbers of types and copies of endogenous peptides on the generation of autoreactive T cells, survival fraction of naive T cells, hypervariable CD3 loop sequence of TCR of those T cells that have survived, and endogenous peptide sequences. From our simulation results, we found that the increase in the number of types of endogenous peptides in the thymus increases the fraction of autoreactive T cells among those T cells that have survived, while increasing the total number of autoreactive T cells up to a certain number of types of peptides and then continuously reducing it. However, such qualitative results may change depending on the negative selection threshold (see S4-8). Otherwise, the fraction of autoreactive T cells among surviving T cells, which determines the quality of T cells in the peripheral tissue, only worsens as the number of types of peptides increases. The increased number of strongly interacting endogenous peptides due to the increased number of types of peptides improves the chances for the death of strongly interacting T cells but does not change much the probability of the death of moderately interacting autoreactive T cells because of a high probability of survival near the negative selection threshold. A sufficiently large number of types of peptides is necessary to generate antigen-specific T cells, but it can result in a

worse quality of T cells in the peripheral tissue. Otherwise, the increase in the number of copies of endogenous peptides reduces the fraction of autoreactive T cells among T cells in the peripheral tissue as well as the total amount of autoreactive T cells that have escaped thymic selection. The chances for the survival of those T cells moderately interacting with peptides by interaction energy just above the negative selection threshold dramatically declines exponentially with the number of copies. This fact implies that increasing copy numbers may help improve the quality of peripheral T cells. Therefore, if there exists a limited amount of peptides that antigen-presenting cells can express in the thymus, there should be optimal numbers of types of peptides as well as numbers of copies to ensure the maximum production of antigen-specific as well as non-autoreactive T cells. To satisfy such criteria, the thymus should be equipped with a large number of endogenous peptides with a sufficiently great diversity of peptides and copies of each of them, but not too large numbers of types and copies of peptides to sacrifice most of the naive T cells.

5.2 Future Steps

5.2.1 The clustered Lat proteins may enhance the stability of signalsome on Lat and Ras nanocluster formations

We have discussed the effect of configurations of membrane system on the bimodality of the steady-state level of RasGTP, which is induced by the positive feedback loop of the production of RasGTP and the negative regulation of RasGTP by RasGAP. Our simulation results indicate that the upper steady-state level of RasGTP in the cluster

system can be more stable than that in the homogenous system. As described in the introduction, many molecules, such as PLC-γ, Gads-SLP76, and GRb2-SOS, can cooperatively interact with a Lat molecule and form a stable signalsome. It would be interesting to see whether this cooperative binding can be also enhanced more in the cluster system, thus causing a further enhanced upper fixed level of RasGTP. I hypothesize that the cluster system may enhance the effective duration of maintaining a signalsome due to rapid rebinding of molecules to phosphorylated Lat molecules in a cluster. To test this hypothesis, it would be necessary to reduce our current model to consider only the cooperative binding between PLC-γ, Gads-SLP76, and GRb2-SOS and to examine the number of signalsomes observed in both the cluster and homogenous systems. If the cluster system indeed improves chances for the proteins to form a signalsome, then we can expect the enhanced production of RasGTP through PLC-γ as well as GRb2-SOS.

The initial formation of a K-RasGTP nanocluster might happen near the SOS, which is bound to the phosphorylated Lat, because SOS is the main molecule that rapidly produces RasGTP by the positive feedback reaction. This highly probable event also implies that, if the diffusivity of Ras nanocluster is small, many Ras nanoclusters can be localized in a Lat protein island, considering the sizes of both the Ras nanocluster (~0.02 μm in diameter) and the Lat cluster (~0.2 μm). We have already discussed several possible mechanisms, supported by experiments and theoretical work, for the formation of these Ras nanoclusters. We note that these Ras nanoclusters are highly likely related to the positive feedback reaction. The positive feedback reaction mediated by the SOS molecule in the cluster system can be enhanced by these highly concentrated Ras

nanoclusters near Lat clusters. This enhancement might induce spatial positive feedback formation of Ras nanoclusters because the formation of Ras nanoclusters is positively enhanced by its own product, which is newly created Ras nanoclusters. Although we did not carefully examine Ras nanocluster formation, it would be important to investigate whether the formation of Ras nanoclusters is more prominent in the cluster system than in the homogenous system. If so, it would be interesting to explore how this enhanced formation of Ras nanoclusters can affect the stability of the system by examining the degree of bimodality in the level of RasGTP at equilibrium.

Lommerse et al. claim that the diffusivity of Ras and Lck molecules in the membrane depends on the region where they are [108]. For example, the diffusivities of these molecules become much slower when they are in lipid rafts than when they are outside lipid rafts. In addition, Murakoshi et al. suggest that the diffusivity of Ras molecules also becomes slower after T-cell activation [109]. We have already examined how diffusivity of molecules affects the bimodality of the steady-state level of RasGTP in both the cluster and homogenous systems. However, imposing non-uniform diffusivity of Ras molecules on our systems might provide an interesting insight into how the non-uniform diffusivity of molecules can affect the amount of downstream signal. I hypothesize that rapid diffusion of Ras molecules outside Lat clusters might transport RasGDP or RasGTP rapidly from outside a Lat cluster to SOS molecules bound to Lat molecules in a Lat cluster. Then, there will be no significant time delay in supplying RasGDP to catalytic sites of SOS molecules in a cluster system. In addition, the slow diffusion of Ras molecules inside a cluster could also enhance the rebinding of RasGTP molecules to allosteric pockets of SOS molecules highly localized in a Lat cluster.

5.2.2 The amplification of fully phosphorylated ITAM in a cluster system

We have discussed how a sufficiently strong negative regulation of phosphorylated ITAM can help a T cell to generate stronger downstream signals in accordance with the strength of affinity of pMHC molecules, the phenomenon which is observed in experiments. However, the increased amount of downstream signal created by stronger antigenic pMHC is not significant because the amount of antigenic pMHC presented by APC is small. The T cells might need strong signals upon stimulation by antigenic pMHC. Although our models and results suggest that strong negative regulation might be necessary in order to eliminate the unwanted high production of downstream signals by moderately interacting pMHC molecules, there might be a mechanism of how the T cell can initiate production of a large amount of downstream signals such as fully phosphorylated ITAM upon stimulation. Interestingly, SHP-1, one of the possible negative regulators of ITAM, consists of two important sites that can regulate its own activity. When Y536 of SHP-1 is phosphorylated, the phosphatase activity of SHP-1 becomes the greatest, while the phosphoryaltion of S591 inhibits its phosphatase activity. Holdorf et al. has shown that the phosphoryaltion of S591 starts to occur after the initial stimulation of human peripheral blood T cells (PBT) and maintains such inhibition of phosphatase activity strongly for 1 minute, and then the level of the inhibition declines within 10 minutes [92]. This result may suggest that the activity of phosphase is initially strong enough for a T cell to detect a threshold amount of doubly phosphorylated ITAM generated by antigenic pMHC, which is required for the initial stimulation. We do not know how a T cell can respond so sensitively to a small increase in the amount of fully phosphoryalted ITAM, considering the small amount of antigenic pMHC that can

stimulate a T cell. However, we note that the negative regulation mediated by SHP-1 is inhibited initially upon stimulation of a T cell, and this inhibition might significantly increase the amount of downstream signal induced by antigenic pMCH molecules. In conclusion, I propose two steps of initial T cell stimulation. The first step is a specific detection of antigenic pMHC, in the presence of a sufficiently strong negative regulation that is required for the elimination of spurious triggering induced by weakly or moderately interacting pMHC, and the next step is the amplification of downstream signals by the negative regulation of the activity of phosphatases.

How could a T cell amplify downstream signals even further once it responds to its interaction with antigenic pMHC, while the negative regulation is weak? The pseudodimer model suggests possible answers to this question. As described before, the model suggests that while TCR interacts with an antigenic pMHC, the activated Lck bound to the coreceptor interacting with the complex of TCR-antigenic pMHC can phosphorylate many other ITAM molecules of TCR interacting with endogenous pMHC molecules brought to the coreceptor. If we impose this pseudodimer model on our cluster system, we might be able see another role of clusters in amplifying the amount of fully phosphorylated ITAM. To summarize, with unknown mechanisms, a T cell may begin to reduce the activity of phosphatases of phosphorylated ITAM, once some TCR proteins on the surface membrane interact with a few antigenic pMHC. When a TCR in a TCR cluster occasionally interacts with an antigenic pMHC molecule, and a coreceptor bound to an active Lck molecule interacts with the pMHC, many nearby TCR interacting with endogenous pMHC will be brought to the coreceptor and their ITAMs will be quickly fully phosphorylated.

There is another important protein to be considered to explore how the cluster system could induce production of a greater amount of downstream signal: CD45. It would be interesting to include CD45 in our cluster and homogenous system based on its topology and reaction with its associated proteins. CD45 transforms the inactive or fully active state of Lck into basally active Lck. This molecule is known to be an important phosphatase for T-cell activation through a phosphatidyl inositol pathway and is found to be excluded from TCR clusters [38,110]. CD45 is essential for the T-cell activation as many papers indicate, because it dephosphorylates the inhibitory tyrosine of the Src family of tyrosine kinase such as Lck [89,90,110]. It would be interesting to examine the roles of CD45 more closely in the cluster system because of the well known characteristics of this molecule. I hypothesize that CD45 outside of TCR clusters would be able to supply basally active Lck to TCR clusters, but its activity to dephosphorylate the fully active Lck would be prohibited while the fully active Lck stays in the TCR clusters. However, the homogeneous system in which TCRs and Lcks are more exposed to CD45s would have fewer chances to produce fully active Lcks.

5.3 Concluding remarks

As mentioned in the beginning of this thesis, immunology provides many interesting questions to both theoretical and experimental scientists. I have been interested in clustered proteins in the membrane of a T cell, which is the key mediator of the immune system, and proposed some interesting roles of clustered proteins. I hope that my research findings have contributed to advancing understanding of some aspects of the immune system.

Appendix

Supporting Information for Chapter 2

Materials and Methods

Reaction network S2-1. Phosphorylation of Lat

$$pZAP70 + Lat \xrightarrow{k_{on,pZAP70-Lat}} pZAP70 - Lat$$
$$pZAP70 - Lat \xrightarrow{k_{off,pZAP70-Lat}} pZAP70 + Lat$$
$$pZAP70 - Lat \xrightarrow{k_p} pZAP70 - pLat$$
$$pZAP70 - pLat \xrightarrow{k_{off,pZAP70-pLat}} pZAP70 + pLat$$

Reaction network S2-2. Dephosphorylation of active ZAP-70

$$P + pZAP70 \xrightarrow{k_{on,P-pZAP70}} P - pZAP70$$
$$P - pZAP70 \xrightarrow{k_{off,P-pZAP70}} P + pZAP70$$
$$P - pZAP70 \xrightarrow{k_{dp}} P - ZAP70$$
$$P - ZAP70 \xrightarrow{k_{off,P-ZAP70}} P + ZAP70$$

Reaction network S2-3. Dephosphorylation of pLat by its phosphatase, I

$$I + pLat \xrightarrow{k_{on,I-pLat}} I - pLat$$
$$I - pLat \xrightarrow{k_{off,I-pLat}} I + pLat$$
$$I - pLat \xrightarrow{k_{dp,pLat}} I - Lat$$
$$I - Lat \xrightarrow{k_{off,I-Lat}} I + Lat$$

Simulation Methodology

We employed the Stochastic Simulation Compiler [75] to simulate reaction events and diffusion in our system. All reaction rate constants and diffusion constants are converted into units of s^{-1} for use in the simulations [8,75]. First order reaction constants (s^{-1}) are unmodified for our simulation. However, experimentally obtained second order rate constants have units of $M^{-1}s^{-1}$. To convert into simulation units, we first change the bulk on-rate into an effective two-dimensional on-rate by dividing it by a distance associated with the distance proteins can sample in the direction perpendicular to the membrane (we assume this is of the same order of magnitude as the radius of gyration of molecules). For our simulation, we set the length of a lattice site as 0.01 μm and take the radius of gyration of molecules as 0.001 μm. Then, the experimental value of k_2 in $M^{-1}s^{-1}$ can be converted into s^{-1} by a multiplication factor of 1/60.2 ($1\ M^{-1}s^{-1} = \frac{1\ L}{1\ mole \times sec} = \frac{10^{15}\ \mu m^3}{6.02 \times 10^{23}\ molecules \times sec}$. After dividing this unit by the square of the length of a lattice site and then by the radius gyration, we obtain 1/60.2 s^{-1}). Diffusion is modeled by molecules hopping to nearest neighbor lattice sites. The diffusion coefficient, measured in units of $\mu m^2/s$, is converted into a hopping rate by dividing the by the square of the length of a lattice site.

Table S2-1. Rate constants for simulation

Rate Constants	Reaction
0.2 $\mu M^{-1}s^{-1}$ [17]	$k_{on,pZAP70-Lat}$: pZAP70 binding to Lat
1 s^{-1} [17]	$k_{off,pZAP70-Lat}$: pZAP70 unbinding from Lat
1 s^{-1} [17]	k_p: pZAP70 phosphorylating Lat
1 s^{-1} [17]	$k_{off,pZAP70-pLat}$: pZAP70 unbinding from Lat
0.2 $\mu M^{-1}s^{-1}$	$k_{on,P-pZAP70}$: pZAP70 binding to its phosphatase, P
1 s^{-1}	$k_{off,P-pZAP70}$: pZAP70 unbinding from its phosphatase
1 s^{-1}	k_{dp}: phosphatase dephosphorylating pZAP70
1 s^{-1}	$k_{off,P-ZAP70}$: ZAP70 unbinding from its phosphatase
0.2 $\mu M^{-1}s^{-1}$	$k_{on,I-pLat}$: pLat binding to its phosphatase, I
1 s^{-1}	$k_{off,I-pLat}$: pLat unbinding from its phosphatase
1 s^{-1}	$k_{dp,pLat}$: phosphatase dephosphorylating pLat
1 s^{-1}	$k_{off,I-Lat}$: Lat unbinding from its phosphatase

Table S2-2. Concentration of species for simulation

Species	Number of molecules in a 2 μm-diameter membrane system
LAT	20 per 0.2 μm-diameter cluster (75/ μm^2 [16], 28.5 per cluster [76])
ZAP-70	20 per 0.2 μm-diameter cluster (72000/ μm^3 [16])
SHP-1	800 (20000/ μm^3 [111])

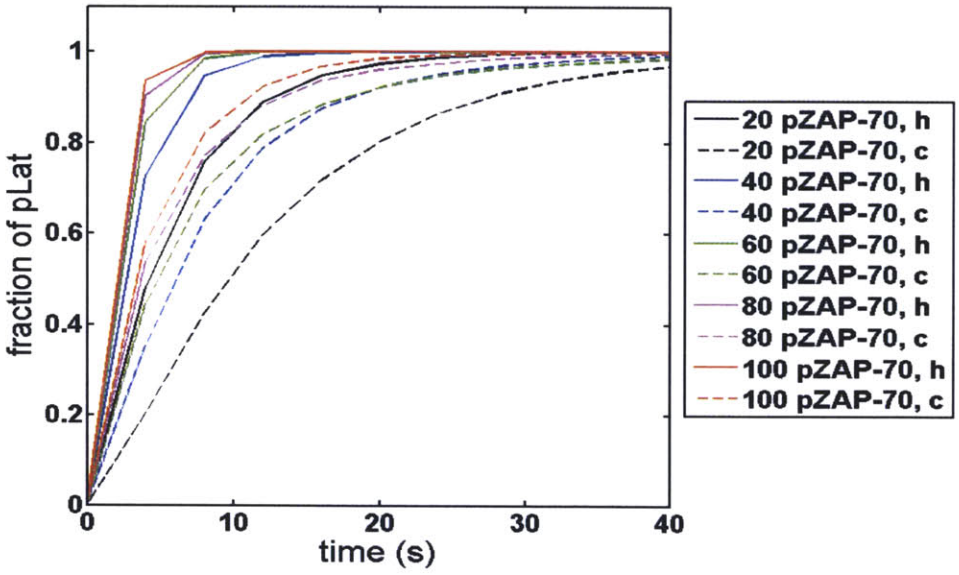

Figure S2-1. The effect of concentration of pZAP-70 on the production of pLat. Each cluster system contains 5 ZAP-70 and 5 Lat clusters. There is no phosphatase. "20 pZAP-70, c" stands for the cluster system in which each cluster initially contains 20 pZAP-70. "20 pZAP-70, h" is the homogenous system that contains the same amount of reactants as "20 pZAP-70, c." Each Lat cluster contains 20 Lat molecules. See Figure 2 for a description of simulation method.

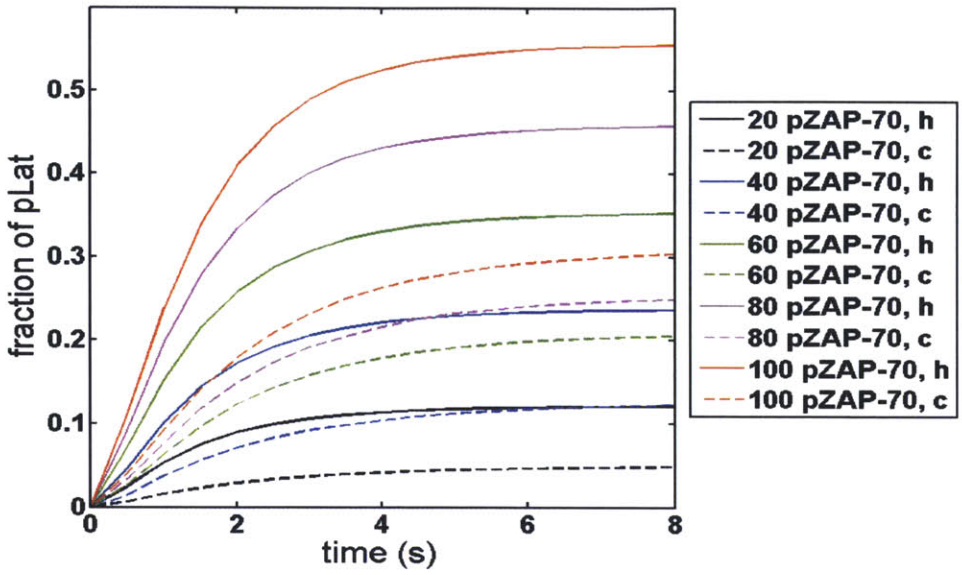

Figure S2-2. The effect of the presence of phosphatase of pZAP-70 at various concentrations of pZAP-70 on the production of pLat. Each system contains 800 phosphatases per π μm^2. In the system with clustered proteins, ZAP-70 molecules are initially located inside their clusters. See Figure S1 for a description of legend terminology.

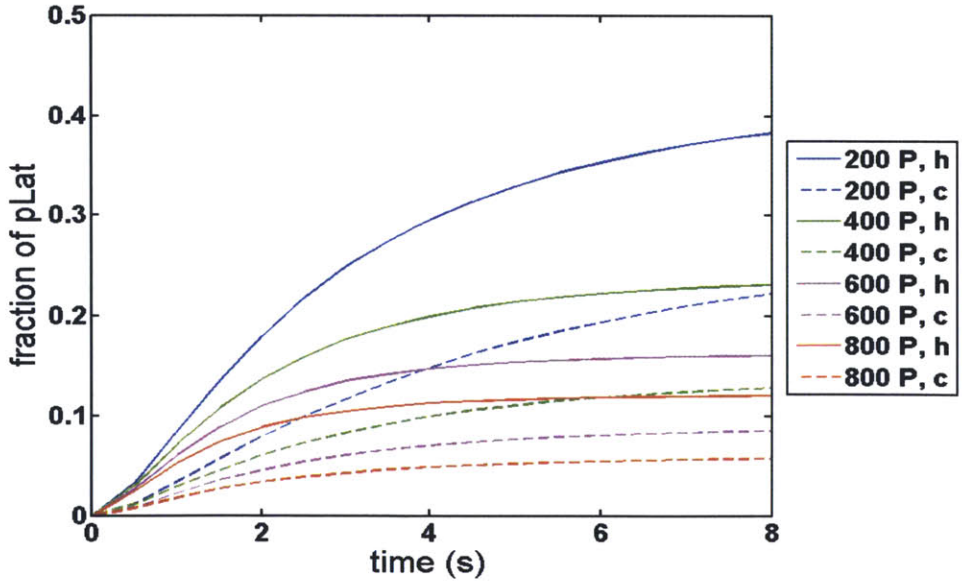

Figure S2-3. The effect of phosphatase concentration on the production of pLat. Each cluster contains 20 molecules. "200 P, h" and "200 P, c" stand for the homogenous system and the cluster system, respectively, that contains 200 phosphatases. In the system with clustered proteins, ZAP-70 molecules are initially located inside their clusters. Each cluster system contains 5 ZAP-70 and 5 Lat clusters and each cluster contains 20 molecules.

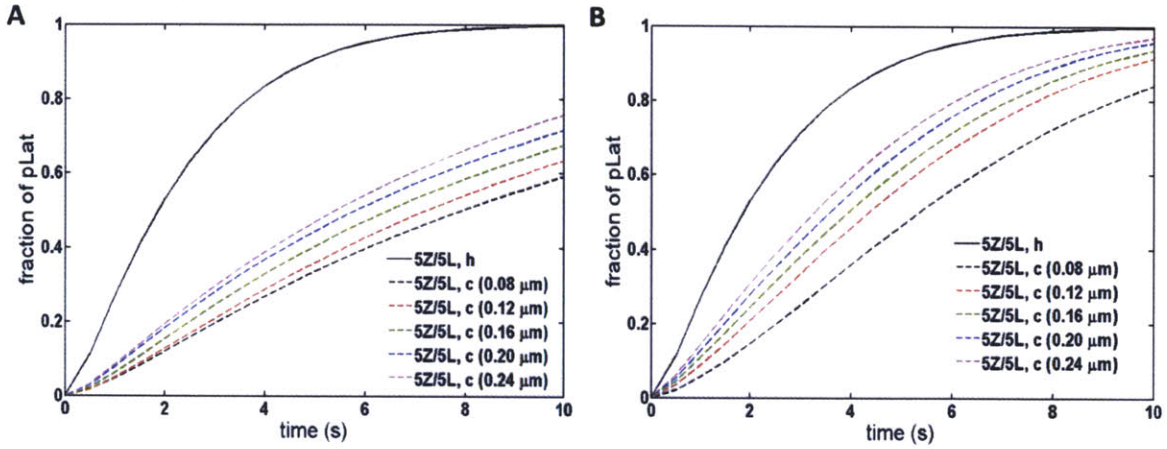

Figure S2-4. Fraction of pLat in the cluster system for various cluster sizes in the presence of no phosphatases. Each system contains 400 Lat and 400 pZAP-70 molecules. "5Z/5L, c (0.08 μm)" denotes the cluster system that consists of clusters with a diameter of 0.08 μm, while "5Z/5L, h" denotes the homogeneous system. We obtain the fraction of pLat over 60 different cluster-system configurations with 25 trajectories for each configuration. **(A)** pZAP-70 molecules are initially confined inside clusters. **(B)** pZAP-70 molecules are initially homogenously distributed.

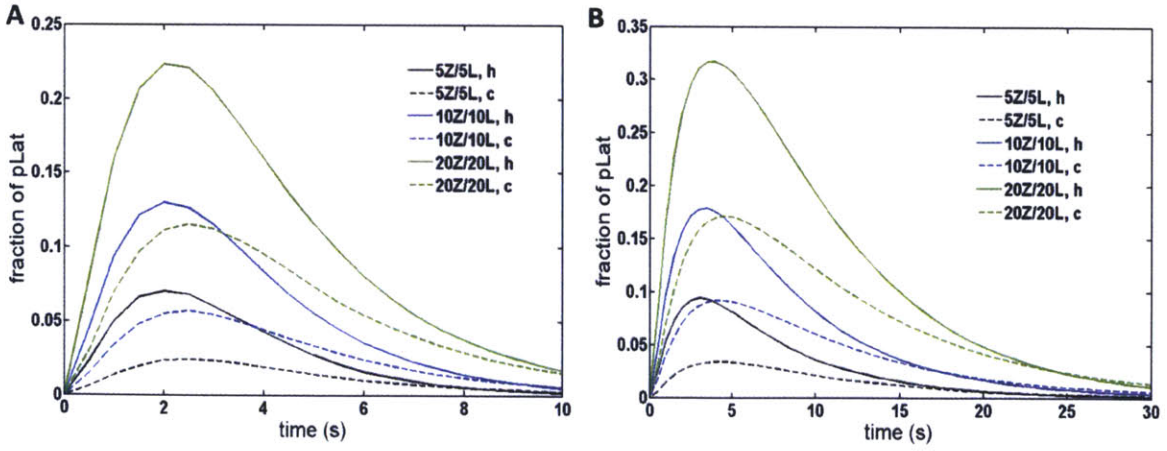

Figure S2-5. Fraction of pLat as a function of time, with dephosphorylation of Lat molecules. Each system contains 800 phosphatases of pZAP-70. In the system with

clustered proteins, each ZAP-70 and Lat cluster initially contains 20 molecules. We obtain the average fraction of pLat over 20 different cluster-system configurations with 25 trajectories for each configuration. "5Z/5L, c" stands for the cluster system that contains 5 pZAP and 5 Lat clusters. "5Z/5L, h" is the homogeneous system that contains the same number of reactants as in the "5Z/5L, c" system. **(A)** 800 phosphatases of pLat **(B)** 80 phosphatases of pLat

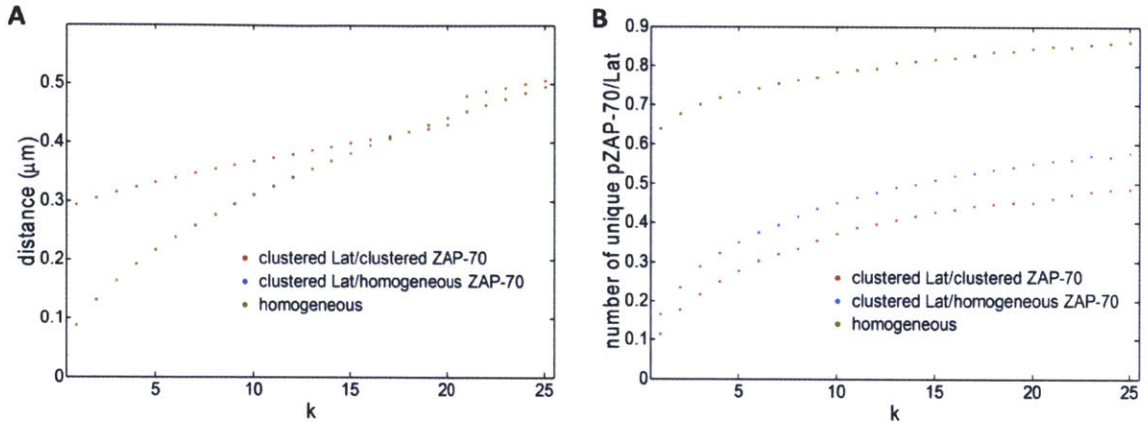

Figure S2-6. The effect of reduced cluster number on the mean distance from a Lat molecule to the k^{th} nearest pZAP-70 and the number of unique pZAP-70 per Lat. The "clustered Lat/cluster ZAP-70" system contains 5 Lat and 5 ZAP-70 clusters. We obtain the mean distances and the number of unique pZAP-70 per Lat by averaging over 1000 configurations. See Figure 4 for a description of legend terminology.

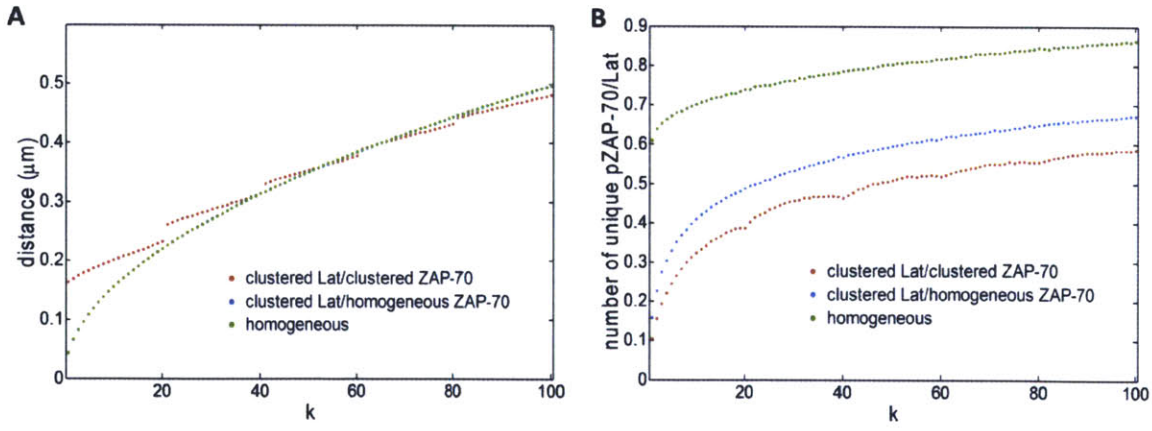

Figure S2-7. The effect of reduced size of clusters on the mean distance from a Lat molecule to the k^{th} nearest pZAP-70 and the number of unique pZAP-70 per Lat. The "clustered Lat/cluster ZAP-70" system contains 20 Lat and 20 ZAP-70 clusters. The diameter of each cluster is reduced by a factor of 2. We obtain the mean distances and the number of unique pZAP-70 per Lat by averaging over 1000 configurations.

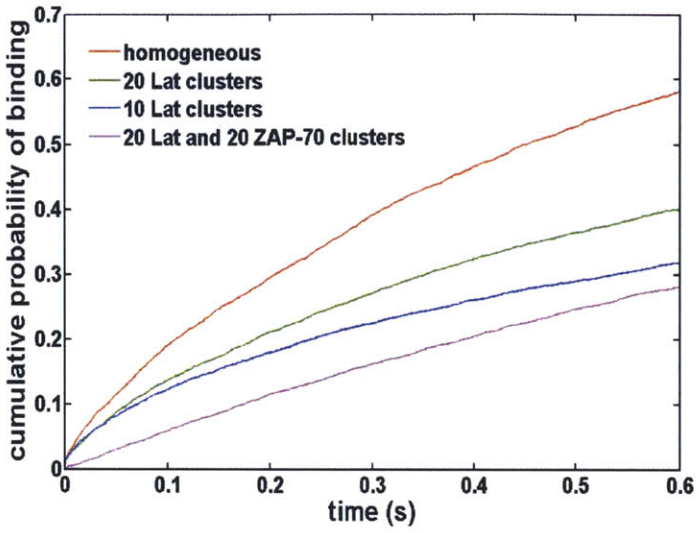

Figure S2-8. The cumulative probability of observing Lat-pZAP binding as a function of time for a single pZAP. Each system contains 400 Lat molecules, either homogeneously distributed or confined in clusters. One pZAP-70 is randomly located initially, and we determine the probability that the first binding between the pZAP-70 and a Lat molecules has occurred by a given time. For the cluster system, we obtain the probability of observing Lat-pZAP-70 over 100 different configurations with 50 trajectories for each configuration. The diffusivity of molecules in system is 0.0033 $\mu m^2/s$.

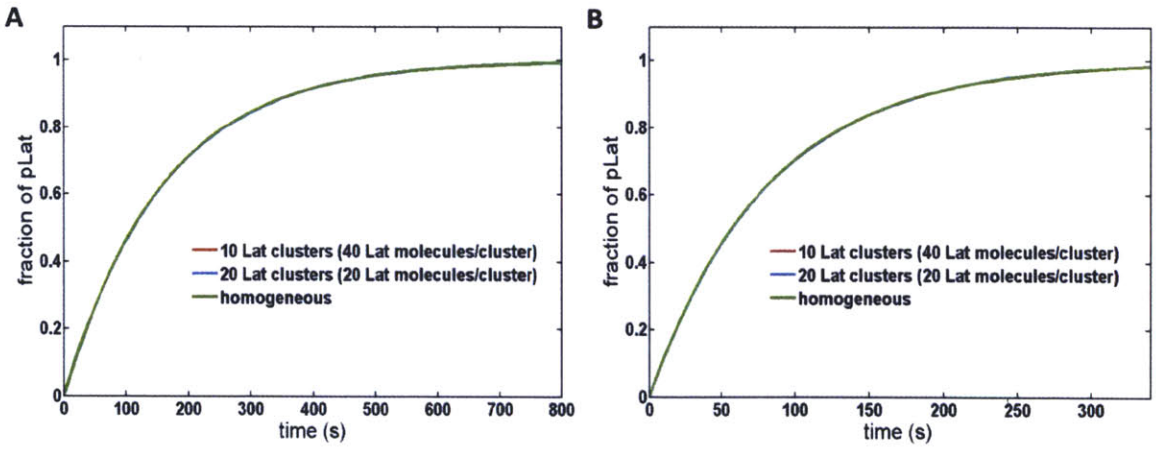

Figure S2-9. The effect of a change in the rate constant for the association or dissociation between pZAP and Lat. Other kinetic parameters are the same as those in Table S1. See Figure 5 for a description of legend terminology. **(A)** The rate constant $k_{on,pZAP70-Lat}$ is reduced by a factor of 2000. **(B)** The rate constant $k_{off,pZAP70-Lat}$ is increased by a factor of 2000.

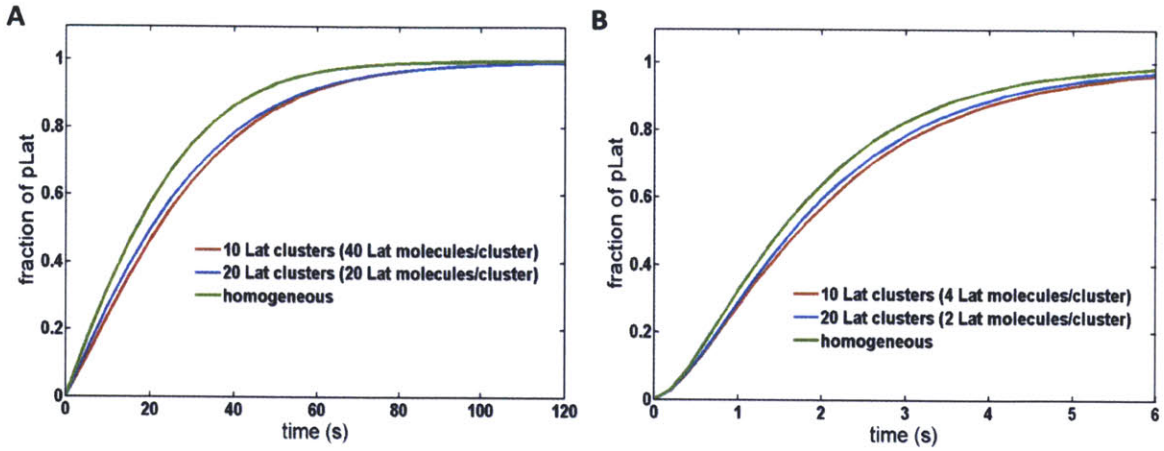

Figure S2-10. The effect of a change in the number of reactants. Other kinetic parameters are the same as those in Table S1. **(A)** The number of pZAP-70 in the system is reduced by a factor of 10. **(B)** The number of Lat in the system is reduced by a factor of 10.

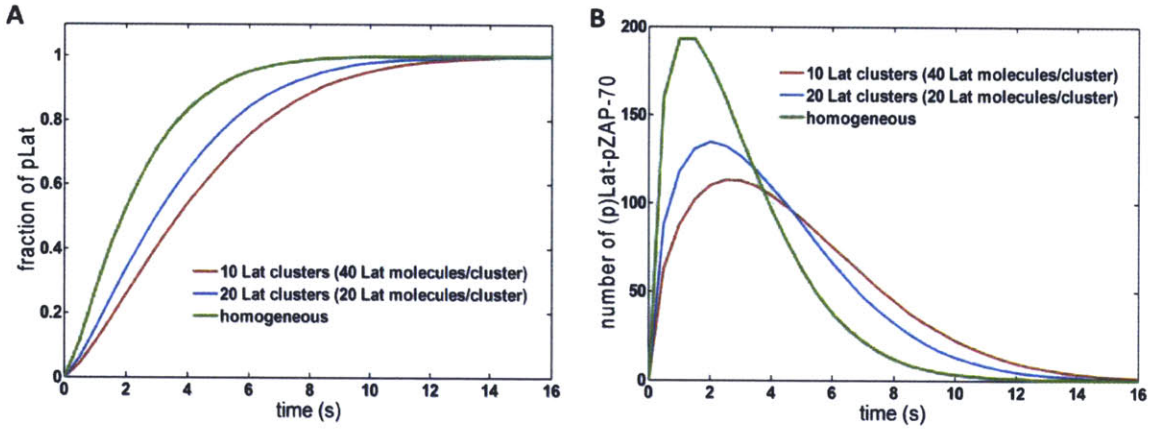

Figure S2-11. The effect of a decrease in the size of each cluster. The diameter of each cluster is reduced by a factor of 2.

Hitting rate calculation in the cluster system

We have already shown that the hitting rate in the homogenous system, for the case in which there is no competition among A molecules for binding to B molecules, can be found as the inverse of the sum of times of the association and dissociation between A and B molecules. We also want to find the analytical form of the hitting rate in the cluster system in which A molecules do not compete each other for binding to the same B molecule. As shown in Fig. 2-8, we can discretize the cluster system into subdomains, each of which contains one A molecules, which can freely diffuse through all domains, and one cluster that confines B molecules. We want to compare the hitting rate in this cluster system with the homogenous system that contains the same amount of reactants.

We notice that there exist period events in the cluster system. For example, when an A molecule starts diffusing from the boundary of subdomain, it will eventually hit the edge of the cluster with a mean time scale, $\tau_{R_+ \to R_-}$, and once it is at the edge of the cluster, it will eventually comeback to the edge of the subdomain with a mean time scale, $\tau_{R_- \to R_+}$, where R_+ and R_- are the radii of the subdomain and cluster, respectively. During the latter time duration, an A molecule can cross the cluster for a mean number of C_n, and once an A molecule is inside the cluster there exists a mean hitting rate, H_{cl}. In addition, there exists a mean time duration for an A molecule spending inside a cluster per crossing the edge of the cluster. Then, we can approximate the hitting rate in the cluster system as the following.

$$H_c = \frac{C_n H_{cl} \tau_{cl}}{\tau_{R_+ \to R_-} + \tau_{R_- \to R_+}} \qquad \text{S2.1}$$

We first define crossing the reflective boundary and crossing the boundary of the cluster as the events that A molecule diffuses from R_+ to $R_+ - \varepsilon$ and from R_- to $R_- - \varepsilon$, respectively, where ε is a very small arbitrary distance, which makes the time scale for an A molecule to diffuse from R_- to $R_- - \varepsilon$ is negligible compared to any other time scale for the reaction between A and B molecules (see Fig. 2-9).

The conditional first passage time for a molecule, initially located at r ($R_- < r < R_+$), to hit the edge of the inner circle, R_-, without hitting the boundary of the outer circle, R_+, $t_-\left(\vec{r}\right)$, can be solved by satisfying the following equations and conditions [112].

$$\nabla^2\left[\varepsilon_+(r)\right] = 0$$

$$\varepsilon_-(R_-) = 1 \qquad \text{S2.2}$$

$$\varepsilon_-(R_+) = 0$$

$$D\nabla^2\left[\varepsilon_-(r) t_-(r)\right] = -\varepsilon_-(r) \qquad \text{S2.3}$$

$$\varepsilon_-(r) t_-(r) = 0 \text{ at } r = R_- \text{ and } r = R_+$$

$$t_{-}(r)=\frac{\left(r^2-R_{-}^2\right)}{4D\ln\left(\frac{R_{+}}{r}\right)}\left(\ln\left(\frac{r}{R_{+}}\right)-1\right)+\frac{\ln\left(\frac{r}{R_{-}}\right)\left(R_{+}^2-R_{-}^2\right)}{4D\ln\left(\frac{R_{+}}{R_{-}}\right)\ln\left(\frac{R_{+}}{r}\right)} \qquad \text{S2.4}$$

$$\varepsilon_{-}(r)=\frac{\ln\left(\frac{R_{+}}{r}\right)}{\ln\left(\frac{R_{+}}{R_{-}}\right)} \qquad \text{S2.5}$$

where $\varepsilon_{-}(\vec{r})$ is the splitting probability of an A particle, which starts diffusing at r to hit the edge of the inner circle.

Analogously, the conditional first passage time for a molecule, initially located at r to hit R_{+} without hitting R_{-}, $t_{+}(\vec{r})$, can be solved:

$$t_{+}(r)=\frac{\left(R_{+}^2-r^2\right)}{4D}+\frac{\left(r^2-R_{-}^2\right)}{4D\ln\left(\frac{r}{R_{-}}\right)}-\frac{\left(R_{+}^2-R_{-}^2\right)}{4D\ln\left(\frac{R_{+}}{R_{-}}\right)} \qquad \text{S2.6}$$

$$\varepsilon_{+}(r)=1-\varepsilon_{-}(r) \qquad \text{S2.7}$$

Then, we can derive the expected time duration for an A molecule which starts diffusing at the boundary of the subdomain of size R_{+}, to reach the boundary of a cluster, R_{-}, for the first time ($\tau_{R_{+}\to R_{-}}$). When an A molecule starts diffusing from near the boundary of the subdomain ($R_{+}-\varepsilon$), it can directly hit the edge of the cluster with an expected probability ε_{-}. It also can cross the edge of the subdomain for one time, two

times, or any number of times. As we can expect, the mean time scale for A molecule to hit the edge of the cluster, when it start diffusing from the edge of the subdomain can be calculated by the following geometric distribution:

$$\tau_{R_+ \to R_-} = \varepsilon_- \left(\tau_{\varepsilon i} + \tau_{\varepsilon o}\varepsilon_+\right)\sum_{n=0}^{\infty}(n+1)\varepsilon_+^n + \tau_i \varepsilon_- \sum_{n=0}^{\infty}\varepsilon_+^n \qquad \text{S2.8}$$

where,

τ_i =conditional first passage time for A diffusing from $R_+ - \varepsilon$ to hit R_- without hitting R_+

$\tau_{\varepsilon o}$ =conditional first passage time for A diffusing from $R_+ - \varepsilon$ to hit R_+ without hitting R_-

$\tau_{\varepsilon i}$ = first passage time for A molecule diffusing from R_+ to hit $R_+ - \varepsilon$

ε_+ =probability for A diffusing from $R_+ - \varepsilon$ to hit R_+ first

ε_- = probability for A diffusing from $R_+ - \varepsilon$ to hit R_- first, 1-ε_+

$$\varepsilon_+ = \frac{\ln\left(\frac{R_+ - \varepsilon}{R_-}\right)}{\ln\left(\frac{R_+}{R_-}\right)} \qquad \text{S2.9}$$

$$\tau_i = \frac{\left((R_+ - \varepsilon)^2 - R_-^2\right)}{4D\ln\left(\frac{R_+}{R_+ - \varepsilon}\right)}\left(\ln\left(\frac{R_+ - \varepsilon}{R_+}\right) - 1\right) + \frac{\ln\left(\frac{R_+ - \varepsilon}{R_-}\right)\left(R_+^2 - R_-^2\right)}{4D\ln\left(\frac{R_+}{R_-}\right)\ln\left(\frac{R_+}{R_+ - \varepsilon}\right)} \qquad \text{S2.10}$$

$$\tau_{\varepsilon o}=\frac{\left(R_+^2-\left(R_+-\varepsilon\right)^2\right)}{4D}+\frac{\left(\left(R_+-\varepsilon\right)^2-R_-^2\right)}{4D\ln\left(\frac{R_+-\varepsilon}{R_-}\right)}-\frac{\left(R_+^2-R_-^2\right)}{4D\ln\left(\frac{R_+}{R_-}\right)} \qquad \text{S2.11}$$

$$\tau_{\varepsilon i}=\frac{\varepsilon^2}{2D} \qquad \text{S2.12}$$

Finally, after implementing the above analytical form of each term into equation S2.8, we obtain the following form of $\tau_{R_+\to R_-}$:

$$\tau_{R_+\to R_-}=\frac{\varepsilon^2}{2D}\left(\frac{\ln\left(\frac{R_+}{R_-}\right)}{\ln\left(\frac{R_+}{R_+-\varepsilon}\right)}\right)+\frac{\left(\left(R_+-\varepsilon\right)^2-R_-^2\right)}{4D\ln\left(\frac{R_+}{R_+-\varepsilon}\right)}\ln\left(1-\frac{\varepsilon}{R_+}\right)+\left(\frac{\ln\left(\frac{R_+-\varepsilon}{R_-}\right)}{\ln\left(\frac{R_+}{R_+-\varepsilon}\right)}\right)\frac{\left(2\varepsilon R_+-\varepsilon^2\right)}{4D} \qquad \text{S2.13}$$

Employing the similar approaches, we can also derive the expected time duration for an A molecule which starts diffusing at R_-, to return to R_+, for the first time ($\tau_{R_-\to R_+}$).

$$\tau_{R_-\to R_+}=\tau_o\varepsilon_+\sum_{n=1}^{\infty}\varepsilon_-^n+\varepsilon_-\varepsilon_+\left(\tau_{\varepsilon i}+\tau_{\varepsilon o}\right)\sum_{n=0}^{\infty}\left(n+1\right)\varepsilon_-^n \qquad \text{S2.14}$$

where,

τ_o =conditional first passage time for A diffusing from R_- to hit R_+ without hitting $R_--\varepsilon$

$\tau_{\varepsilon o}$ =first passage time for A diffusing from $R_- - \varepsilon$ to hit R_-

$\tau_{\varepsilon i}$ =conditional first passage time for A diffusing from R_- to hit $R_- - \varepsilon$ without hitting R_+

ε_+ =probability for A diffusing from R_- to hit R_+ first

ε_- = probability for A diffusing from R_- to hit $R_- - \varepsilon$ first, 1-ε_+

$$\varepsilon_+ = \frac{\ln\left(\frac{R_-}{R_- - \varepsilon}\right)}{\ln\left(\frac{R_+}{R_- - \varepsilon}\right)} \qquad \text{S2.15}$$

$$\tau_o = \frac{\left(R_+^2 - R_-^2\right)}{4D} + \frac{\left(R_-^2 - \left(R_- - \varepsilon\right)^2\right)}{4D\ln\left(\frac{R_-}{R_- - \varepsilon}\right)} - \frac{\left(R_+^2 - \left(R_- - \varepsilon\right)^2\right)}{4D\ln\left(\frac{R_+}{R_- - \varepsilon}\right)} \qquad \text{S2.16}$$

$$\tau_{\varepsilon i} = \frac{\left(R_-^2 - \left(R_- - \varepsilon\right)^2\right)}{4D\ln\left(\frac{R_+}{R_-}\right)}\left(\ln\left(\frac{R_-}{R_+}\right) - 1\right) + \frac{\ln\left(\frac{R_-}{R_- - \varepsilon}\right)\left(R_+^2 - \left(R_- - \varepsilon\right)^2\right)}{4D\ln\left(\frac{R_+}{R_- - \varepsilon}\right)\ln\left(\frac{R_+}{R_-}\right)} \qquad \text{S2.17}$$

Once an A molecule crosses the cluster boundary, it will spend inside a cluster for an expected time, before it comes back to the edge of the cluster. Wofsy et al. have examined the first passage time for an A particle, which is located at r in a circular domain of radius R, to reach the edge of the domain. The circular domain contains B particles which interact with A particle as the following reaction scheme.

$$A + B \underset{k_{off}}{\overset{k_{on}}{\rightleftarrows}} A - B$$

Wofsy et al. considered the case in which diffusivities of A, B and A-B molecules are the same and the case the diffusivity of A-B is zero, while diffusivities of A and B molecules are the same [79]. The first passage time for the prior case can be also derived by simply taking limit of R_- to zero for $t_+\left(\vec{r}\right)$ (see Eq. S2.6). Implementing the analytical solution derived by Wofsy et al., we obtain the first passage time for a A molecules located at $R_- - \varepsilon$ to comeback to R_-, $\tau_{\varepsilon o}$, as the following.

$$\tau_{\varepsilon o} = \frac{\left(2\varepsilon R_- - \varepsilon^2\right)}{4D}\left(1 + K\left[B\right]_{cl}\right) \quad (\text{if } D_A = D_B = D \text{ and } D_{A-B} = 0) \qquad \text{S2.18}$$

For the case when diffusivities of all molecules are the same, while the diffusivity of a complex is zero, we can directly implement the result derived by Wofsy et al. because A molecules at the edge of the cluster is unbound. However, when diffusivities of all molecules are the same, the A molecule can be bound or unbound to a B molecule, when A molecules is at the edge of the cluster. If A molecules is bound, it will bounce back to $R_- - \varepsilon$. Therefore, the mean time for an unbound A molecule to reach the edge of the cluster is the following.

If we define $\tau_\sigma = \frac{\left(2\varepsilon R_- - \varepsilon^2\right)}{4D}$, then

$$\tau_{\varepsilon o} = \tau_\sigma P_{unbound} + 2\tau_\sigma P_{unbound} P_{bound} + 3\tau_\sigma P_{unbound} P_{bound}^2 + \ldots$$
$$= \frac{\tau_\sigma}{P_{unbound}} = \frac{\left(2\varepsilon R_- - \varepsilon^2\right)}{4D}\left(1 + K\left[B\right]_{cl}\right) \qquad (\text{if } D_L = D_Z = D_{LZ} = D)$$

S2.19

Then, for either case, $D_L = D_Z = D_{LZ} = D$ or $D_A = D_B = D$ and $D_{A-B} = 0$,

$$\tau_{R_- \to R_+} = \frac{\left(R_+^2 - R_-^2\right)}{4D} + \frac{\left(2\varepsilon R_- - \varepsilon^2\right)}{4D\ln\left(\frac{R_-}{R_- - \varepsilon}\right)} - \frac{\left(R_+^2 - \left(R_- - \varepsilon\right)^2\right)}{4D\ln\left(\frac{R_+}{R_- - \varepsilon}\right)}$$
$$+ \frac{\ln\left(\frac{R_+}{R_-}\right)}{\ln\left(\frac{R_-}{R_- - \varepsilon}\right)}\left(\frac{\left(2\varepsilon R_- - \varepsilon^2\right)}{4D\ln\left(\frac{R_+}{R_-}\right)}\left(\ln\left(\frac{R_-}{R_+}\right) - 1\right) + \frac{\ln\left(\frac{R_-}{R_- - \varepsilon}\right)\left(R_+^2 - \left(R_- - \varepsilon\right)^2\right)}{4D\ln\left(\frac{R_+}{R_- - \varepsilon}\right)\ln\left(\frac{R_+}{R_-}\right)} + \frac{\left(2\varepsilon R_- - \varepsilon^2\right)}{4D}\left(1 + K\left[B\right]_c\right)\right)$$

S2.20

After taking limit of value of ε to an infinitely small value,

$$\lim_{\varepsilon \to 0} \tau_{R_+ \to R_-} = -\frac{\left(R_+^{\,2} - R_-^2\right)}{4D} + \frac{R_+^{\,2}}{2D}\ln\left(\frac{R_+}{R_-}\right) \qquad \text{S2.21}$$

$$\lim_{\varepsilon \to 0} \tau_{R_- \to R_+} = \frac{\left(R_+^{\,2} - R_-^2\right)}{4D} + \frac{R_-^{\,2}}{2D}K\left[B\right]_c \ln\left(\frac{R_+}{R_-}\right) \qquad \text{S2.22}$$

C_n, the mean number of crossing of an A molecule over the boundary of a cluster before coming back to the edge of the subdomain can be obtained by the number of diffusion of A from R_- to $R_- - \varepsilon$ before coming back to R_+.

$$C_n = \varepsilon_- \varepsilon_+ \sum_{n=0}^{\infty} (n+1)\varepsilon_-^n = \left(\frac{1}{\varepsilon_+} - 1\right) \tag{S2.23}$$

$$\varepsilon_+ = \frac{\ln\left(\frac{R_-}{R_- - \varepsilon}\right)}{\ln\left(\frac{R_+}{R_- - \varepsilon}\right)} \tag{S2.24}$$

Then, the total duration of time for an A particle spending inside a cluster before it comes back to a cluster, $\tau_{cl,\Sigma}$, is

$$\tau_{cl,\Sigma} = C_n \frac{\left(2\varepsilon R_- - \varepsilon^2\right)}{4D}\left(1 + K[B]_c\right) \tag{S2.25}$$

$$\lim_{\varepsilon \to 0} \tau_{cl,\Sigma} = \frac{R_-^{\,2}}{2D} K[B]_c \ln\left(\frac{R_+}{R_-}\right) \tag{S2.26}$$

Now, we know all analytical form for each term in Eq. S2.1. After implementing these forms, we find the hitting rate in the cluster system is the same as that in the homogenous system. We note that this results is obtained based on the diffusion rate constant suggested by Bell, and different forms of diffusion rate constant strongly affect

the analytical form of hitting rate between A and B molecules in the homogenous system or in a cluster.

For example, implementing the diffusion rate constant derived by Lauffenburger and Linderman, we find that the hitting rate in the cluster system can be larger than that in the homogenous system.

$$H_{\mathrm{h}} \approx \frac{k_{on}[B]_{\mathrm{h}}}{\left(1+\frac{k_{on}\ln\left(\frac{b_h}{s}\right)}{2\pi\left(D_A+D_B\right)}\right)\left(1+K[B]_{\mathrm{h}}\right)} \qquad \text{S2.27}$$

where b_h in the equation for H_h is the mean half distance between B molecules. This distance is inversely proportional to the square root of the concentration of B molecules considering the size of reflective subdomain that we have already described ($b_{\mathrm{h}} \approx 1/\sqrt{\pi[B]_h}$) [113]. The analytical solution for H_c can be obtained by substituting b_h by b_c ($b_c \approx b_h \frac{R_-}{R_+}$).

$$H_c - H_h \approx \frac{k_{on}^2 \ln\left(\frac{R_+}{R_-}\right)[B]_h}{2\pi\left(D_A+D_B\right)\left(1+K[B]_h\right)\left(1+\frac{k_{on}\ln\left(\frac{b_h}{s}\frac{R_-}{R_+}\right)}{2\pi\left(D_A+D_B\right)}\right)\left(1+\frac{k_{on}\ln\left(\frac{b_h}{s}\right)}{2\pi\left(D_A+D_B\right)}\right)} \geq 0 \qquad \text{S2.28}$$

where the meaning of b and s are the same as those used for the description of diffusion rate constant.

As we can notice from the above analytical solution, the difference between hitting rates in the cluster and homogenous systems becomes negligible as the size of the cluster approaches to the size of the subdomain, diffusivities of molecules increase, or the intrinsic reaction rate constant for the association between reactants decreases.

The discrepancy between analytical descriptions of the hitting rate for both the cluster and homogenous system may suggest the importance of developing analytical forms of the two dimensional diffusion rate constant to analyze the effect of configuration on the downstream signals. The mathematical approaches and assumptions employed by Lauffenburger and Linderman, and Goldstein to obtain diffusion rate constant is plausible and capture the dependency of the constant on the bulk concentration of molecules and the size of reaction radius [83,84]. The discrepancy between hitting rates at steady state between the cluster and homogenous systems suggests the possibility of that, when there exists no competition among A molecules for binding to B molecules, the cluster system could induce the greater downstream signals. As mentioned in Chapter 2, the increased rebinding between reactants mainly due to reduced size of clusters or diffusivities of molecules, or increased association reaction rate constants, could help the cluster system to enhance the production of downstream signals, although our current study with extensive parameter regimes did not show such prediction. We may need further studies on the two dimensional diffusion rate constant. We note that more precise comparison of the hitting rates between the cluster and

homogenous system depends on the further investigation on the derivation of analytical form of the two dimensional diffusion rate constant.

Supporting Information for Chapter 3

Materials and Methods

The simulation methods are similar to those described in the supporting information for Chapter 2.

Reaction network S3-1. Interactions between TCR, pMHC, coreceptors for the generation of doubly phosphorylated ITAM and the negative regulation of phosphorylated ITAM.

$$TCR + pMHC \xrightarrow{k_{on,TCR-pMHC}} TCR - pMHC$$
$$TCR - (ag)pMHC \xrightarrow{k_{off,TCR-(ag)pMHC}} TCR + (ag)pMHC$$
$$TCR - (en)pMHC \xrightarrow{k_{off,TCR-(en)pMHC}} TCR + (en)pMHC$$
$$TCR + CD4/8 \xrightarrow{k_{on,TCR-CD4/8}} TCR - CD4/8$$
$$TCR - CD4/8 \xrightarrow{k_{off,TCR-CD4/8}} TCR + CD4/8$$
$$pMHC + CD4/8 \xrightarrow{k_{on,pMHC-CD4/8}} pMHC - CD4/8$$
$$pMHC - CD4/8 \xrightarrow{k_{off,pMHC-CD4/8}} pMHC + CD4/8$$
$$TCR - pMHC - CD4/8 \xrightarrow{k_{p,TCR-pMHC-CD4/8}} pTCR - pMHC - CD4/8$$
$$pTCR - pMHC - CD4/8 \xrightarrow{k_{p,pTCR-pMHC-CD4/8}} ppTCR - pMHC - CD4/8$$
$$pTCR + SHP1 \xrightarrow{k_{on,TCR-SHP1}} pTCR - SHP1$$
$$ppTCR + SHP1 \xrightarrow{k_{on,TCR-SHP1}} ppTCR - SHP1$$
$$TCR - SHP1 \xrightarrow{k_{off,TCR-SHP1}} TCR + SHP1$$
$$pTCR - SHP1 \xrightarrow{k_{off,TCR-SHP1}} pTCR + SHP1$$
$$ppTCR - SHP1 \xrightarrow{k_{off,TCR-SHP1}} ppTCR + SHP1$$
$$pTCR \xrightarrow{k_{dp,pTCR}} TCR$$
$$ppTCR \xrightarrow{k_{dp,ppTCR}} pTCR$$

The first reaction, $TCR + pMHC \xrightarrow{k_{on,TCR-pMHC}} TCR - pMHC$ implies the interaction between TCR and pMHC with an association rate constant of $k_{on,TCR-pMHC}$. However, either TCR or pMHC are either bound or unbound to a coreceptor when they interact, and this is not shown explicitly in the reaction. This rule also similarly applies to the other reactions assuming TCR, pMHC, and coreceptors independently interact with each other. The reaction $pTCR + SHP1 \xrightarrow{k_{on,TCR-SHP1}} pTCR - SHP1$ describes only singly phosphorylated TCR, which is either bound or unbound to a pMHC molecule that is not bound to a coreceptor, can associate with a SHP-1 molecule.

Table S3-1. Rate constants for reaction network S3-1.

Rate Constants	Reaction
0.015 $\mu M^{-1}s^{-1}$ [8]	$k_{on,TCR-pMHC}$: TCR binding to $pMHC$
0.02 s^{-1} [8]	$k_{off,TCR-(ag)pMHC}$: TCR unbinding from antigenic $pMHC$
20 s^{-1} [8]	$k_{off,TCR-(en)pMHC}$: TCR unbinding from endogenous $pMHC$
0.0001 $\mu M^{-1}s^{-1}$ [8]	$k_{on,TCR-CD4/8}$: TCR binding to a coreceptor
1 s^{-1} [8]	$k_{off,TCR-CD4/8}$: TCR unbinding from a coreceptor
0.1 $\mu M^{-1}s^{-1}$ [8]	$k_{on,pMHC-CD4/8}$: $pMHC$ binding to a coreceptor
20 s^{-1} [8]	$k_{off,pMHC-CD4/8}$: $pMHC$ unbinding from a coreceptor
0.1 s^{-1} [8]	$k_{p,TCR-pMHC-CD4/8}$: a coreceptor bound to $pMHC$ phosphorylating bare ITAM of TCR bound to $pMHC$
0.05 s^{-1} [8]	$k_{p,pTCR-pMHC-CD4/8}$: a coreceptor bound to $pMHC$ phosphorylating singly phosphorylated ITAM of TCR bound to $pMHC$
0.02 $\mu M^{-1}s^{-1}$	$k_{on,TCR-SHP1}$: phosphorylated TCR binding to $SHP1$
1 s^{-1}	$k_{off,TCR-SHP1}$: TCR unbinding from $SHP1$
0.2 s^{-1} [8]	$k_{dp,pTCR}$: $SHP1$ dephosphorylating unprotected singly phosphorylated TCR bound to $SHP1$
0.4 s^{-1} [8]	$k_{dp,ppTCR}$: $SHP1$ dephosphorylating unprotected doubly phosphorylated TCR bound to $SHP1$

characteristic length used for SSC=0.001 μm

Table S3-2. Concentration of species for the simulation of reaction network S3-1.

Species	Number of molecules in a 2 μm-diameter membrane system
TCR	20 clusters, 20 per 0.2 μm-diameter cluster (300 μm^{-2} [8])
(en) pMHC	300 (100 μm^{-2} [8])
(ag) pMHC	30
CD4/8	300 (100 μm^{-2} [8])
SHP-1	600 (20000/ μm^3 [111])

Reaction network S3-2. The generation of RasGTP by the positive feedback reaction and the negative regulation of RasGAP.

$$Lat + SOS \xrightarrow{k_{on,Lat-SOS}} Lat - SOS$$
$$Lat - SOS \xrightarrow{k_{off,Lat-SOS}} Lat + SOS$$
$$Lat - SOS + RasGDP \xrightarrow{k_{on,Lat-SOS-(RasGDP)_{allo}}} Lat - SOS - (RasGDP)_{allo}$$
$$Lat - SOS - (RasGDP)_{allo} \xrightarrow{k_{off,Lat-SOS-(RasGDP)_{allo}}} Lat - SOS + RasGDP$$
$$Lat - SOS + RasGTP \xrightarrow{k_{on,Lat-SOS-(RasGTP)_{allo}}} Lat - SOS - (RasGTP)_{allo}$$
$$Lat - SOS - (RasGTP)_{allo} \xrightarrow{k_{off,Lat-SOS-(RasGTP)_{allo}}} Lat - SOS + RasGTP$$

$$Lat - SOS - (RasGDP)_{allo} + RasGDP \xrightarrow{k_{on,Lat-SOS-(RasGDP)_{allo}-RasGDP}} Lat - SOS - (RasGDP)_{allo} - RasGDP$$

$$Lat - SOS - (RasGTP)_{allo} + RasGDP \xrightarrow{k_{on,Lat-SOS-(RasGTP)_{allo}-RasGDP}} Lat - SOS - (RasGTP)_{allo} - RasGDP$$

$$Lat - SOS - (RasGDP)_{allo} - RasGDP \xrightarrow{k_{p,Lat-SOS-(RasGDP)_{allo}-RasGDP}} Lat - SOS - (RasGDP)_{allo} - RasGTP$$

$$Lat - SOS - (RasGDP)_{allo} - RasGTP \xrightarrow{k_{off,Lat-SOS-(RasGDP)_{allo}-RasGTP}} Lat - SOS - (RasGDP)_{allo} + RasGTP$$

$$Lat - SOS - (RasGTP)_{allo} - RasGDP \xrightarrow{k_{p,Lat-SOS-(RasGTP)_{allo}-RasGDP}} Lat - SOS - (RasGTP)_{allo} - RasGTP$$

$$Lat - SOS - (RasGTP)_{allo} - RasGTP \xrightarrow{k_{off,Lat-SOS-(RasGTP)_{allo}-RasGTP}} Lat - SOS - (RasGTP)_{allo} + RasGTP$$

$$RasGTP + RasGAP \xrightarrow{k_{on,RasGTP-RasGAP}} RasGTP - RasGAP$$
$$RasGTP - RasGAP \xrightarrow{k_{off,RasGTP-RasGAP}} RasGTP + RasGAP$$
$$RasGTP - RasGAP \xrightarrow{k_{dp,RasGTP-RasGAP}} RasGDP - RasGAP$$
$$RasGDP - RasGAP \xrightarrow{k_{off,RasGDP-RasGAP}} RasGDP + RasGAP$$

Table S3-3. Rate constants for reaction network S3-2.

Rate Constants	Reaction
6.24 $\mu M^{-1}s^{-1}$ [17]	$k_{on,Lat-SOS}$: SOS binding to Lat
1 s^{-1}	$k_{off,Lat-SOS}$: SOS unbinding from Lat
0.102 $\mu M^{-1}s^{-1}$ [17]	$k_{on,Lat-SOS-(RasGDP)_{allo}}$: $RasGDP$ binding to the allosteric pocket of SOS
3 s^{-1} [17]	$k_{off,Lat-SOS-(RasGDP)_{allo}}$: $RasGDP$ unbinding from the allosteric pocket of SOS
0.102 $\mu M^{-1}s^{-1}$ [17]	$k_{on,Lat-SOS-(RasGTP)_{allo}}$: $RasGTP$ binding to the allosteric pocket of SOS
0.4 s^{-1} [17]	$k_{off,Lat-SOS-(RasGTP)_{allo}}$: $RasGTP$ unbinding from the allosteric pocket of SOS
0.04 $\mu M^{-1}s^{-1}$ [17]	$k_{on,Lat-SOS-(RasGDP)_{allo}-RasGDP}$: $RasGDP$ binding to the catalytic site of SOS bound to $(RasGDP)_{allo}$
0.06 $\mu M^{-1}s^{-1}$ [17]	$k_{on,Lat-SOS-(RasGTP)_{allo}-RasGDP}$: $RasGDP$ binding to the catalytic site of SOS bound to $(RasGTP)_{allo}$
0.003 s^{-1} [17]	$k_{p,Lat-SOS-(RasGDP)_{allo}-RasGDP}$: SOS bound to $(RasGDP)_{allo}$ converting $RasGDP$ to $RasGDP$ at a catalytic site
1 s^{-1} [17]	$k_{off,Lat-SOS-(RasGDP)_{allo}-RasGTP}$: $RasGTP$ unbinding from the catalytic site of SOS bound to $(RasGDP)_{allo}$
0.04 s^{-1} [17]	$k_{p,Lat-SOS-(RasGTP)_{allo}-RasGDP}$: SOS bound to $(RasGTP)_{allo}$ converting $RasGDP$ to $RasGDP$ at a catalytic site
1 s^{-1}	$k_{off,Lat-SOS-(RasGTP)_{allo}-RasGTP}$: $RasGTP$ unbinding from the catalytic site of SOS bound to $(RasGTP)_{allo}$
2.4 $\mu M^{-1}s^{-1}$ [17]	$k_{on,RasGTP-RasGAP}$: $RasGTP$ binding to $RasGAP$
1 s^{-1} [17]	$k_{off,RasGTP-RasGAP}$: $RasGTP$ unbinding from $RasGAP$
0.1 s^{-1} [17]	$k_{dp,RasGTP-RasGAP}$: $RasGAP$ dephosphorylating $RasGTP$
1	$k_{off,RasGDP-RasGAP}$: $RasGDP$ unbinding from $RasGAP$

characteristic length used for SSC=0.01 μm

Table S3-4. Concentration of species for the simulation of reaction network S3-2.

Species	Number of molecules in a 2 μm-diameter membrane system
Lat	20 per 0.2 μm-diameter cluster (75/ μm^2 [16], 28.5 per cluster [76])
SOS	250
Ras	500 (75/μm^2[16])
RasGAP	Varied from 25 to 50, but 25 is for the reference (250/μm^3 [16])

Reaction network S3-3. Most comprehensive network for the generation of RasGTP. In addition to the reaction network S3-2, the cooperative binding between PLC-γ and GRb2-SOS to Lat, the generation of RasGTP by RasGRP, and the basal activity of SOS molecules are considered.

$$Lat + PLC\gamma \xrightarrow{k_{on,Lat-PLC\gamma}} Lat - PLC\gamma$$
$$Lat - PLC\gamma \xrightarrow{k_{off,Lat-PLC\gamma}} Lat + PLC\gamma$$
$$Lat + SOS \xrightarrow{k_{on,Lat-SOS}} Lat - SOS$$
$$Lat - SOS \xrightarrow{k_{off,Lat-SOS}} Lat + SOS$$
$$Lat - SOS - PLC\gamma \xrightarrow{k_{off,Lat-SOS-PLC\gamma}} Lat - SOS + PLC\gamma$$
$$Lat - SOS - PLC\gamma \xrightarrow{k_{off,Lat-SOS-PLC\gamma}} Lat - PLC\gamma + SOS$$
$$Lat - PLC\gamma + PIP2 \xrightarrow{k_{on,Lat-PLC\gamma-PIP2}} Lat - PLC\gamma - PIP2$$
$$PLC\gamma - PIP2 \xrightarrow{k_{off,PLC\gamma-PIP2}} PLC\gamma + PIP2$$
$$Lat - PLC\gamma - PIP2 \xrightarrow{k_{c,Lat-PLC\gamma-PIP2}} Lat - PLC\gamma + DAG + IP3$$
$$DAG + RasGRP \xrightarrow{k_{on,DAG-RasGRP}} DAG - RasGRP$$
$$DAG - RasGRP \xrightarrow{k_{off,DAG-RasGRP}} DAG + RasGRP$$
$$DAG - RasGRP + RasGDP \xrightarrow{k_{on,DAG-RasGRP-RasGDP}} DAG - RasGRP - RasGDP$$
$$DAG - RasGRP - RasGDP \xrightarrow{k_{off,DAG-RasGRP-RasGDP}} DAG - RasGRP + RasGDP$$
$$DAG - RasGRP - RasGDP \xrightarrow{k_{c,DAG-RasGRP-RasGDP}} DAG - RasGRP + RasGTP$$
$$Lat - SOS + RasGDP \xrightarrow{k_{on,Lat-SOS-RasGDP}} Lat - SOS - RasGDP$$
$$Lat - SOS - RasGDP \xrightarrow{k_{off,Lat-SOS-RasGDP}} Lat - SOS + RasGDP$$
$$Lat - SOS - RasGDP \xrightarrow{k_{p,Lat-SOS-RasGDP}} Lat - SOS - RasGTP$$
$$Lat - SOS - RasGTP \xrightarrow{k_{off,Lat-SOS-RasGTP}} Lat - SOS + RasGTP$$
$$Lat - SOS + RasGDP \xrightarrow{k_{on,Lat-SOS-(RasGDP)_{allo}}} Lat - SOS - (RasGDP)_{allo}$$
$$Lat - SOS - (RasGDP)_{allo} \xrightarrow{k_{off,Lat-SOS-(RasGDP)_{allo}}} Lat - SOS + RasGDP$$
$$Lat - SOS + RasGTP \xrightarrow{k_{on,Lat-SOS-(RasGTP)_{allo}}} Lat - SOS - (RasGTP)_{allo}$$
$$Lat - SOS - (RasGTP)_{allo} \xrightarrow{k_{off,Lat-SOS-(RasGTP)_{allo}}} Lat - SOS + RasGTP$$
$$Lat - SOS - (RasGDP)_{allo} + RasGDP \xrightarrow{k_{on,Lat-SOS-(RasGDP)_{allo}-RasGDP}} Lat - SOS - (RasGDP)_{allo} - RasGDP$$
$$Lat - SOS - (RasGTP)_{allo} + RasGDP \xrightarrow{k_{on,Lat-SOS-(RasGTP)_{allo}-RasGDP}} Lat - SOS - (RasGTP)_{allo} - RasGDP$$
$$Lat - SOS - (RasGDP)_{allo} - RasGDP \xrightarrow{k_{p,Lat-SOS-(RasGDP)_{allo}-RasGDP}} Lat - SOS - (RasGDP)_{allo} - RasGTP$$

$$Lat - SOS - (RasGDP)_{allo} - RasGTP \xrightarrow{k_{off,Lat-SOS-(RasGDP)_{allo}-RasGTP}} Lat - SOS - (RasGDP)_{allo} + RasGTP$$

$$Lat - SOS - (RasGTP)_{allo} - RasGDP \xrightarrow{k_{p,Lat-SOS-(RasGTP)_{allo}-RasGDP}} Lat - SOS - (RasGTP)_{allo} - RasGTP$$

$$Lat - SOS - (RasGTP)_{allo} - RasGTP \xrightarrow{k_{off,Lat-SOS-(RasGTP)_{allo}-RasGTP}} Lat - SOS - (RasGTP)_{allo} + RasGTP$$

$$RasGTP + RasGAP \xrightarrow{k_{on,RasGTP-RasGAP}} RasGTP - RasGAP$$
$$RasGTP - RasGAP \xrightarrow{k_{off,RasGTP-RasGAP}} RasGTP + RasGAP$$
$$RasGTP - RasGAP \xrightarrow{k_{dp,RasGTP-RasGAP}} RasGDP - RasGAP$$
$$RasGDP - RasGAP \xrightarrow{k_{off,RasGDP-RasGAP}} RasGDP + RasGAP$$

Table S3-5. Rate constants for reaction network S3-3.

Rate Constants	Reaction
7.92 $\mu M^{-1}s^{-1}$ [17]	$k_{on,Lat-PLC\gamma}$: $PLC\gamma$ binding to Lat
0.5 s^{-1} [17]	$k_{off,Lat-PLC\gamma}$: $PLC\gamma$ unbinding from Lat, which is unbound to SOS
6.24 $\mu M^{-1}s^{-1}$ [17]	$k_{on,Lat-SOS}$: SOS binding to Lat
1.1 s^{-1} [17]	$k_{off,Lat-SOS}$: SOS unbinding from Lat, which is unbound to $PLC\gamma$
0.01 s^{-1} [17]	$k_{off,Lat-SOS-PLC\gamma}$: SOS or $PLC\gamma$ unbinding from Lat, which is bound to both $PLC\gamma$ and SOS
4.08 $\mu M^{-1}s^{-1}$ [17]	$k_{on,Lat-PLC\gamma-PIP2}$: $PIP2$ binding to $Lat - PLC\gamma$
1 s^{-1} [17]	$k_{off,PLC\gamma-PIP2}$: $PIP2$ binding to $Lat - PLC\gamma$
0.5 s^{-1} [17]	$k_{c,Lat-PLC\gamma-PIP2}$: $Lat - PLC\gamma$ cleaves $PIP2$ and produces $DAG$and $IP3$
4.08 $\mu M^{-1}s^{-1}$ [17]	$k_{on,DAG-RasGRP}$: $RasGRP$ binding to DAG
0.08 s^{-1} [17]	$k_{off,DAG-RasGRP}$: $RasGRP$ unbinding from DAG
0.32 $\mu M^{-1}s^{-1}$ [17]	$k_{on,DAG-RasGRP-RasGDP}$: $RasGDP$ binding to $DAG - RasGRP$
1 s^{-1} [17]	$k_{off,DAG-RasGRP-RasGDP}$: $RasGDP$ unbinding from $DAG -$

	$RasGRP$
0.01 s^{-1} [17]	$k_{c,DAG-RasGRP-RasGDP}$: $DAG - RasGDP$ converting $RasGDP$ to $RasGTP$ and releasing $RasGTP$
0.04 $\mu M^{-1}s^{-1}$ [17]	$k_{on,Lat-SOS-RasGDP}$: $RasGDP$ binding to the catalytic site of SOS, which has an empty allosteric pocket
4 s^{-1} [16]	$k_{off,Lat-SOS-RasGDP}$: $RasGDP$ unbinding from the catalytic site of SOS, which has an empty allosteric pocket
0.0005 s^{-1} [16]	$k_{p,Lat-SOS-RasGDP}$: SOS with an empty allosteric pocket basally converting $RasGDP$ to $RasGTP$
4 s^{-1} [16]	$k_{off,Lat-SOS-RasGTP}$: $RasGTP$ unbinding from the catalytic site of SOS, which has an empty allosteric pocket
0.102 $\mu M^{-1}s^{-1}$ [17]	$k_{on,Lat-SOS-(RasGDP)_{allo}}$: $RasGDP$ binding to the allosteric pocket of SOS
3 s^{-1} [17]	$k_{off,Lat-SOS-(RasGDP)_{allo}}$: $RasGDP$ unbinding from the allosteric pocket of SOS
0.102 $\mu M^{-1}s^{-1}$ [17]	$k_{on,Lat-SOS-(RasGTP)_{allo}}$: $RasGTP$ binding to the allosteric pocket of SOS
0.4 s^{-1} [17]	$k_{off,Lat-SOS-(RasGTP)_{allo}}$: $RasGTP$ unbinding from the allosteric pocket of SOS
0.04 $\mu M^{-1}s^{-1}$ [17]	$k_{on,Lat-SOS-(RasGDP)_{allo}-RasGDP}$: $RasGDP$ binding to the catalytic site of SOS bound to $(RasGDP)_{allo}$
0.06 $\mu M^{-1}s^{-1}$ [17]	$k_{on,Lat-SOS-(RasGTP)_{allo}-RasGDP}$: $RasGDP$ binding to the catalytic site of SOS bound to $(RasGTP)_{allo}$
0.003 s^{-1} [17]	$k_{p,Lat-SOS-(RasGDP)_{allo}-RasGDP}$: SOS bound to $(RasGDP)_{allo}$ converting $RasGDP$ to $RasGDP$ at a catalytic site
1 s^{-1} [17]	$k_{off,Lat-SOS-(RasGDP)_{allo}-RasGTP}$: $RasGTP$ unbinding from the catalytic site of SOS bound to $(RasGDP)_{allo}$
0.04 s^{-1} [17]	$k_{p,Lat-SOS-(RasGTP)_{allo}-RasGDP}$: SOS bound to $(RasGTP)_{allo}$ converting $RasGDP$ to $RasGDP$ at a catalytic site
1 s^{-1}	$k_{off,Lat-SOS-(RasGTP)_{allo}-RasGTP}$: $RasGTP$ unbinding from the catalytic site of SOS bound to $(RasGTP)_{allo}$
2.4 $\mu M^{-1}s^{-1}$ [17]	$k_{on,RasGTP-RasGAP}$: $RasGTP$ binding to $RasGAP$
1 s^{-1} [17]	$k_{off,RasGTP-RasGAP}$: $RasGTP$ unbinding from $RasGAP$
0.1 s^{-1} [17]	$k_{dp,RasGTP-RasGAP}$: $RasGAP$ dephosphorylating $RasGTP$
1	$k_{off,RasGDP-RasGAP}$: $RasGDP$ unbinding from $RasGAP$

characteristic length used for SSC=0.01 μm

Table S3-6. Concentration of species for the simulation of reaction network S3-3.

Species	Number of molecules in a 2 μm-diameter membrane system
Lat	20 per 0.2 μm-diameter cluster (75/μm^2 [16], 28.5 per cluster [76])
SOS	250
Ras	500 (75/μm^2[16])
RasGAP	Varied from 25 to 50, but 15 is for the reference (250/μm^3 [16])
PLCγ	40 (1250/μm^2 [17])
PIP2	40 (1250/μm^2 [17])
RasGRP	20 (625/μm^2 [17])

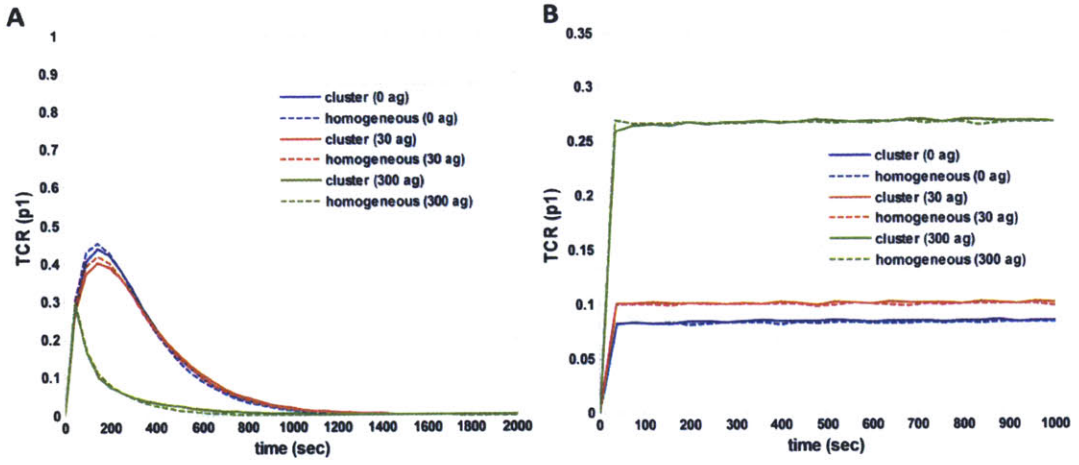

Figure S3-1. The fraction of singly phosphorylated ITAM at various concentrations of antigenic pMHC. Simulation results for the cluster system in which 20 TCR molecules are placed in each of 20 TCR clusters and homogeneous system which contains randomly distributed 400 TCR molecules. The fraction of singly phosphorylated TCR is obtained by the number of singly phosphorylated TCR divided by 400. Eech system contains a fixed amount of pMHC molecules (330 pMHC molecules), but only the number of antigenic pMHC is varied to examine the effect of the concentration of antigenic pMHC on the downstream signals. "cluster (30 ag)" denotes the cluster system that contains 30 antigenic pMHC (k_{off}=0.02 s^{-1}) and 300 endogenous pMHC molecules (k_{off}=20 s^{-1}). "homogeneous (30 ag)" denotes the homogenous system that is compared to the system "cluster (30 ag)." The diffusivity of molecules is 0.0033 μm^2/s. The fraction of doubly phosphorylated ITAM in the same system is shown in Fig. 3-1. **(A)** The system with no phosphatase of ITAM. **(B)** The system with 600 phosphatases of ITAM per π μm^2.

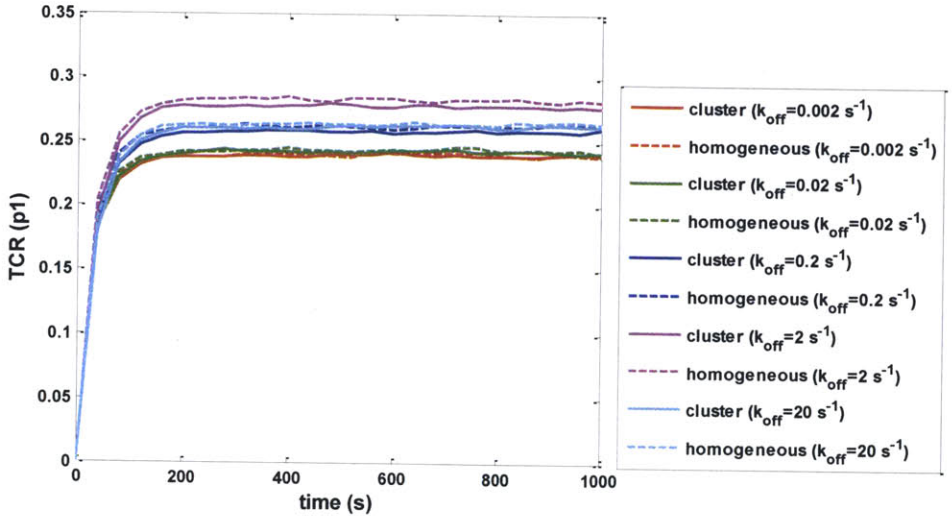

Figure S3-2. The fraction of singly phosphorylated ITAM at various affinities of antigenic pMHC. Simulation results for the cluster system in which 20 TCR molecules are placed in each of 20 TCR clusters and homogenous system which contains randomly distributed 400 TCR molecules. Each system, except "homogeneous (k_{off}=20 s^{-1})" and "cluster (k_{off}=20 s^{-1})", contains 30 antigenic pMHC, 300 endogenous pMHC, and 60 phosphatases of ITAM. "cluster (k_{off}=0.02 s^{-1})" denotes the cluster system that contains 30 antigenic pMHC with k_{off} of 0.02 s^{-1}. Likewise, "homogeneous (k_{off}=20 s^{-1})" denotes the homogeneous system that contains only endogenous pMHC with k_{off} of 20 s^{-1}. The diffusivity of molecules is 0.0033 $\mu m^2/s$.

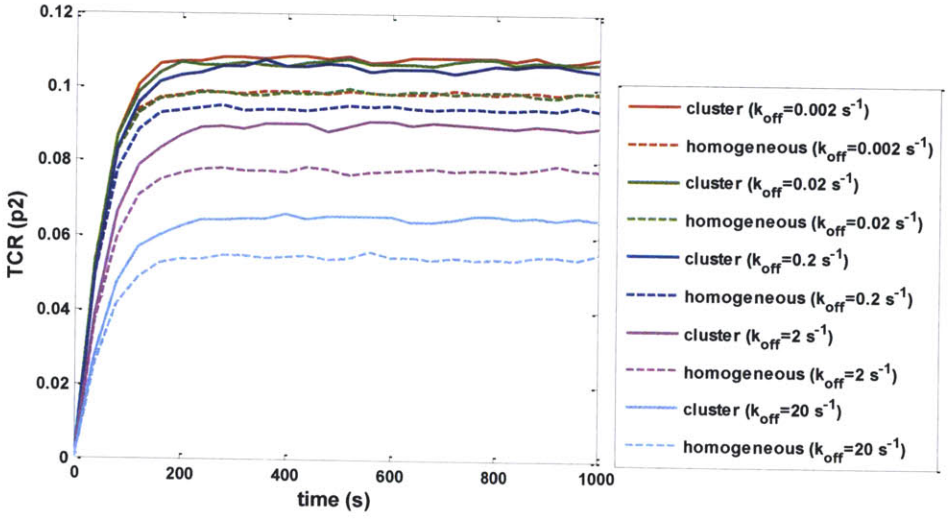

Figure S3-3. The fraction of doubly phosphorylated ITAM at various affinities of antigenic pMHC. The legendary description is the same as that in Fig. S3-2.

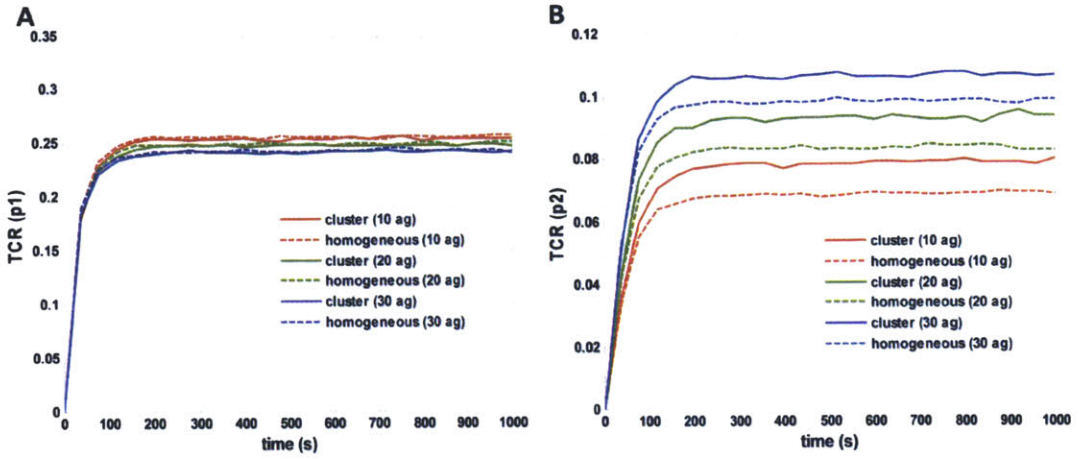

Figure S3-4. The fraction of singly and doubly phosphorylated ITAM in the homogenous and cluster systems at various low concentration of antigenic pMHC molecules. Each system consists of 60 phosphatases of ITAM per π μm^2. The diffusivity of molecules is 0.0033 $\mu m^2/s$. The total amount of pMHC molecules in each system is fixed at 330. "cluster (30 ag)" denotes the cluster system that contains 30 antigenic pMHC with k_{off} of 0.02 s^{-1}. **(A)** The fraction of singly phosphorylated ITAM. **(B)** The fraction of doubly phosphorylated ITAM.

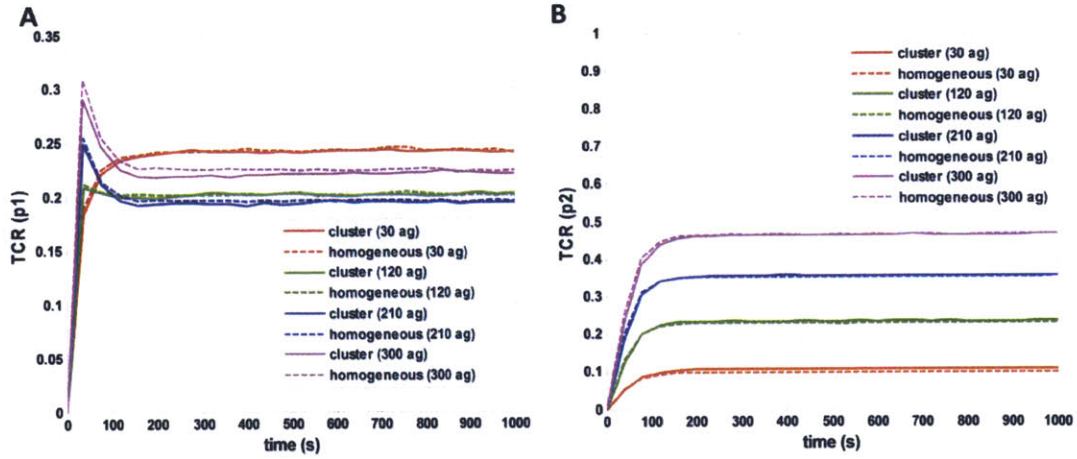

Figure S3-5. The fraction of singly and doubly phosphorylated ITAM in the homogenous and cluster systems at various high concentration of antigenic pMHC molecules. Each system consists of 60 phosphatases of ITAM per π μm^2. The diffusivity of molecules is 0.0033 $\mu m^2/s$. The total amount of pMHC molecules in each system is fixed at 330. "cluster (30 ag)" denotes the cluster system that contains 30 antigenic

pMHC with k_{off} of 0.02 s^{-1}. **(A)** The fraction of singly phosphorylated ITAM. **(B)** The fraction of doubly phosphorylated ITAM.

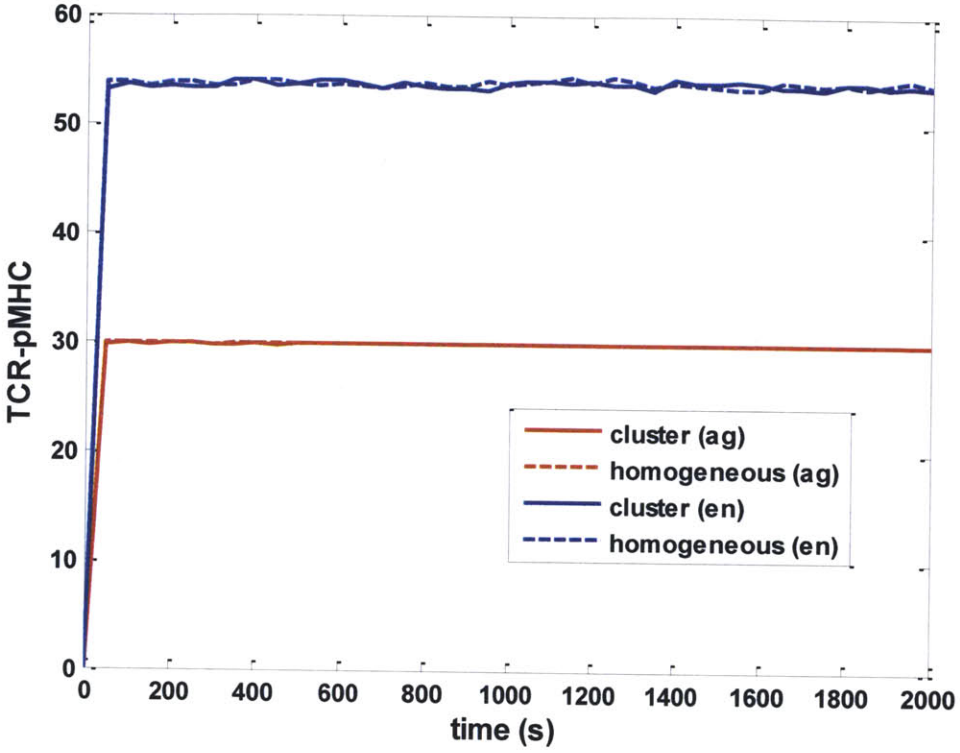

Figure S3-6. The total amount of TCR bound to pMHC in both cluster and homogenous systems. Simulation results for the cluster system in which 20 TCR molecules are placed in each of 20 TCR clusters and homogenous system which contains randomly distributed 400 TCR molecules. Each system contains 30 antigenic pMHC (k_{off}=0.02 s^{-1}) and 300 endogenous pMHC molecules (k_{off}=20 s^{-1}). The system contains 600 phosphatases of ITAM per π μm^2. The diffusivity of molecules is 0.0033 $\mu m^2/s$. "cluster (ag)" and "cluster (en)" denote the amount of TCR bound to antigenic pMHC molecules and to endogenous pMHC, respectively. The similar legendary description applies to the homogenous system.

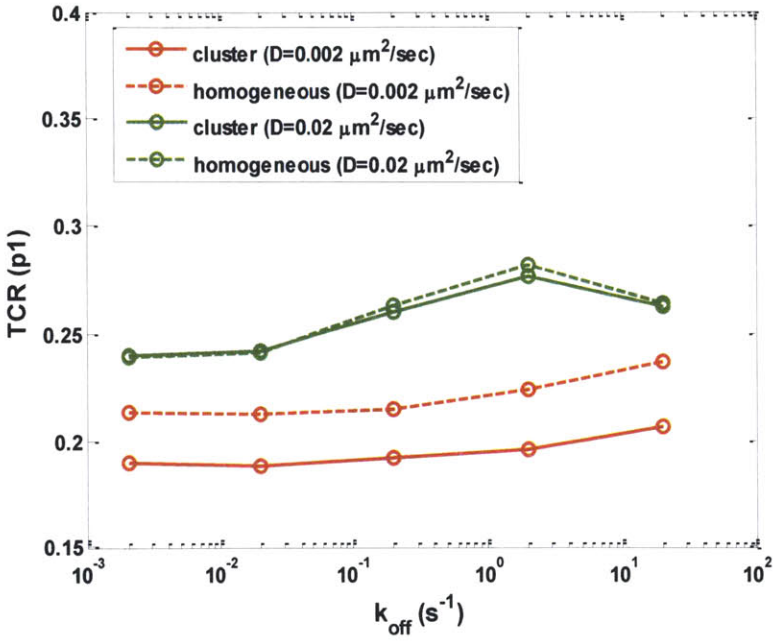

Figure S3-7. The effect of clustering of proteins, diffusivity of molecules, and potency of antigenic pMHC on the level of singly phosphorylated ITAM at equilibrium. Simulation results for the cluster system in which 20 TCR molecules are placed in each of 20 TCR clusters and homogenous system which contains randomly distributed 400 TCR molecules. Each system consists of 300 endogenous pMHC, 30 antigenic pMHC, and 60 phosphatases of ITAM per π μm^2. The level of doubly phosphorylated ITAM in the same system is shown in Fig. 3-2.

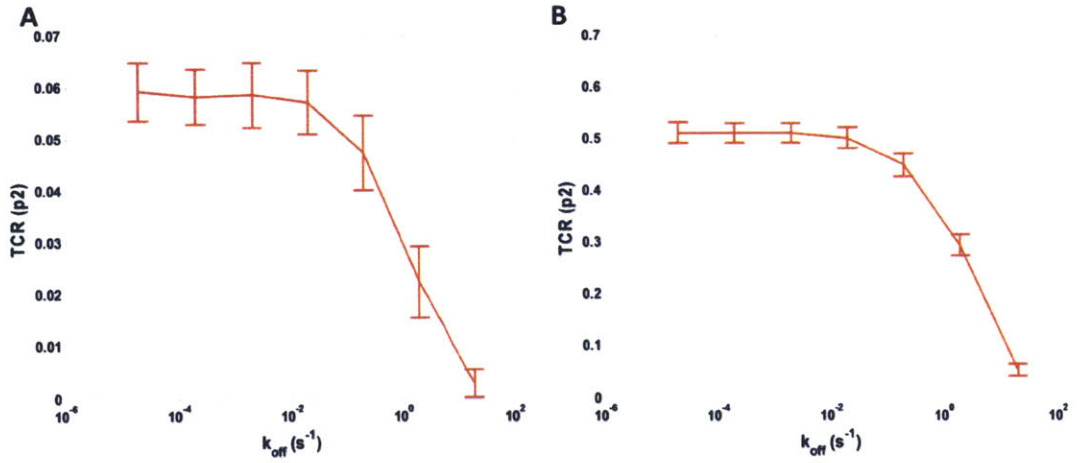

Figure S3-8. The steady-state fraction of doubly phosphorylated ITAM in homogenous system that consists of pMHC molecules of the same potency. Each system consists of 60 phosphatases of ITAM per π μm^2. The diffusivity of molecules is

0.0033 $\mu m^2/s$. **(A)** The system contains 30 pMHC molecules. **(B)** The system contains 330 pMHC molecules.

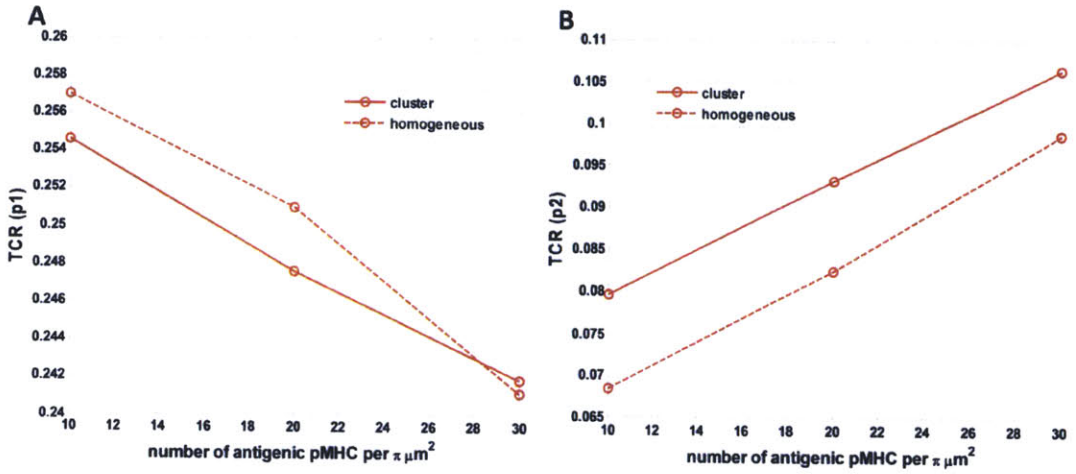

Figure S3-9. The steady-state fraction of singly and doubly phosphorylated ITAM in the homogenous and cluster systems at various low concentration of antigenic pMHC molecules. Each system consists of 60 phosphatases of ITAM per π μm^2. The diffusivity of molecules is 0.0033 $\mu m^2/s$. The total amount of pMHC molecules in each system is fixed at 330. **(A)** The fraction of singly phosphorylated ITAM. **(B)** The fraction of doubly phosphorylated ITAM.

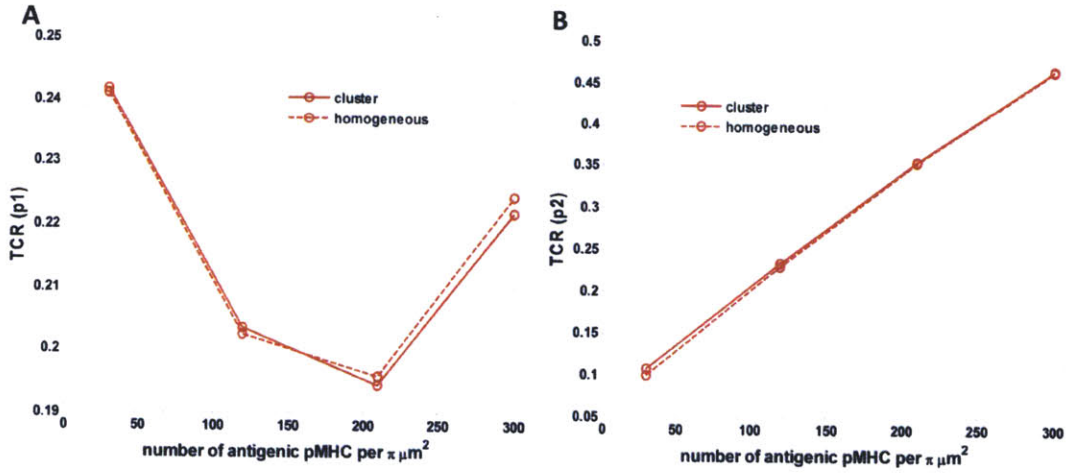

Figure S3-10. The steady-state fraction of singly and doubly phosphorylated ITAM in the homogenous and cluster systems at various high concentrations of antigenic pMHC molecules. Each system consists of 60 phosphatases of ITAM per π μm^2. The diffusivity of molecules is 0.0033 $\mu m^2/s$. The total amount of pMHC molecules in each

system is fixed at 330. **(A)** The fraction of singly phosphorylated ITAM. **(B)** The fraction of doubly phosphorylated ITAM.

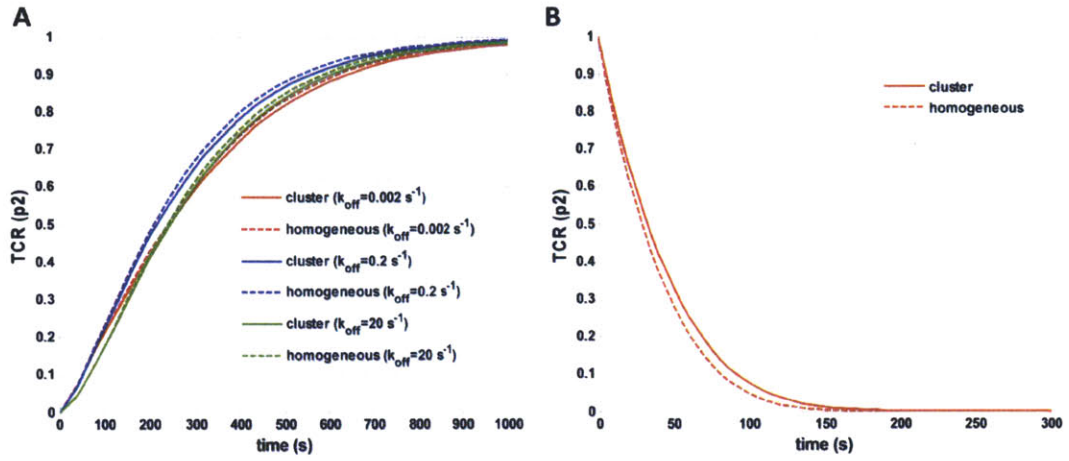

Figure S3-11. The fraction of singly and doubly phosphorylated ITAM over time in the homogenous and cluster systems at various potencies of antigenic pMHC molecules. The diffusivity of molecules is 0.0033 $\mu m^2/s$. **(A)** Each system consists of 300 endogenous pMHC and 30 antigenic pMHC molecules per π μm^2. There is no phosphatase of ITAM. "cluster (k_{off}=20 s^{-1})" denotes the cluster system that contains the antigenic pMHC with k_{off} of 20 s^{-1}. **(B)** Each system initially contains 400 doubly phosphorylated ITAM and 60 phosphatases of ITAM. The cluster system initially locates doubly phosphorylated 20 TCR molecules per cluster. There are no pMHC and coreceptors.

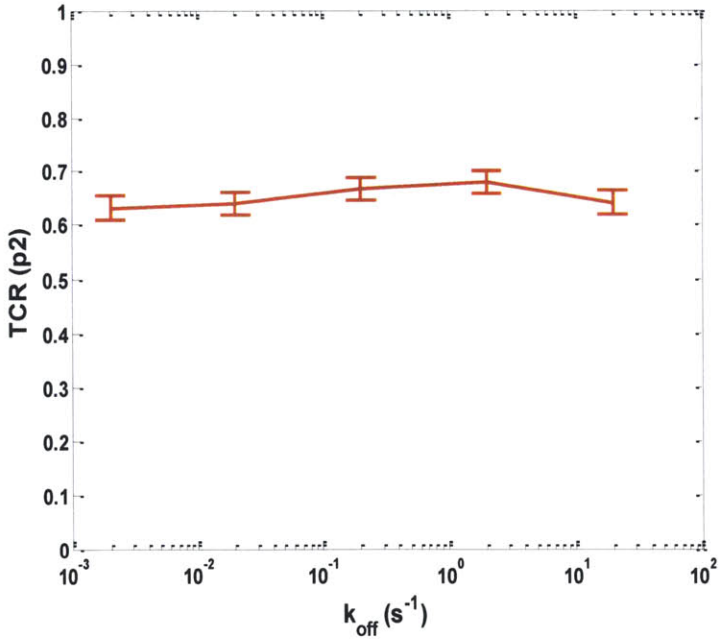

Figure S3-12. The fraction of doubly phosphorylated ITAM at equilibrium in the homogeneous system at various potencies of 30 antigenic pMHC molecules among 330 pMHC in the system. The diffusivity of molecules is 0.0033 $\mu m^2/s$. Each system consists of 400 TCR, 300 coreceptors, 300 endogenous pMHC, 30 antigenic pMHC, and 6 phosphatases of ITAM per π μm^2.

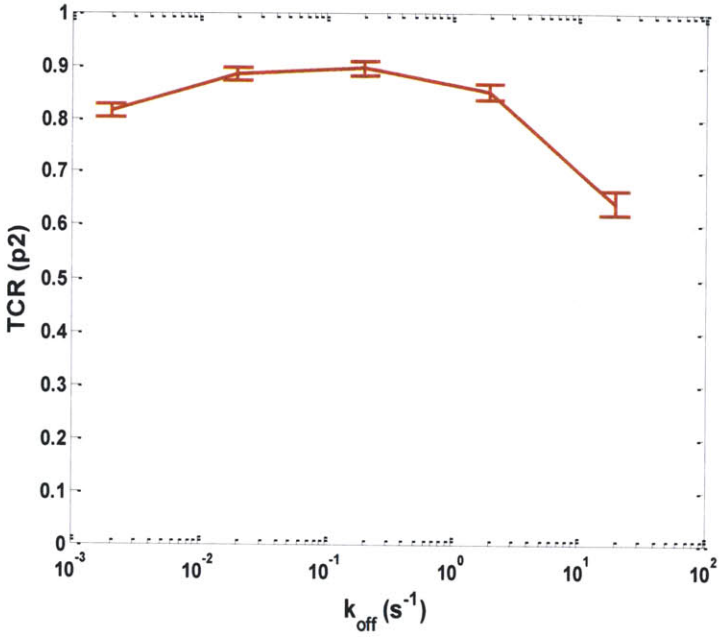

Figure S3-13. The fraction of doubly phosphorylated ITAM at equilibrium in the homogeneous system at various potencies of 330 pMHC molecules. The diffusivity of molecules is 0.0033 $\mu m^2/s$. Each system consists of 400 TCR, 300 coreceptors, 330 antigenic pMHC, and 6 phosphatases of ITAM per π μm^2.

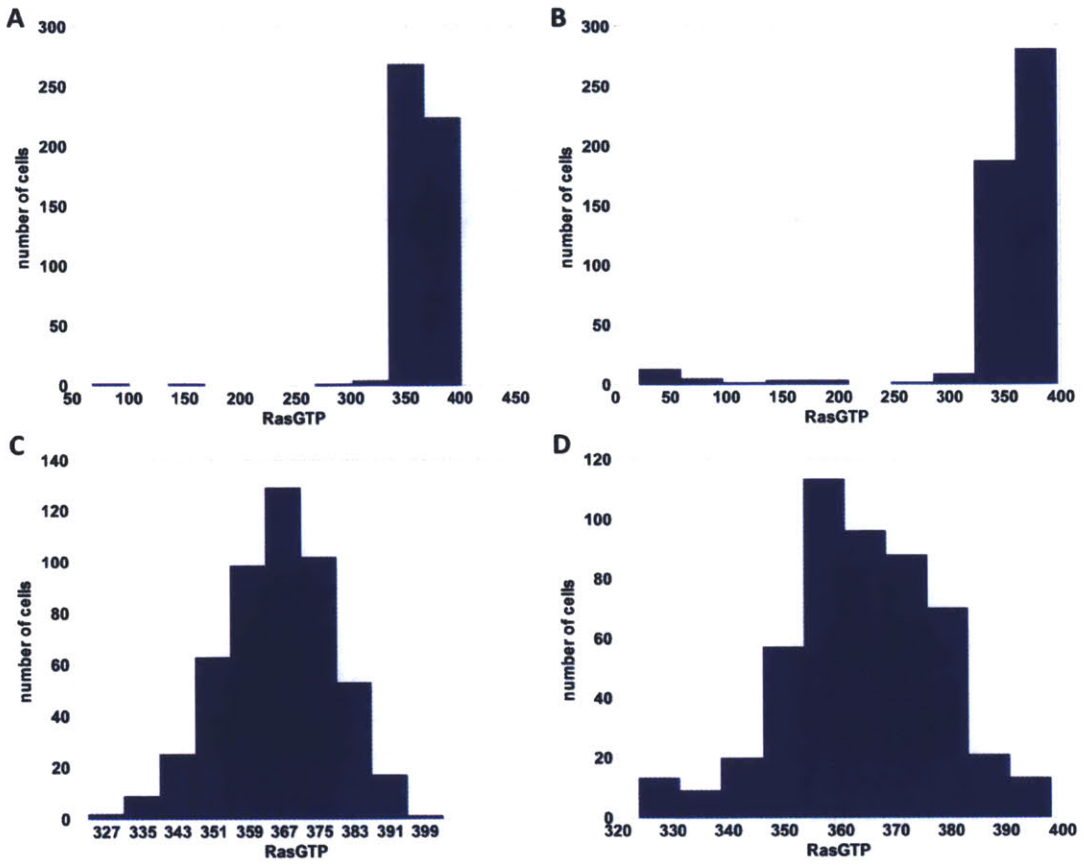

Figure S3-14. The steady-state level of RasGTP and the number of cells containing a given steady-state level of RasGTP. The diffusivity of molecules is 0.0167 $\mu m^2/s$. Each system consists of 500 Ras and 15 RasGAP molecules per π μm^2. **(A)** The cluster system that initially consists of Ras as a form of RasGDP. **(B)** The homogenous system that initially consists of Ras as a form of RasGDP. **(C)** The cluster system that initially consists of Ras as a form of RasGTP. **(D)** The homogenous system that initially consists of Ras as a form of RasGTP.

Supporting Information for Chapter 4

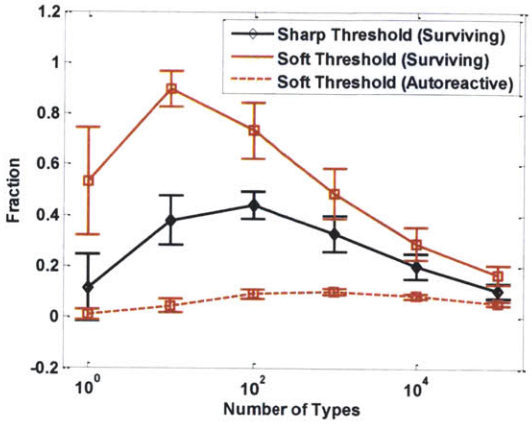

Figure S4-1. The effect of the number of types of peptides at a single copy. R denotes the number of copies of each type of endogenous peptides. **(A)** Fraction of surviving T cells (the number of surviving T cells/the original number of T cells made in the thymus). **(B)** Fraction of autoreactive T cells (the number of autoreative T cells/the original number of T cells made in the thymus). **(C)** The percentage of the number of autoreactive T cells among the number of surviving T cells.

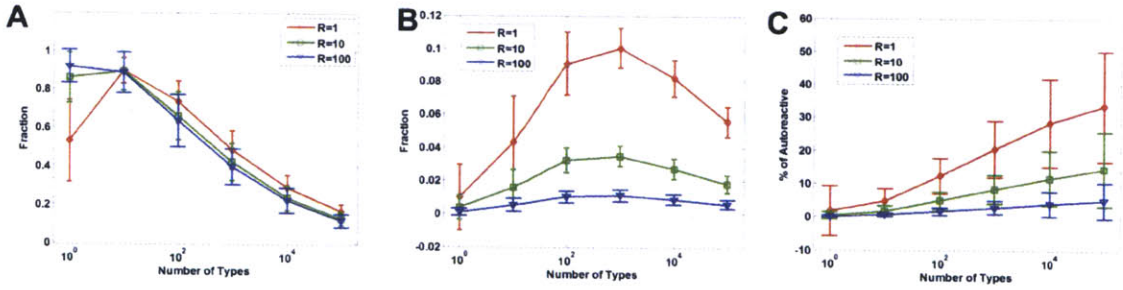

Figure S4-2. The effect of the number of types of peptides. R denotes the number of copies of each type of endogenous peptides. **(A)** Fraction of surviving T cells (the number of surviving T cells/the original number of T cells made in the thymus). **(B)** Fraction of autoreactive T cells (the number of autoreative T cells/the original number of T cells made in the thymus). **(C)** The percentage of the number of autoreactive T cells among the number of surviving T cells.

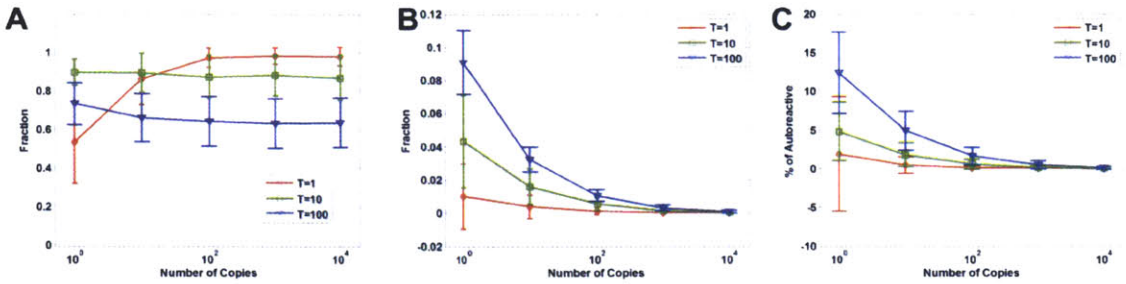

Figure S4-3. The effect of the number of copies (repeats) of each type of peptide. T stands for the number of types of endogenous peptides. **(A)** Fraction of surviving T cells (the number of surviving T cells/the original number of T cells made in the thymus). **(B)** Fraction of autoreactive T cells (the number of autoreative T cells/the original number of T cells made in the thymus). **(C)** The percentage of the number of autoreactive T cells among the number of surviving T cells.

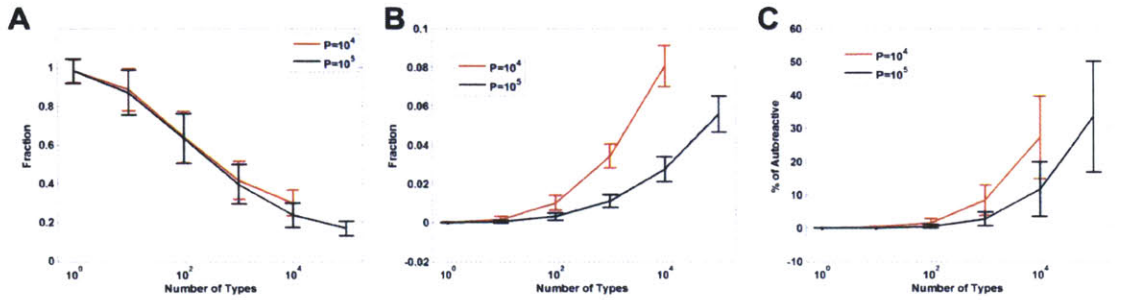

Figure S4-4. The effect of the number of types of peptides at a fixed total number of peptides. P denotes the total number of peptides. **(A)** Fraction of surviving T cells (the number of surviving T cells/the original number of T cells made in the thymus). **(B)** Fraction of autoreactive T cells (the number of autoreative T cells/the original number of T cells made in the thymus). **(C)** The percentage of the number of autoreactive T cells among the number of surviving T cells.

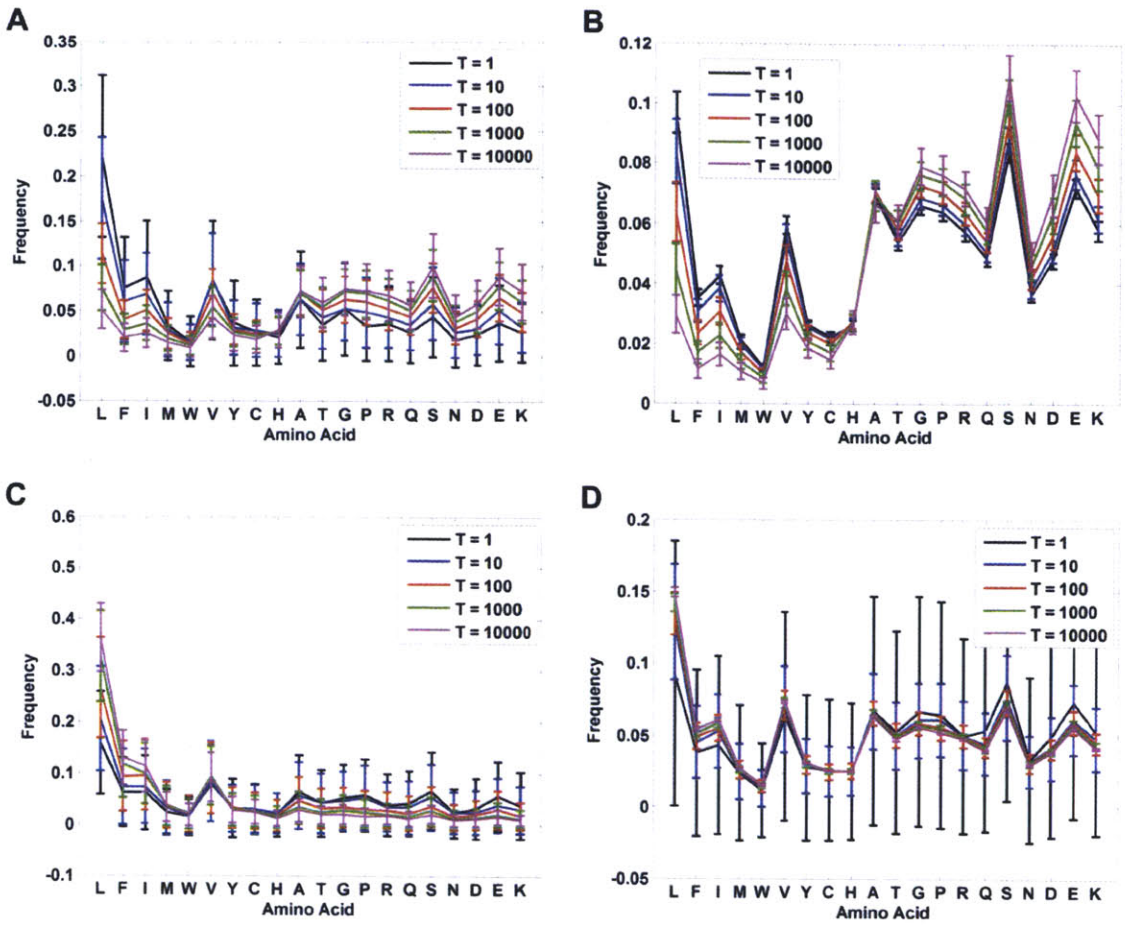

Figure S4-5. The consequence of increasing the number of types of peptides on amino acids frequencies of TCR and endogenous peptides. T stands for the number of types of endogenous peptides. The number of copies of each type of peptides is 100. The order of amino acids in the abscissa is in accordance with the mean interaction free energy with all 20 amino acids. **(A)** Autoreactive TCR. **(B)** Non-autoreactive TCR. **(C)** Autoreactive endogenous peptide (peptides that have reacted with TCR and made it autoreactive). **(D)** Non-autoreactive endogenous peptide (peptides that have reacted with TCR, making it non-autoreactive).

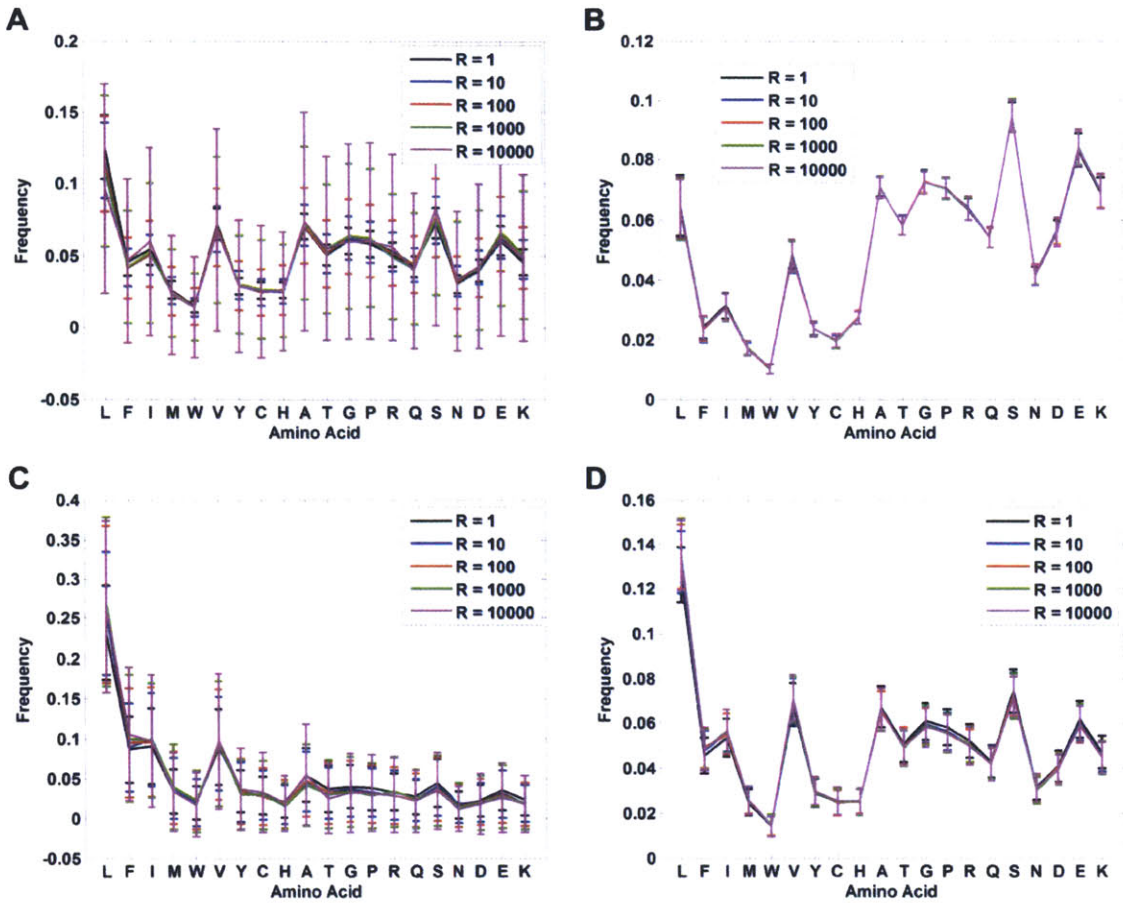

Figure S4-6. The consequence of increasing the number of copies of each type of peptides on amino acids frequencies of TCR and endogenous peptides at a fixed number of types of peptides. R stands for the number of copies of each type of endogenous peptides. The number of types of peptides is 100. The order of amino acids in the abscissa is in accordance with the mean interaction free energy with all 20 amino acids. **(A)** Autoreactive TCR. **(B)** Non-autoreactive TCR. **(C)** Autoreactive endogenous peptide (peptides that have reacted with TCR and made it autoreactive). **(D)** Non-autoreactive endogenous peptide (peptides that have reacted with TCR, making it non-autoreactive).

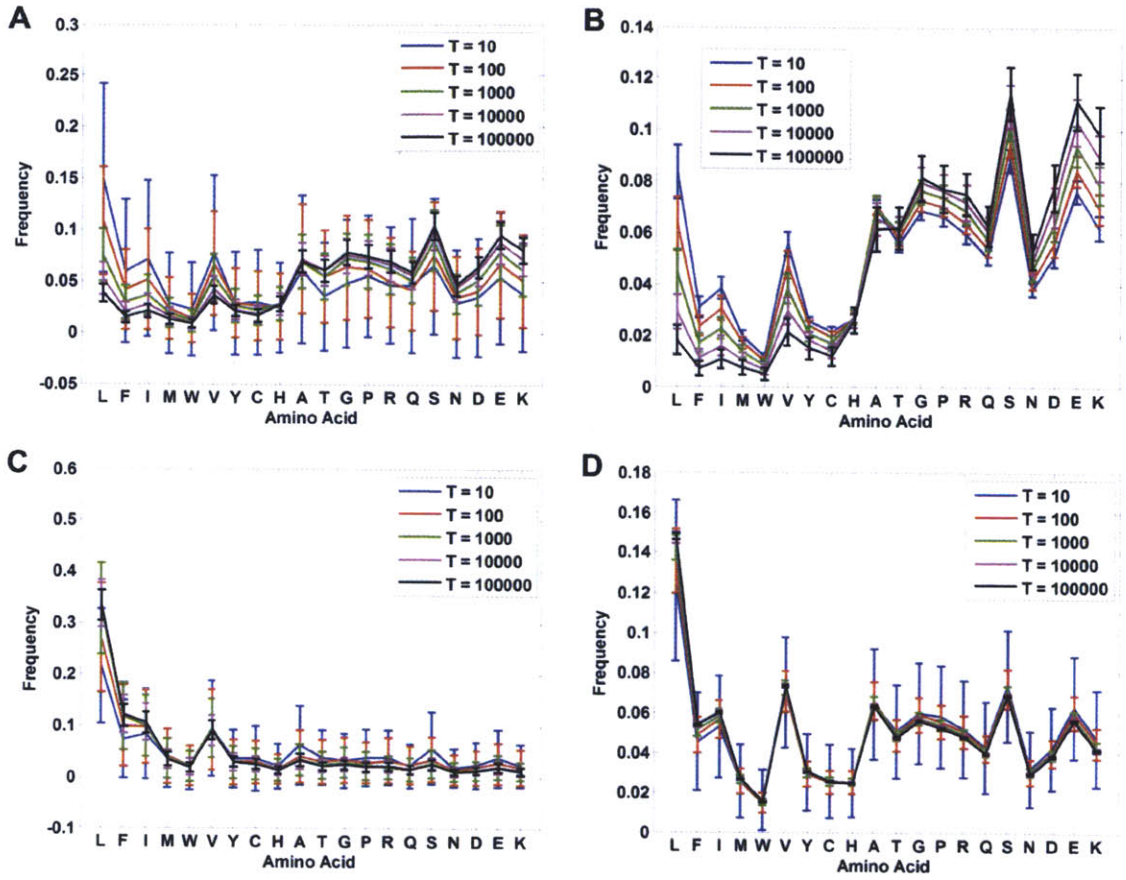

Figure S4-7. The consequence of increasing the number of types of peptides on amino acids frequencies of TCR and endogenous peptides at a fixed total number of peptides. T stands for the number of types of endogenous peptides. The total number of peptides is 10^4. The order of amino acids in the abscissa is in accordance with the mean interaction free energy with all 20 amino acids. **(A)** Autoreactive TCR. **(B)** Non-autoreactive TCR. **(C)** Autoreactive endogenous peptide (peptides that have positively selected TCR and have made it autoreactive). **(D)** Non-autoreactive endogenous peptide (peptides that have positively selected TCR, making it non-autoreactive).

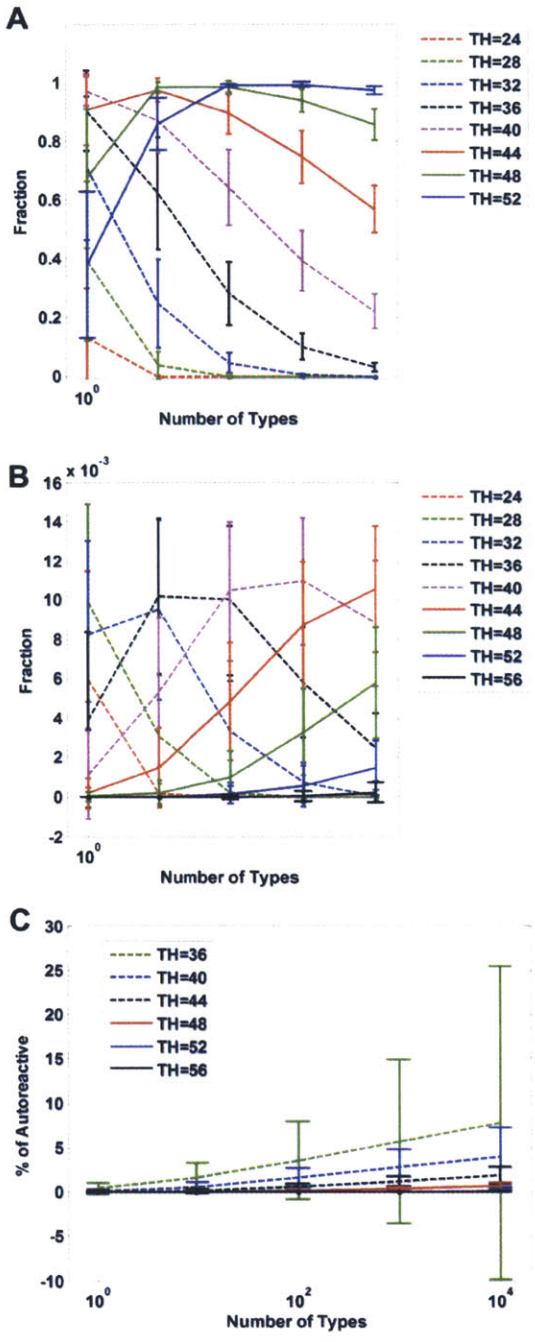

Figure S4-8. The comparison of the effect of the number of types of peptides at a constant number of copies across different values of the negative selection threshold. TH denotes the magnitude of the negative selection threshold. The difference between the negative selection threshold and the positive selection threshold is -5 k_BT. The number of copies of each type of peptides is fixed at 100. **(A)** Fraction of surviving T cells (the

number of surviving T cells/the original number of T cells made in the thymus). **(B)** Fraction of autoreactive T cells (the number of autoreative T cells/the original number of T cells made in the thymus). **(C)** The percentage of the number of autoreactive T cells among the number of surviving T cells.

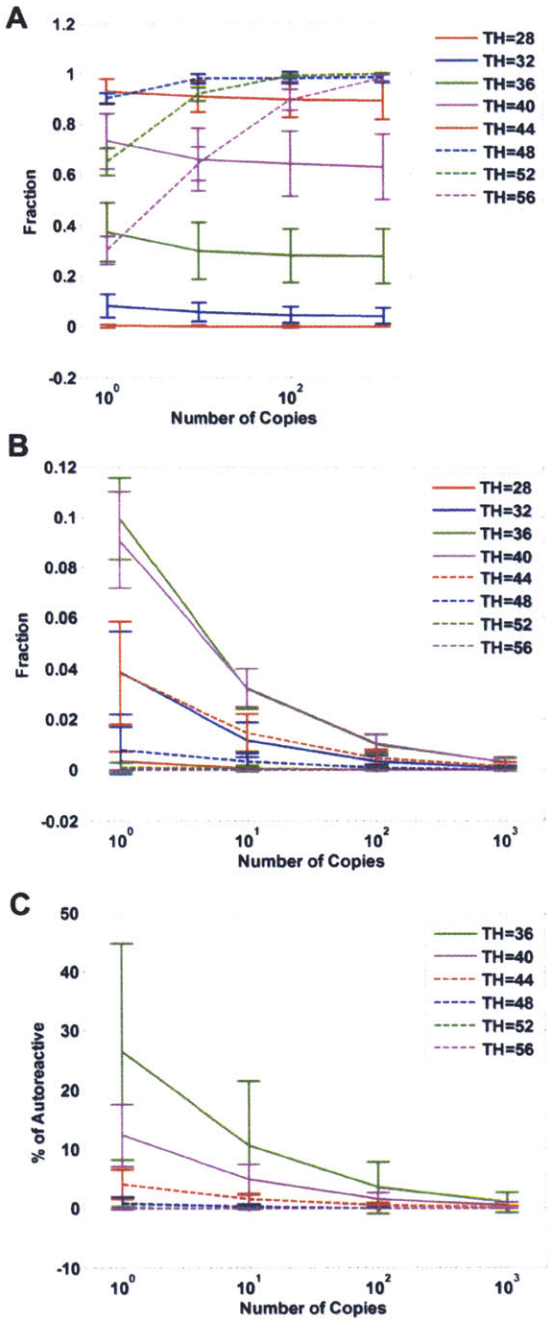

Figure S4-9. The comparison of the effect of the number of copies of each type of peptides at a fixed number of types of peptides across different values of the negative selection threshold. TH denotes the magnitude of the negative selection threshold. The difference between the negative selection threshold and the positive

selection threshold is -5 k_BT. The number of types of peptides is fixed at 100. **(A)** Fraction of surviving T cells (the number of surviving T cells/the original number of T cells made in the thymus). **(B)** Fraction of autoreactive T cells (the number of autoreative T cells/the original number of T cells made in the thymus). **(C)** The percentage of the number of autoreactive T cells among the number of surviving T cells.

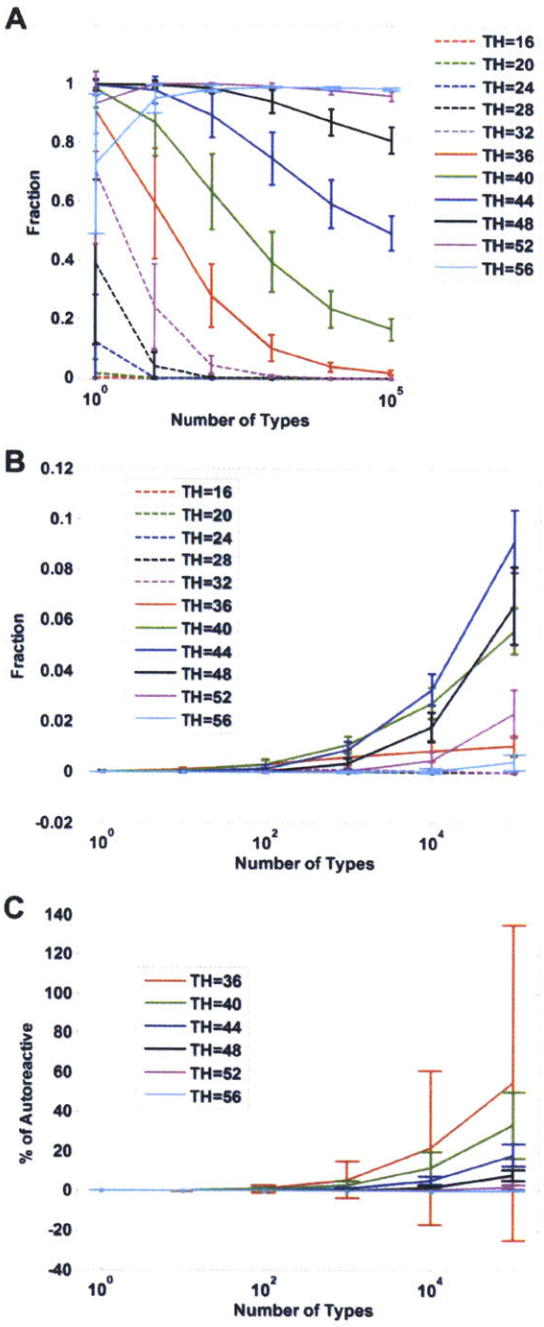

Figure S4-10. The comparison of the effect of the number of types of peptides at a constant total number of peptides across different values of the negative selection threshold. TH denotes the magnitude of the negative selection threshold. The difference between the negative selection threshold and the positive selection threshold is -5 k_BT. The total number of peptides is fixed at 10^4. **(A)** Fraction of surviving T cells (the number of surviving T cells/the original number of T cells made in the thymus). **(B)** Fraction of

autoreactive T cells (the number of autoreative T cells/the original number of T cells made in the thymus). **(C)** The percentage of the number of autoreactive T cells among the number of surviving T cells.

Bibliography

1. Dushek O, Coombs D (2008) Analysis of serial engagement and peptide-MHC transport in T cell receptor microclusters. Biophys J 94: 3447-3460.
2. Dushek O, Das R, Coombs D (2009) A role for rebinding in rapid and reliable T cell responses to antigen. PLoS Comput Biol 5: e1000578.
3. Kosmrlj A, Jha AK, Huseby ES, Kardar M, Chakraborty AK (2008) How the thymus designs antigen-specific and self-tolerant T cell receptor sequences. Proc Natl Acad Sci U S A 105: 16671-16676.
4. Jiang N, Huang J, Edwards LJ, Liu B, Zhang Y, et al. (2011) Two-stage cooperative T cell receptor-peptide major histocompatibility complex-CD8 trimolecular interactions amplify antigen discrimination. Immunity 34: 13-23.
5. Huse M, Klein LO, Girvin AT, Faraj JM, Li QJ, et al. (2007) Spatial and temporal dynamics of T cell receptor signaling with a photoactivatable agonist. Immunity 27: 76-88.
6. Malissen B (2008) CD3 ITAMs count! Nat Immunol 9: 583-584.
7. Kabouridis PS, Jury EC (2008) Lipid rafts and T-lymphocyte function: implications for autoimmunity. FEBS Lett 582: 3711-3718.
8. Artyomov MN, Lis M, Devadas S, Davis MM, Chakraborty AK (2010) CD4 and CD8 binding to MHC molecules primarily acts to enhance Lck delivery. Proc Natl Acad Sci U S A 107: 16916-16921.
9. Krummel MF, Sjaastad MD, Wulfing C, Davis MM (2000) Differential clustering of CD4 and CD3zeta during T cell recognition. Science 289: 1349-1352.
10. Kindt TJ, Godsby RA, Osborne BA (2007) Kuby Immunology. New York: W. H. Freeman & Company.
11. Holler PD, Lim AR, Cho BK, Rund LA, Kranz DM (2001) CD8(-) T cell transfectants that express a high affinity T cell receptor exhibit enhanced peptide-dependent activation. J Exp Med 194: 1043-1052.
12. Huppa JB, Axmann M, Mortelmaier MA, Lillemeier BF, Newell EW, et al. (2010) TCR-peptide-MHC interactions in situ show accelerated kinetics and increased affinity. Nature 463: 963-967.
13. Liu H, Purbhoo MA, Davis DM, Rudd CE (2010) SH2 domain containing leukocyte phosphoprotein of 76-kDa (SLP-76) feedback regulation of ZAP-70 microclustering. Proc Natl Acad Sci U S A 107: 10166-10171.
14. Yokosuka T, Sakata-Sogawa K, Kobayashi W, Hiroshima M, Hashimoto-Tane A, et al. (2005) Newly generated T cell receptor microclusters initiate and sustain T cell activation by recruitment of Zap70 and SLP-76. Nat Immunol 6: 1253-1262.
15. Wang H, Kadlecek TA, Au-Yeung BB, Goodfellow HE, Hsu LY, et al. (2010) ZAP-70: an essential kinase in T-cell signaling. Cold Spring Harb Perspect Biol 2: a002279.
16. Das J, Ho M, Zikherman J, Govern C, Yang M, et al. (2009) Digital signaling and hysteresis characterize ras activation in lymphoid cells. Cell 136: 337-351.

17. Prasad A, Zikherman J, Das J, Roose JP, Weiss A, et al. (2009) Origin of the sharp boundary that discriminates positive and negative selection of thymocytes. Proc Natl Acad Sci U S A 106: 528-533.
18. Coombs D, Dushek, O, van der Merwe, PA (2011) A review of mathematical models for T cell receptor triggering and antigen discrimination; Molina-Paris C, Lythe, G., editor. New York: Springer.
19. Li QJ, Dinner AR, Qi S, Irvine DJ, Huppa JB, et al. (2004) CD4 enhances T cell sensitivity to antigen by coordinating Lck accumulation at the immunological synapse. Nat Immunol 5: 791-799.
20. Irvine DJ, Purbhoo MA, Krogsgaard M, Davis MM (2002) Direct observation of ligand recognition by T cells. Nature 419: 845-849.
21. Yachi PP, Ampudia J, Zal T, Gascoigne NR (2006) Altered peptide ligands induce delayed CD8-T cell receptor interaction--a role for CD8 in distinguishing antigen quality. Immunity 25: 203-211.
22. Luescher IF, Vivier E, Layer A, Mahiou J, Godeau F, et al. (1995) CD8 modulation of T-cell antigen receptor-ligand interactions on living cytotoxic T lymphocytes. Nature 373: 353-356.
23. Wooldridge L, van den Berg HA, Glick M, Gostick E, Laugel B, et al. (2005) Interaction between the CD8 coreceptor and major histocompatibility complex class I stabilizes T cell receptor-antigen complexes at the cell surface. J Biol Chem 280: 27491-27501.
24. Holler PD, Kranz DM (2003) Quantitative analysis of the contribution of TCR/pepMHC affinity and CD8 to T cell activation. Immunity 18: 255-264.
25. Laugel B, van den Berg HA, Gostick E, Cole DK, Wooldridge L, et al. (2007) Different T cell receptor affinity thresholds and CD8 coreceptor dependence govern cytotoxic T lymphocyte activation and tetramer binding properties. J Biol Chem 282: 23799-23810.
26. McKeithan TW (1995) Kinetic proofreading in T-cell receptor signal transduction. Proc Natl Acad Sci U S A 92: 5042-5046.
27. Govern CC, Paczosa MK, Chakraborty AK, Huseby ES Fast on-rates allow short dwell time ligands to activate T cells. Proc Natl Acad Sci U S A 107: 8724-8729.
28. Valitutti S, Muller S, Cella M, Padovan E, Lanzavecchia A (1995) Serial triggering of many T-cell receptors by a few peptide-MHC complexes. Nature 375: 148-151.
29. Zhang W, Sloan-Lancaster J, Kitchen J, Trible RP, Samelson LE (1998) LAT: the ZAP-70 tyrosine kinase substrate that links T cell receptor to cellular activation. Cell 92: 83-92.
30. Zhu M, Janssen E, Zhang W (2003) Minimal requirement of tyrosine residues of linker for activation of T cells in TCR signaling and thymocyte development. J Immunol 170: 325-333.
31. Lin J, Weiss A (2001) Identification of the minimal tyrosine residues required for linker for activation of T cell function. J Biol Chem 276: 29588-29595.
32. Houtman JC, Higashimoto Y, Dimasi N, Cho S, Yamaguchi H, et al. (2004) Binding specificity of multiprotein signaling complexes is determined by both

cooperative interactions and affinity preferences. Biochemistry 43: 4170-4178.
33. Gureasko J, Galush WJ, Boykevisch S, Sondermann H, Bar-Sagi D, et al. (2008) Membrane-dependent signal integration by the Ras activator Son of sevenless. Nat Struct Mol Biol 15: 452-461.
34. Sondermann H, Soisson SM, Boykevisch S, Yang SS, Bar-Sagi D, et al. (2004) Structural analysis of autoinhibition in the Ras activator Son of sevenless. Cell 119: 393-405.
35. Groves JT, Kuriyan J Molecular mechanisms in signal transduction at the membrane. Nat Struct Mol Biol 17: 659-665.
36. Das J, Kardar M, Chakraborty AK (2009) Positive feedback regulation results in spatial clustering and fast spreading of active signaling molecules on a cell membrane. J Chem Phys 130: 245102.
37. Abel SM, Roose JP, Groves JT, Weiss A, Chakraborty AK (2012) The membrane environment can promote or suppress bistability in cell signaling networks. J Phys Chem B 116: 3630-3640.
38. Bunnell SC, Hong DI, Kardon JR, Yamazaki T, McGlade CJ, et al. (2002) T cell receptor ligation induces the formation of dynamically regulated signaling assemblies. J Cell Biol 158: 1263-1275.
39. Lillemeier BF, Pfeiffer JR, Surviladze Z, Wilson BS, Davis MM (2006) Plasma membrane-associated proteins are clustered into islands attached to the cytoskeleton. Proc Natl Acad Sci U S A 103: 18992-18997.
40. Campi G, Varma R, Dustin ML (2005) Actin and agonist MHC-peptide complex-dependent T cell receptor microclusters as scaffolds for signaling. J Exp Med 202: 1031-1036.
41. Manz BN, Groves JT (2010) Spatial organization and signal transduction at intercellular junctions. Nat Rev Mol Cell Biol 11: 342-352.
42. Lavi Y, Gov N, Edidin M, Gheber LA (2012) Lifetime of major histocompatibility complex class-I membrane clusters is controlled by the actin cytoskeleton. Biophys J 102: 1543-1550.
43. Hui KL, Wang C, Grooman B, Wayt J, Upadhyaya A. (2012) Membrane dynamics correlate with formation of signaling clusters during cell spreading. Biophys J 102.
44. Harder T (2004) Lipid raft domains and protein networks in T-cell receptor signal transduction. Curr Opin Immunol 16: 353-359.
45. Treanor B, Batista FD (2010) Organisation and dynamics of antigen receptors: implications for lymphocyte signalling. Curr Opin Immunol 22: 299-307.
46. Huppa JB, Davis MM (2003) T-cell-antigen recognition and the immunological synapse. Nat Rev Immunol 3: 973-983.
47. Kaizuka Y, Douglass AD, Varma R, Dustin ML, Vale RD (2007) Mechanisms for segregating T cell receptor and adhesion molecules during immunological synapse formation in Jurkat T cells. Proc Natl Acad Sci U S A 104: 20296-20301.
48. Tsuchida M, Manthei ER, Knechtle SJ, Hamawy MM (1999) CD28 ligation induces rapid tyrosine phosphorylation of the linker molecule LAT in the

absence of Syk and ZAP-70 tyrosine phosphorylation. Eur J Immunol 29: 2354-2359.
49. Kholodenko BN, Hancock JF, Kolch W (2010) Signalling ballet in space and time. Nat Rev Mol Cell Biol 11: 414-426.
50. Kenworthy AK (2007) Nanoclusters digitize Ras signalling. Nat Cell Biol 9: 875-877.
51. Harding A, Hancock JF (2008) Ras nanoclusters: combining digital and analog signaling. Cell Cycle 7: 127-134.
52. Henis YI, Hancock JF, Prior IA (2009) Ras acylation, compartmentalization and signaling nanoclusters (Review). Mol Membr Biol 26: 80-92.
53. Boykevisch S, Zhao C, Sondermann H, Philippidou P, Halegoua S, et al. (2006) Regulation of ras signaling dynamics by Sos-mediated positive feedback. Curr Biol 16: 2173-2179.
54. Tian T, Plowman SJ, Parton RG, Kloog Y, Hancock JF (2010) Mathematical modeling of K-Ras nanocluster formation on the plasma membrane. Biophys J 99: 534-543.
55. Gurry T, Kahramanogullari O, Endres RG (2009) Biophysical mechanism for ras-nanocluster formation and signaling in plasma membrane. PLoS One 4: e6148.
56. Siggs OM, Makaroff LE, Liston A (2006) The why and how of thymocyte negative selection. Curr Opin Immunol 18: 175-183.
57. von Boehmer H, Aifantis I, Gounari F, Azogui O, Haughn L., Apostolou I, Jaeckel E, Grassi F, Klein L (2003) Thymic selection revisited: How essential is it? Immunol Rev 191: 62-78.
58. Werlen G, Hausmann B, Naeher D, Palmer E (2003) Signaling life and death in the thymus: timing is everything. Science 299: 1859-1863.
59. Palmer E, Naeher, D. (2009) Affinity threshold for thymic selection through a T-cell receptor-co-receptor zipper. Nat Rev Immunol 9: 207-212.
60. Jameson SC, Hogquist KA, Bevan MJ (1995) Positive selection of thymocytes. Annu Rev Immunol 13: 93-126.
61. Le Borgne M, Ladi E, Dzhagalov I, Herzmark P, Liao YF, et al. (2009) The impact of negative selection on thymocyte migration in the medulla. Nat Immunol 10: 823-830.
62. Huseby ES, Crawford F, White J, Marrack P, Kappler JW (2006) Interface-disrupting amino acids establish specificity between T cell receptors and complexes of major histocompatibility complex and peptide. Nat Immunol 7: 1191-1199.
63. Huseby ES, White J, Crawford F, Vass T, Becker D, et al. (2005) How the T cell repertoire becomes peptide and MHC specific. Cell 122: 247-260.
64. Daniels MA, Teixeiro E, Gill J, Hausmann B, Roubaty D, et al. (2006) Thymic selection threshold defined by compartmentalization of Ras/MAPK signalling. Nature 444: 724-729.
65. Altan-Bonnet G, Germain RN (2005) Modeling T cell antigen discrimination based on feedback control of digital ERK responses. PLoS Biol 3: e356.
66. Davis SJ, van der Merwe PA (2006) The kinetic-segregation model: TCR triggering and beyond. Nat Immunol 7: 803-809.

67. Blanchard N, Di Bartolo V, Hivroz C (2002) In the immune synapse, ZAP-70 controls T cell polarization and recruitment of signaling proteins but not formation of the synaptic pattern. Immunity 17: 389-399.
68. Zhang W, Trible RP, Samelson LE (1998) LAT palmitoylation: its essential role in membrane microdomain targeting and tyrosine phosphorylation during T cell activation. Immunity 9: 239-246.
69. Lillemeier BF, Mortelmaier MA, Forstner MB, Huppa JB, Groves JT, et al. (2010) TCR and Lat are expressed on separate protein islands on T cell membranes and concatenate during activation. Nat Immunol 11: 90-96.
70. Lin J, Weiss A, Finco TS (1999) Localization of LAT in glycolipid-enriched microdomains is required for T cell activation. J Biol Chem 274: 28861-28864.
71. Lingwood D, Simons K (2010) Lipid rafts as a membrane-organizing principle. Science 327: 46-50.
72. Horejsi V (2003) The roles of membrane microdomains (rafts) in T cell activation. Immunol Rev 191: 148-164.
73. Sherman E, Barr V, Manley S, Patterson G, Balagopalan L, et al. (2011) Functional nanoscale organization of signaling molecules downstream of the T cell antigen receptor. Immunity 35: 705-720.
74. Plas DR, Johnson R, Pingel JT, Matthews RJ, Dalton M, et al. (1996) Direct regulation of ZAP-70 by SHP-1 in T cell antigen receptor signaling. Science 272: 1173-1176.
75. Lis M, Artyomov MN, Devadas S, Chakraborty AK (2009) Efficient stochastic simulation of reaction-diffusion processes via direct compilation. Bioinformatics 25: 2289-2291.
76. Williamson DJ, Owen DM, Rossy J, Magenau A, Wehrmann M, et al. (2011) Pre-existing clusters of the adaptor Lat do not participate in early T cell signaling events. Nat Immunol 12: 655-662.
77. Peirce M, Metzger H (2000) Detergent-resistant microdomains offer no refuge for proteins phosphorylated by the IgE receptor. J Biol Chem 275: 34976-34982.
78. Govern CC, Paczosa MK, Chakraborty AK, Huseby ES (2010) Fast on-rates allow short dwell time ligands to activate T cells. Proc Natl Acad Sci U S A 107: 8724-8729.
79. Wofsy C, Coombs D, Goldstein B (2001) Calculations show substantial serial engagement of T cell receptors. Biophys J 80: 606-612.
80. Bell GI (1978) Models for the specific adhesion of cells to cells. Science 200: 618-627.
81. Berg HC, Purcell EM (1977) Physics of chemoreception. Biophys J 20: 193-219.
82. Shoup D, Szabo A (1982) Role of diffusion in ligand binding to macromolecules and cell-bound receptors. Biophys J 40: 33-39.
83. Lauffenburger D, Linderman, JJ (1993) Receptors. New York: Oxford University Press, Inc.
84. Goldstein B, Levine, H., Torney, D. (2007) Diffusion limited reactions. SIAM J Appl Math 67: 1147-1165.

85. Torney D, McConnell, HM (1983) Diffusion-limited reaction rate theory for two-dimensional systems. Proc R Soc Lond A 387: 147-170.
86. Purbhoo MA, Liu H, Oddos S, Owen DM, Neil MA, et al. (2010) Dynamics of subsynaptic vesicles and surface microclusters at the immunological synapse. Sci Signal 3: ra36.
87. Gillespie DT (1977) Exact stochastic simulation of coupled chemical reactions. J Phys Chem 81: 2340-2361.
88. Andrews SS, Addy NJ, Brent R, Arkin AP (2010) Detailed simulations of cell biology with Smoldyn 2.1. PLoS Comput Biol 6: e1000705.
89. Sozio MS, Mathis MA, Young JA, Walchli S, Pitcher LA, et al. (2004) PTPH1 is a predominant protein-tyrosine phosphatase capable of interacting with and dephosphorylating the T cell receptor zeta subunit. J Biol Chem 279: 7760-7769.
90. Young JA, Becker AM, Medeiros JJ, Shapiro VS, Wang A, et al. (2008) The protein tyrosine phosphatase PTPN4/PTP-MEG1, an enzyme capable of dephosphorylating the TCR ITAMs and regulating NF-kappaB, is dispensable for T cell development and/or T cell effector functions. Mol Immunol 45: 3756-3766.
91. Poole AW, Jones ML (2005) A SHPing tale: perspectives on the regulation of SHP-1 and SHP-2 tyrosine phosphatases by the C-terminal tail. Cell Signal 17: 1323-1332.
92. Liu Y, Kruhlak MJ, Hao JJ, Shaw S (2007) Rapid T cell receptor-mediated SHP-1 S591 phosphorylation regulates SHP-1 cellular localization and phosphatase activity. J Leukoc Biol 82: 742-751.
93. Holdorf AD, Lee KH, Burack WR, Allen PM, Shaw AS (2002) Regulation of Lck activity by CD4 and CD28 in the immunological synapse. Nat Immunol 3: 259-264.
94. Mugler A, Bailey AG, Takahashi K, ten Wolde PR (2012) Membrane clustering and the role of rebinding in biochemical signaling. Biophys J 102: 1069-1078.
95. Chao DL, Davenport MP, Forrest S, Perelson AS (2005) The effects of thymic selection on the range of T cell cross-reactivity. Eur J Immunol 35: 3452-3459.
96. Pacholczyk R, Kern J (2008) The T-cell receptor repertoire of regulatory T cells. Immunology 125: 450-458.
97. Zheng L, Sharma R, Kung JT, Deshmukh US, Jarjour WN, Fu SM, Ju ST. (2008) Pervasive and stochastic changes in the TCR repertoire of regulatory T-cell-deficient mice. . Int Immunol 20: 517-523.
98. Anderson MS, Venanzi ES, Klein L, Chen Z, Berzins SP, et al. (2002) Projection of an immunological self shadow within the thymus by the aire protein. Science 298: 1395-1401.
99. Mamula MJ (1993) The inability to process a self-peptide allows autoreactive T cells to escape tolerance. J Exp Med 177: 567-571.
100. Danke NA, Koelle DM, Yee C, Beheray S, Kwok WW (2004) Autoreactive T cells in healthy individuals. J Immunol 172: 5967-5972.

101. Chen Z, Benoist C, Mathis D. (2005) How defects in central tolerance impinge on a deficiency in regulatory T cells. . Proc Natl Acad Sci USA 102: 14735-14740.
102. Chan C, George AJ, Stark J (2001) Cooperative enhancement of specificity in a lattice of T cell receptors. Proc Natl Acad Sci U S A 98: 5758-5763.
103. Berg RE, Princiotta MF, Irion S, Moticka JA, Dahl KR, et al. (1999) Positive selection of an H2-M3 restricted T cell receptor. Immunity 11: 33-43.
104. Irion S, Berg RE, Staerz UD (2000) A physiological ligand of positive selection is seen with high specificity. J Immunol 164: 4601-4606.
105. Miyazawa S, Jernigan, R.L. (1996) Estimation of Effective Interresidue Contact Energies for Simulation and Threading. J Mol Biol 256: 623-644
106. Henderson RA, Cox AL, Sakaguchi K, Appella E, Shabanowitz J, et al. (1993) Direct identification of an endogenous peptide recognized by multiple HLA-A2.1-specific cytotoxic T cells. Proc Natl Acad Sci U S A 90: 10275-10279.
107. Goldrath AW, Bevan MJ (1999) Selecting and maintaining a diverse T-cell repertoire. Nature 402: 255-262.
108. Lommerse PH, Vastenhoud K, Pirinen NJ, Magee AI, Spaink HP, et al. (2006) Single-molecule diffusion reveals similar mobility for the Lck, H-ras, and K-ras membrane anchors. Biophys J 91: 1090-1097.
109. Murakoshi H, Iino R, Kobayashi T, Fujiwara T, Ohshima C, et al. (2004) Single-molecule imaging analysis of Ras activation in living cells. Proc Natl Acad Sci U S A 101: 7317-7322.
110. Koretzky GA, Picus J, Thomas ML, Weiss A (1990) Tyrosine phosphatase CD45 is essential for coupling T-cell antigen receptor to the phosphatidyl inositol pathway. Nature 346: 66-68.
111. Wylie DC, Das J, Chakraborty AK (2007) Sensitivity of T cells to antigen and antagonism emerges from differential regulation of the same molecular signaling module. Proc Natl Acad Sci U S A 104: 5533-5538.
112. Redner S (2001) A guide to first-passage processes. New York Cambridge University Press.
113. Goldstein B, Griego R, Wofsy C (1984) Diffusion-limited forward rate constants in two dimensions. Application to the trapping of cell surface receptors by coated pits. Biophys J 46: 573-586.